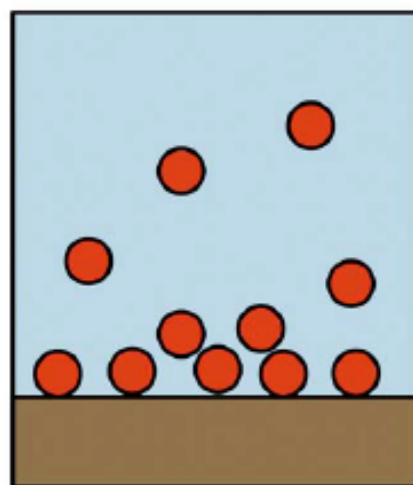
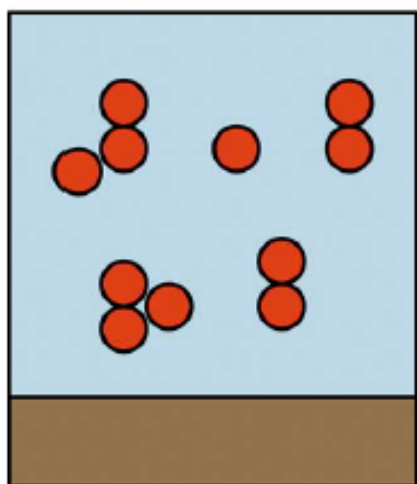


MASTER THESIS

---

# Surface Adsorption versus Bulk Aggregation of Stearyl-Coated Silica Spheres and Surfaces

---



SAMIA OUHAJJI

UNDER SUPERVISION OF:

PROF. A.P. PHILIPSE

PROF. L. PICULELL

PROF. T. NYLANDER

VAN 'T HOFF LABORATORY FOR  
PHYSICAL AND COLLOID CHEMISTRY  
UTRECHT UNIVERSITY



PHYSICAL CHEMISTRY  
LUND UNIVERSITY



**LUND**  
UNIVERSITY

December 11, 2013



## **Abstract**

This thesis describes an experimental study on the competition between surface adsorption and bulk aggregation of particles and surfaces of the same material. The studied system consisted of stearyl silica spheres dispersed in cyclohexane and four different kinds of hydrophobic silica surfaces were used as substrates. Poly(dimethyl)siloxane was used to increase the attraction between the particles in the presence of a surface by means of depletion interaction. Surface adsorption from particle dispersion was found to occur as the interaction between the particles was increased. Ellipsometry experiments revealed that surface adsorption occurred at polymer concentrations far below the bulk phase boundary. As the polymer concentration was increased, an increase in the thickness and the adsorbed amount could be observed. Surface adsorption was found to occur even in the absence of depletant and arose as a consequence of the Van der Waals attraction between spheres and surfaces. The observed minimal polymer concentration needed to overcome the thermal energy correlates well with calculated values. Atomic force microscopy measurements were performed to experimentally visualize the structure of the adsorbed layer. From turbidity and viscosity measurements it was found that no bulk aggregation occurs in the window of the interaction strength where surface adsorption occurs.

The obtained results were compared to recent predictions from theory and simulations by Linse and Wennerström [1] and were found to correspond well.



---

# Contents

---

<b>1</b>	<b>Introduction</b>	<b>7</b>
<b>2</b>	<b>Theory</b>	<b>11</b>
2.1	Colloid-Polymer Mixtures . . . . .	11
2.1.1	Hard Spheres . . . . .	11
2.1.2	Depletion Interaction . . . . .	13
2.1.3	Two Well-Characterized Model Colloid-Polymer Mixtures . . . . .	15
2.2	Ellipsometry . . . . .	17
2.2.1	Null-Ellipsometry . . . . .	18
<b>3</b>	<b>Experimental</b>	<b>21</b>
3.1	Materials . . . . .	21
3.2	Model System . . . . .	22
3.2.1	Characterization . . . . .	22
3.2.2	Phase Diagram . . . . .	23
3.3	Silica Substrates . . . . .	23
3.3.1	Gas-Phase Silanization with Dimethyloctyltrichlorosilane . . . . .	24
3.3.2	Liquid-Phase Silanization with Octadecyltrichlorosilane . . . . .	24
3.3.3	Esterification of the Surface in a Solution of Stearyl Alcohol in Triethyl Phosphate . . . . .	24
3.3.4	Esterification of the Surface in Melt of Stearyl Alcohol . . . . .	25
3.3.5	Characterization . . . . .	25
3.4	Surface Adsorption . . . . .	26
3.4.1	Single-Wavelength Ellipsometry . . . . .	26
3.4.2	The Structure of the Layer . . . . .	28
3.5	Bulk Aggregation . . . . .	29
3.5.1	Turbidity Measurements . . . . .	29
3.5.2	Apparent Hydrodynamic Diameter . . . . .	29
<b>4</b>	<b>Results and Discussion</b>	<b>31</b>
4.1	Model System . . . . .	31
4.2	Silica Substrates . . . . .	32
4.2.1	Characteristics . . . . .	34
4.3	Surface Adsorption . . . . .	36
4.3.1	Ellipsometry . . . . .	37
4.3.2	The Structure of the Layer . . . . .	54

4.4	Bulk Aggregation . . . . .	58
4.4.1	Turbidity Measurements . . . . .	58
4.4.2	Apparent Hydrodynamic Diameter . . . . .	58
<b>5</b>	<b>Van der Waals Attraction and Depletion Interaction</b>	<b>61</b>
5.1	Van der Waals Attraction . . . . .	61
5.1.1	Van der Waals Attraction Between Stearyl-Coated Silica . . . . .	62
5.2	Depletion Interaction . . . . .	64
5.2.1	Depletion Interaction due to Penetrable Hard Spheres . . . . .	64
5.2.2	Depletion Interaction due to Ideal Polymers . . . . .	65
<b>6</b>	<b>Why These Results Could Be Published</b>	<b>67</b>
<b>7</b>	<b>Conclusions and Outlook</b>	<b>69</b>
7.1	Conclusions . . . . .	69
7.2	Outlook . . . . .	69
	<b>Acknowledgements</b>	<b>71</b>
	<b>Bibliography</b>	<b>73</b>
	<b>Appendices</b>	<b>77</b>
	<b>Appendix A Protocol for the Synthesis of Silica Spheres Coated with Stearyl Alcohol</b>	<b>79</b>
A.1	Monodisperse Silica Spheres in Ethanol . . . . .	80
A.2	Hydrophobization with Stearyl Alcohol . . . . .	80
	<b>Appendix B Fluorescent Silica Dispersion</b>	<b>83</b>
B.1	Synthesis of Fluorescent and Hydrophobic Silica Spheres . . . . .	83
B.1.1	Fluorescent, Hydrophilic Silica Spheres . . . . .	83
B.1.2	Hydrophobization . . . . .	84
B.2	Results . . . . .	84
B.2.1	Size and Morphology . . . . .	84
B.2.2	Confocal Microscopy . . . . .	85
B.2.3	AFM . . . . .	85
	<b>Appendix C Quartz Crystal Microbalance with Dissipation Monitoring</b>	<b>91</b>
C.1	Technique . . . . .	91
C.2	Results . . . . .	91
	<b>Appendix D Massive Adsorbed Amount</b>	<b>95</b>
D.1	Incomplete Surface Hydrophobization . . . . .	95
D.2	Incomplete Particle Hydrophobization . . . . .	97
	<b>Appendix E Radius of Gyration of PDMS</b>	<b>99</b>
E.1	Relative Polydispersity . . . . .	100

<b>Appendix F</b>	<b>Volume fractions</b>	<b>103</b>
F.1	Colloid Volume Percent . . . . .	103
F.2	Relative Polymer Concentration . . . . .	103
<b>Appendix G</b>	<b>Adsorbed Amount</b>	<b>105</b>





# Chapter 1

---

## Introduction

---

Surface coatings can be made by particle adsorption from solutions or suspensions onto macroscopic substrates [2], [3]. An example of the latter is convective assembly, also known as vertical deposition method, which is used for the fabrication of colloidal crystals [4], [5]. Adsorption from solutions or suspensions has the advantage that the adsorption rate can be closely controlled by varying parameters such as temperature. Generally, the intention is to obtain surface coatings that are as uniform and homogeneous as possible. However, to achieve close-packed particles in the adsorbed layers is far from trivial. In order for particles to adsorb onto a surface, a particle-surface attraction must exist. In addition, to create uniform, close-packed layers on the substrates, there must be an attraction between the particles as well. If the particle-particle attraction is too large, there is a risk that particles aggregate before adsorbing onto a surface and the resulting coating will not be homogeneous. Particle deposition on surfaces is thus controlled by the balance between particle-particle and particle-surface interactions.

Extensive literature can be found regarding the competition between bulk aggregation and surface adsorption [6], [7], [8], [9], [10]. This competition arises, for example, when a particle dispersion is in contact with a surface. Two scenarios come to mind when the attraction between the particles is increased: the particles can aggregate in the bulk or adsorb onto the surface (figure 1.1).

Okudera studied, among others, the formation and growth mechanisms of thin silica and titania films with varying film thickness on silica substrates [6], [7]. The occurrence of aggregates in the precursor solution had a negative effect on the surface roughness. Similarly, Shin proposed a mechanism for the deposition of various thin metal oxide films onto self-assembled organic monolayers [8]. Zinc oxide films precipitated from solution were the subject of research by Lipowsky [9], [10]. In this particular example, the addition of polymer promoted the formation of smooth films. More recently however, Linse and Wennerström published the results of their theoretical study on the competition between surface adsorption and bulk aggregation [1]. A thermodynamic chemical equilibrium model and Monte Carlo simulations were applied to the adsorption of colloidal particles on a planar surface. The main objective of their research was to answer the following question: does a window in the interaction strength exist at which aggregation in bulk is negligible while adsorption on the surface is substantial?

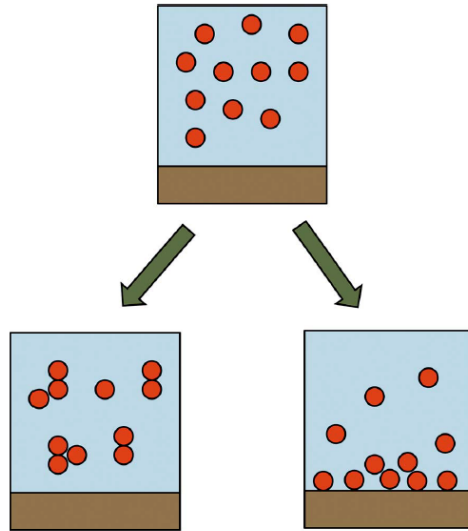


**Figure 1.1:** Two scenarios can be envisaged when a particle suspension comes into contact with a surface and the attraction between the particles is increased: bulk aggregation (left) and surface adsorption (right). Image taken from [1].

In order to elucidate this, two assumptions were made: the particles and surfaces are made of the same material and the interaction range is much smaller than the size of the particles. Under these assumptions the Derjaguin approximation holds (figure 1.2). According to this approximation the sphere-surface interaction is twice as large as the sphere-sphere interaction. However, there are more possibilities for sphere-sphere interactions than for sphere-surface interactions. Therefore, the stronger sphere-surface interaction could be balanced by entropically favoured bulk aggregation [1].

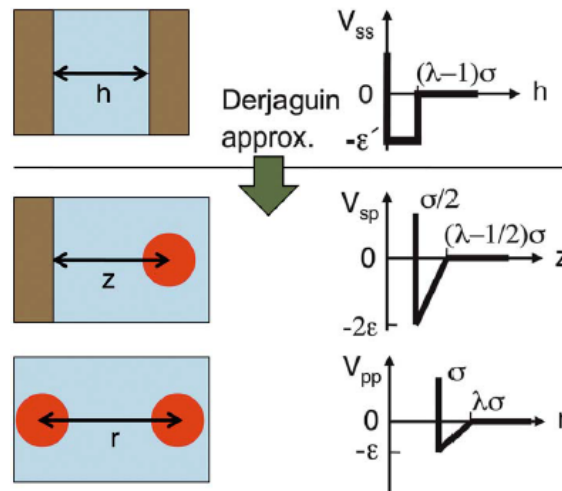


**Figure 1.2:** Derjaguin approximation. The interaction potentials of surface-surface, sphere-surface and sphere-sphere interactions (as illustrated on the left) is shown (on the right). Under the assumptions that the particles and the surfaces are made of the same material and that the interaction range is much smaller than the size of the particles, the Derjaguin approximation holds. The interaction range is the same for both the square-well and the ramp-well potentials, but the depth of the well of the sphere-surface potential, i.e. the interaction strength, is twice as large as that of the sphere-sphere potential. Image taken from [1].

A model for the adsorption was analysed by both theory and computer simulations to determine what happens when the depth of the potential well for sphere-sphere interactions is enlarged. As the attraction between the particles is increased, the following scenarios were found to occur: (A) weak particle adsorption onto the surface, (B) particle association on the surface forming a denser single adsorbed layer, (C) formation of a second adsorbed layer on the surface, (D) multiple adsorbed layers on the surface and (E) bulk phase separation [1]. The simulation results obtained are summarized in figure 1.3.

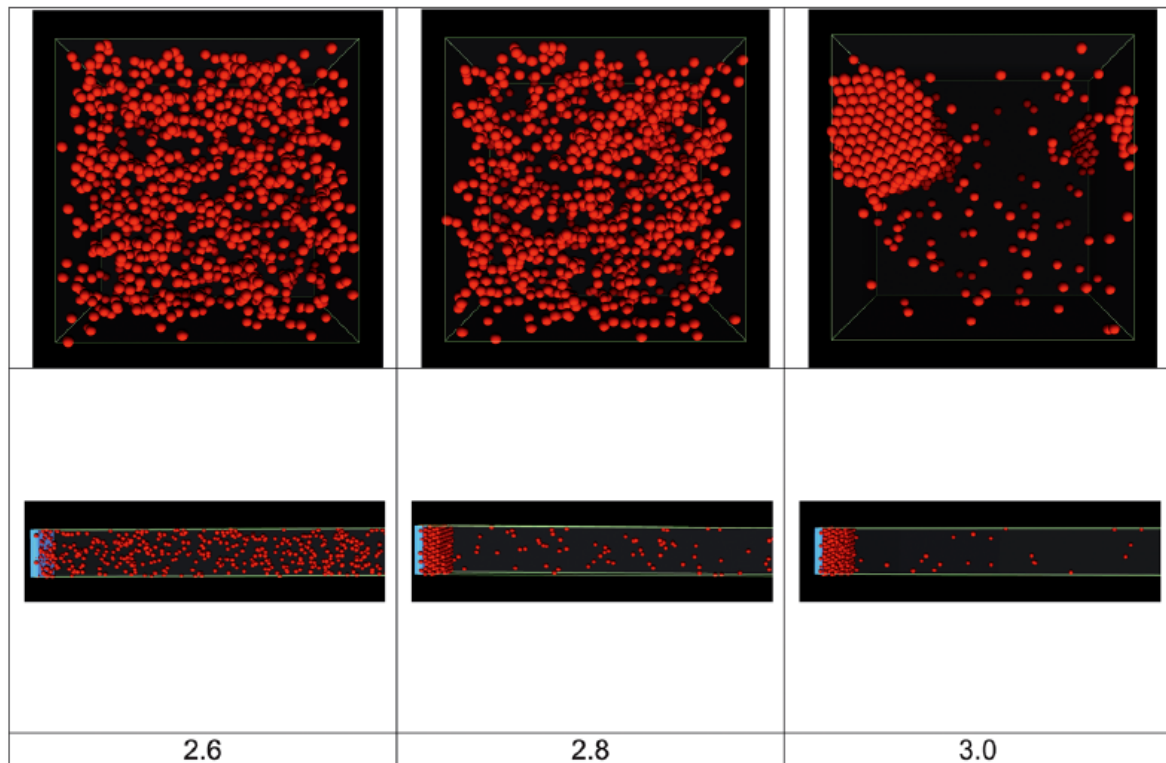


**Figure 1.3:** Final results obtained from Monte Carlo simulations. At the weakest attraction (left), no association occurs in the bulk and there is a slight surface adsorption. However, at slightly higher interaction energy (middle), there still is no sign of bulk aggregation, but multiple layers of particles are adsorbed on the surface. Finally, at even higher interaction strength, bulk aggregation appears while surface adsorption remains. Image taken from [1]

The purpose of my project was to experimentally test these new predictions from theory and simulations and determine what happens when the particles and surface are made of the same material.

The system that was studied in this thesis consisted of hydrophobic stearyl silica spheres dispersed in cyclohexane, a model system for the study of uncharged spheres developed by Vrij and co-workers [11]. Poly(dimethyl)siloxane [12], [13] was used to increase the attraction between the particles by means of depletion-interaction and four different kinds of hydrophobic silica surfaces were used as substrates. Surface adsorption from particle dispersion was monitored by ellipsometry and the structure of the adsorbed layer was investigated experimentally with AFM. The occurrence of bulk aggregation was determined both with turbidity and dynamic light scattering measurements.



# Chapter 2

---

## Theory

---

### 2.1 Colloid-Polymer Mixtures

A model colloid-polymer mixture was chosen to test the theoretical predictions as made by Linse and Wennerström [1]. The model system consist of a dispersion of hard spheres with non-adsorbing polymer. This system is dominated by short-ranged repulsive interactions as there is an effective absence of attractive interactions between the particles. The attractive interactions can then be effectively tuned by depletion interaction. In the following subsections first hard spheres are discussed briefly followed by an explanation of the depletion interaction. Finally, two examples of colloid-polymer mixtures are discussed in section 2.1.3.

#### 2.1.1 Hard Spheres

Hard spheres are impenetrable spheres that are characterized by purely repulsive interactions [14]. The hard-sphere interaction potential,  $W_{hs}(h)$ , is zero at separations larger than the particle diameter and infinite at separations smaller than or equal to the particle diameter:

$$\begin{aligned} W_{hs}(h) &= \infty & h \leq 0 \\ &= 0 & h > 0 \end{aligned} \tag{2.1.1}$$

The hard-sphere interaction potential is sketched in in figure 2.1.

A system of hard spheres, thus, lacks any effective attractions between the particles and only a short-ranged repulsion is present. Such a system can be realized by reducing the Van der Waals attraction between particles. Van der Waals forces act between all atoms and molecules and originate from the collective oscillation of electron clouds at small separations of the particles [14]. Therefore, the Van der Waals attraction is very strong at small separations. The Van der Waals interaction can be minimized by choosing a solvent that is refractive index matched with the particles. In addition, polymers or large organic groups can be attached to the surface of the particles to sterically stabilize the dispersion. If the adsorbed chains are in a *good* solvent, the chains are swollen and

will repel each other. As two particles with polymers attached approach each other and the polymer chains overlap, the osmotic pressure will increase due to steric hindrance of the chains [14].

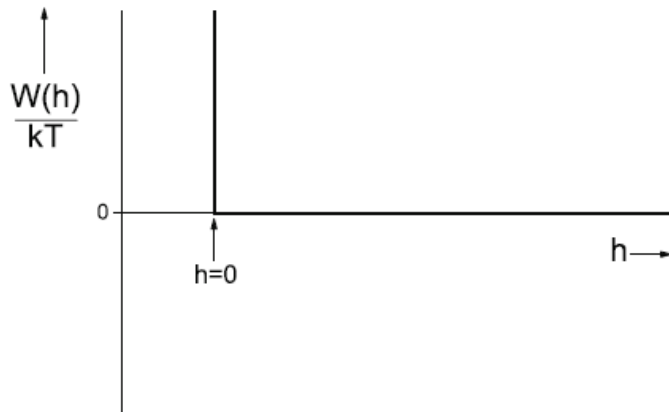


**Figure 2.1:** Hard-sphere interaction potential. At separations larger than the particle diameter the interaction is zero. The interaction potential is infinite at separations equal to or smaller than the particle diameter. Image taken from [14].

The theoretically predicted phase diagram of a system of hard spheres is shown in figure 2.2. At a volume fraction smaller than 0.494 of hard spheres fully fluid phases are observed whereas fully crystal phases appear for volume fractions larger than 0.545. Coexistence of colloidal liquid and crystal phases can be found in the region between 0.494 and 0.545 where a phase transition from the fluid to crystal phase occurs.

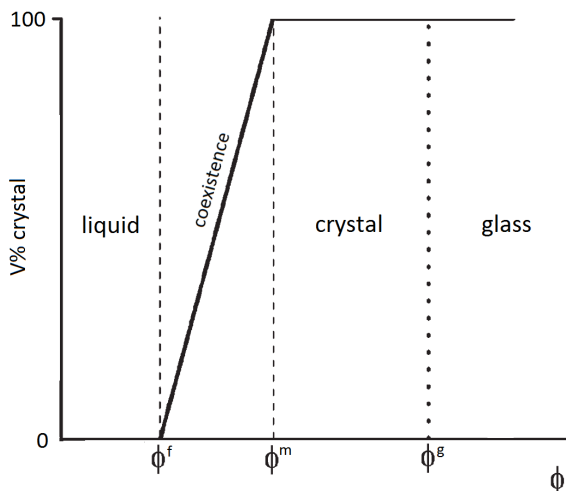


**Figure 2.2:** Theoretically predicted phase diagram for hard spheres. Upon increasing concentrations of hard spheres, the particles undergo a freezing transition (at  $\phi^f = 0.494$ ), a melting transition (at  $\phi^m = 0.545$ ) and a non-equilibrium glass transition (at  $\phi^g \approx 0.58$ ). Image adapted from [15].

## 2.1.2 Depletion Interaction

This section is largely based on the book titled *Colloids and the Depletion Interaction* by Henk Lekkerkerker and Remco Tuinier [14].

Depletion interaction is induced in mixtures of colloidal particles and non-adsorbing polymer. The polymer does not adsorb onto the surface of the colloids and thus creates a depletion layer around the particles which the center of mass of the polymer cannot penetrate due to loss of configurational entropy. When two or more depletion layers overlap (as depicted schematically in figure 2.3 for spherical particles), the free volume available for the polymers increases. To minimize their free energy, the polymers thus exert a net osmotic pressure on the spheres forcing the particles together. This apparent attraction between the colloidal particles is called the depletion interaction. Depletion interaction is entropically driven and arises as result of purely repulsive interactions as the colloid-colloid and colloid-polymer interactions are both repulsive.

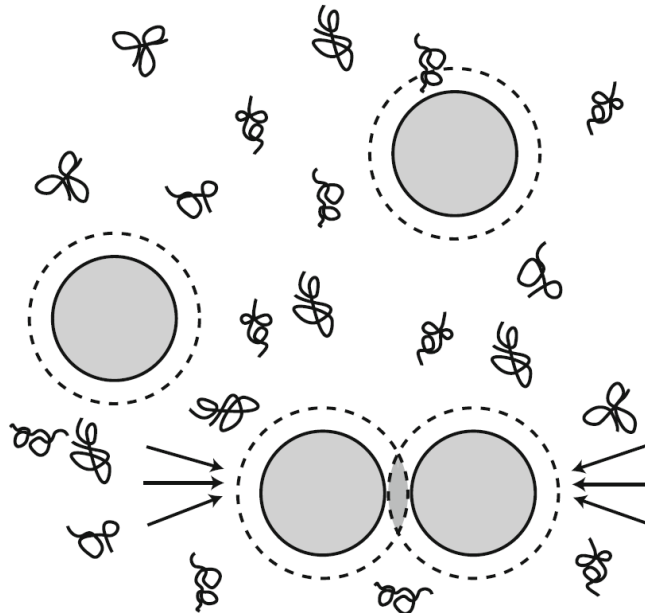


**Figure 2.3:** Illustration depicting the depletion interaction. In a mixture of colloidal spheres and non-adsorbing polymer, a depletion layer arises around the spheres as indicated by the short dashes. The center of mass of the polymer is excluded (depleted) from this layer due to loss of configurational entropy. When two or more depletion layers overlap (lower two spheres), the free volume available for the polymers increases. The polymers thus exert a net osmotic pressure on the colloids (as indicated by the arrows) forcing the particles together. Image taken from [14].

The standard expression for the depletion potential between two spheres with diameter  $2R_c$ , surrounded by a depletion layer with thickness  $\delta$  and for small depletant concentrations is given by:

$$\begin{aligned}
W_{dep}(h) &= \infty & h < 0 \\
&= -PV_{ov}(h) & 0 \leq h \leq 2\delta \\
&= 0 & h \geq 2\delta
\end{aligned} \tag{2.1.2}$$

Here,  $W_{dep}(h)$  is the Asakura-Oosawa-Vrij (AOV) depletion potential,  $h$  is the separation between the colloidal spheres,  $P = n_b kT$  is the ideal osmotic pressure of depletants with bulk number density  $n_b$  and  $V_{ov}$  is the overlap volume of the depletion layers. The overlap volume is depicted in figure 2.3 (hatched area) and is given by the following equation:

$$V_{ov}(h) = \frac{\pi}{6}(2\delta - h)^2(3R_c + 2\delta + \frac{h}{2}) \tag{2.1.3}$$

The depletion interaction potential is sketched schematically in figure 2.4. As indicated in this figure, the range of the depletion potential is determined by the size  $2\delta$  ( $\approx 2R_g$ ) of the depletant, whereas the attraction strength depends on the osmotic pressure and the overlap volume (and thus on the depletant concentration and diameters of polymers and colloids).

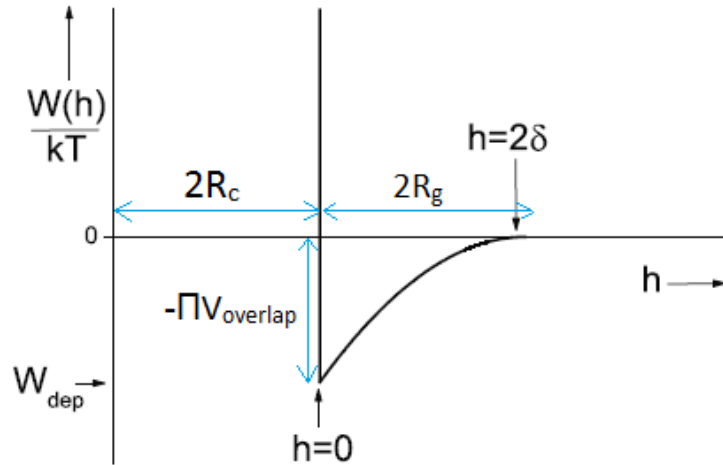


**Figure 2.4:** A sketch of the depletion potential between two hard spheres in a solution containing depletants. The range of the depletion potential depends on the size of the depletant. The depth of the potential well is determined by the osmotic pressure and the overlap volume. Image adapted from [14].

## Phase Diagrams

Colloid-polymer mixtures show interesting phase behaviour upon increasing the colloid and depletant concentrations. The topology of the phase diagram of these systems depends sensitively on the size ratio  $q$  of the polymer ( $R_g$ ) to colloid radii ( $R_c$ ):

$$q = \frac{R_g}{R_c} \tag{2.1.4}$$

A size ratio smaller than 0.3 will give rise to a fluid, solid and coexistence phases. The addition of small polymers thus only expands the fluid-solid coexistence region of the



hard spheres system. The topology of the phase diagram for a size ratio larger than 0.3, exhibits more rich phase behaviour; colloidal liquid, solid and gas and a combination of the three appear as the depletant concentration is increased (see figure 2.5).

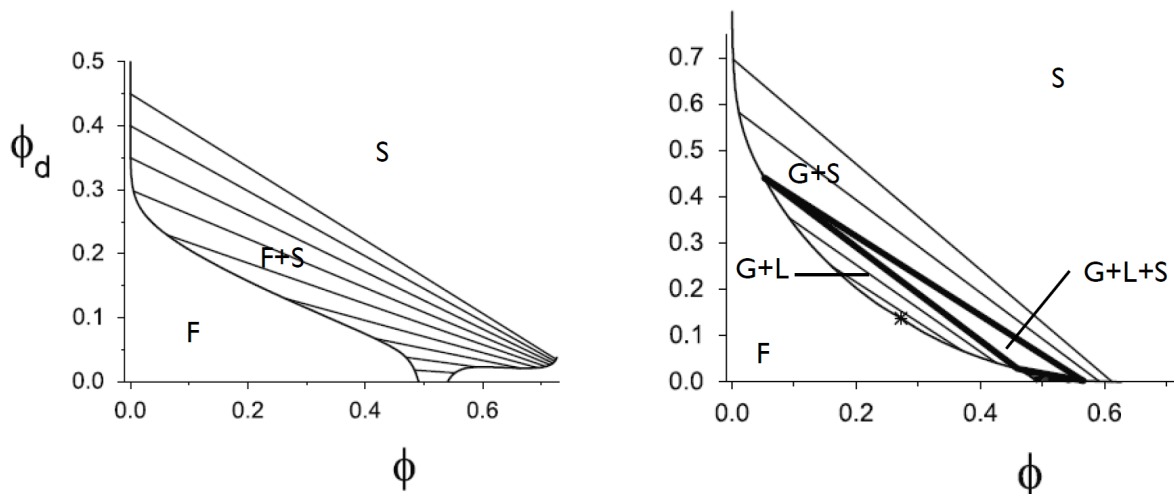


**Figure 2.5:** Theoretically predicted phase diagrams of colloid-polymer mixtures where the depletants are modelled as hard spheres. For a size ratio  $q < 0.3$ , addition of polymer merely expands the fluid-solid crystal coexistence region (left). Colloidal liquid, solid and gas and a combination of the three are observed for a size ratio larger than 0.3 (right). Image adapted from [14].

### 2.1.3 Two Well-Characterized Model Colloid-Polymer Mixtures

There are two model colloid-polymer mixtures that have been extensively studied (both theoretically and experimentally) in the past decades and these will be briefly discussed below.

#### PMMA Spheres and Polystyrene

Poly(methyl methacrylate) spheres sterically stabilized by chemically grafted poly-12-hydroxystearic acid (PHSA) and dispersed in mixtures of decalin and carbondisulfide or tetralin behave as hard spheres as shown by Pusey's group in the 1980s [16], [17]. As the concentration of hard spheres was increased, different phases could be observed (see figure 2.6). The experimental phase diagram was determined and compared to the theoretical hard-sphere phase diagram (as depicted in figure 2.2). From left to right the volume fraction of PMMA spheres is increased and phase transitions occur (as indicated by the arrows). The experimental phase diagram is almost in complete agreement with the theoretical phase diagram, that is also shown in figure 2.7.

In combination with a well-characterized, non-adsorbing, close-to-ideal polymer the PMMA spheres could be used as a model colloid-polymer mixture. Polystyrene satisfies all these conditions in the used solvent and thus PMMA spheres with polystyrene as a depletant are a model colloid-polymer mixture [16].



**Figure 2.6:** Dispersions of PMMA particles. The volume fraction of the hard-sphere like particles increases from left to right. The phase of each sample can be found in figure 2.7 (samples are labelled *a* to *i* from left to right). Image taken from [17].

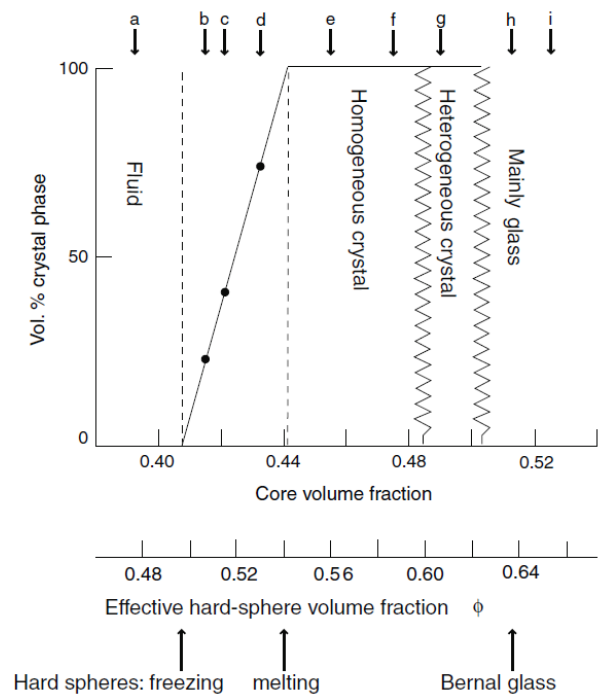


**Figure 2.7:** Experimental phase diagram of PMMA particles. The labels *a* to *i* relate to dispersions as shown in figure 2.6. Below the experimental phase diagram, the theoretical phase diagram is shown with the phase transitions indicated by the arrows.

### Silica Spheres and PDMS

A considerable amount of literature can also be found on the hard spheres system consisting of silica spheres sterically stabilized by octadecyl chains and dispersed in cyclohexane [18]. Numerous experiments have been performed to characterize this particular system by Vrij and collaborators [19], [20], [11]. Sterically stabilized silica

spheres behave like hard spheres as was established by comparison of, among others, diffusion coefficients and sedimentation constants of this system with theoretical values for hard spheres [21], [22].

Upon addition of polydimethylsiloxane (PDMS) to uncharged, hydrophobic silica spheres in cyclohexane, a model colloid-polymer mixture is obtained [23], [24], [25], [26]. Cyclohexane is a good solvent for PDMS and this polymer behaves like an inert molecule in the system as it does not interact with the silica particles [27].

The advantage of a system of silica spheres is the fact that well-characterized particles with small radii (on the order of a few nanometre) can be synthesized (following Stöber [28]).

## 2.2 Ellipsometry

Ellipsometry is an optical technique which can measure the (optical) thickness and refractive index of adsorbed films on substrates. The basic principle of ellipsometry relies on the fact that the polarization state of elliptically polarized light (see figure 2.8) changes upon reflection [29], [30]. There are different types of ellipsometry including null ellipsometry, recording ellipsometry (light intensity is measured) and spectroscopic ellipsometry (measurements are performed at multiple wavelengths) [31]. Experiments as described in this thesis were performed with a Rudolph Research single-wavelength thin-film null ellipsometer (more details on the instrument can be found in section 3.4.1). Null-ellipsometry provides the advantage that the refractive index and the thickness of adsorbed films can be accurately determined. In addition, adsorption processes and growth of adsorbed films can be followed *in situ* [32].

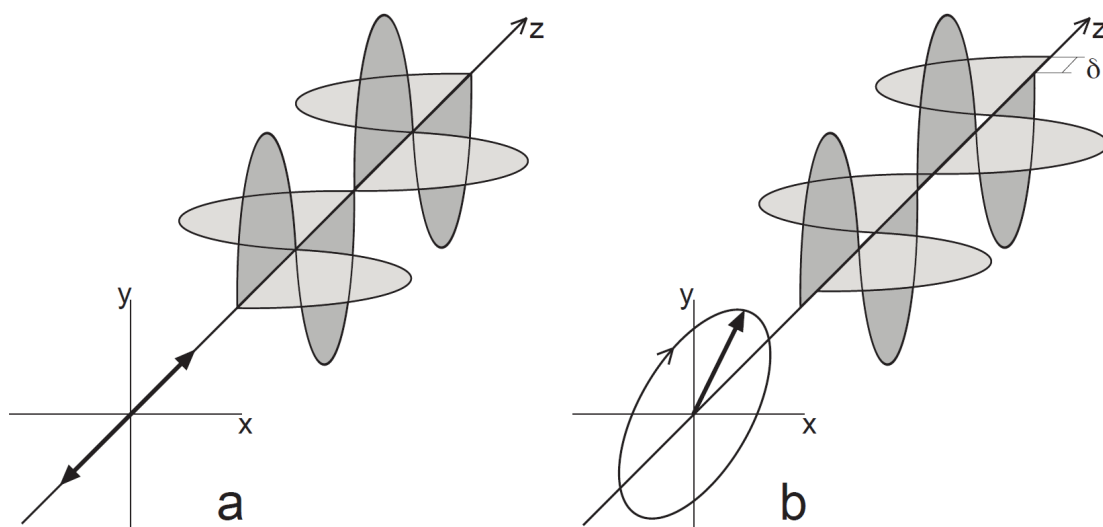


**Figure 2.8:** Linearly (a) and elliptically (b) polarized light. Combining a horizontally polarized light beam with a vertically polarized light beam with the same frequency and phase yields linearly polarized light. However, if the two light beams are combined out of phase, the resultant wave is elliptically polarized [33]. Image taken from [34].

### 2.2.1 Null-Ellipsometry

The main optical components of a null ellipsometer are the polarizer (P), compensator (C), sample (S) and analyzer (A). These can be set-up in either the PCSA or PSCA arrangement [31]. The ellipsometer that was used was arranged in the PCSA configuration and is schematically depicted in figure 2.9.

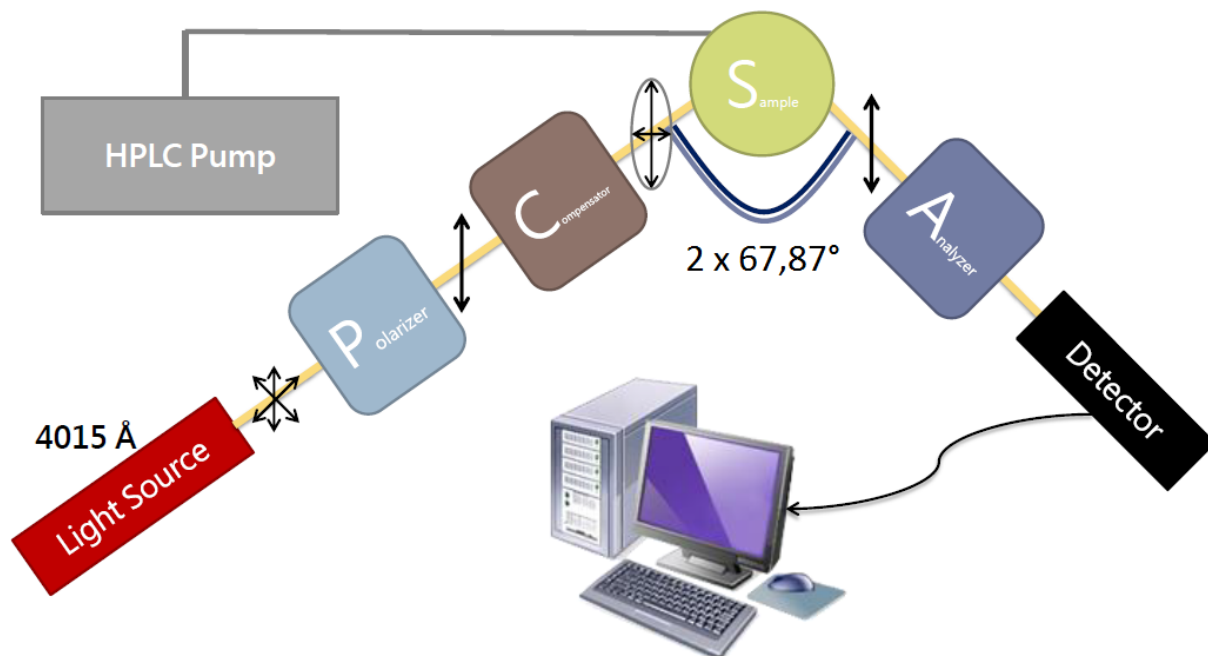


**Figure 2.9:** Ellipsometry set-up used to monitor particle deposition. The Rudolph ellipsometer is set up in a PCSA arrangement; respectively the polarizer (P), compensator (C), sample (S) and analyzer (A). The polarizer and compensator create elliptically polarized light from the light from the light source which is filtered to 4015 Å. This light becomes linearly polarized after reflection on the sample, with an angle of incidence of 67,87 degrees, and is subsequently extinguished by the analyzer. The position of the compensator is fixed and the polarizer and analyzer are turned to determine the ellipsometric angles that give minimum light intensity. The HPLC pump is added to the set-up due to the volatile nature of cyclohexane (refer to section 3.4.1 for more details).

The polarizer creates linearly polarized light from the light from the light source which is filtered to a single wavelength (4015 Å in this case). The linearly polarized light then passes through a retardation plate or compensator after which it is transformed into elliptically polarized light. The retardation plate is made of a birefringent material, which means that it consists of a material that has different refractive indices in perpendicular directions [34]. As the light beam passes through the compensator one of the two components of the polarized light is retarded with respect to the other one. Thus, a phase shift arises between the two electric field vectors making the light elliptically polarized. Due to this phase shift, the two light components will be affected differently while reflecting on a surface. The amplitudes and the phases of the parallel and perpendicular vectors will be altered and the polarization of the light will be changed. Elliptically polarized light with a specific ellipticity can become linearly polarized as it reflects on a surface [33]. This specific ellipticity is obtained by turning either the polarizer or

the compensator. However, in most ellipsometers (as in the Rudolph ellipsometer) the compensator is usually fixed. A second polarizer, the analyzer, can now be turned so as to extinguish the plane polarized light. The angles of the polarizer and the analyzer at which minimum light intensity reaches the detector are called the ellipsometric nulling angles [34]. To find the position of the polarizer and analyzer that give minimum light intensity the method of swings is used [31]. At a fixed position of the analyzer, the polarizer is turned to increase the light intensity to a predetermined value. Subsequently, the position of the polarizer is reversed until the same light intensity is reached at the other side. The position of the minimum is then found by taking the average of the two positions (assuming symmetry). The position of the polarizer is now fixed at this minimum position and the analyzer undergoes the same procedure.

The Rudolph ellipsometer has a fixed compensator angle of  $\pm 45^\circ$ . At this angle, there are four sets of nulling angles at which light is extinguished after passing the analyzer [34]. Each set is referred to as a zone and measurements can be made in each one of these four zones (see table 2.1). The nulling angles can be converted to the ellipsometric angles  $\Psi$  and  $\Delta$  which are the same in each zone in the absence of optical imperfections of the instrument. In reality these angles differ slightly and measurements of the adsorbed film are corrected for the optical imperfections by performing four zone measurements on the bare substrate.

**Table 2.1:** Ellipsometric nulling angles. The conversion from polarizer and analyzer positions to  $\Psi$  and  $\Delta$  in the four zones. The compensator is fixed at  $\pm 45^\circ$  [34].

Zone	C	$\Delta$	$\Psi$
1	$-45^\circ$	$2P_1 + \pi/2$	$A_1$
2	$45^\circ$	$-2P_2 - \pi/2$	$A_2$
3	$-45^\circ$	$2P_3 - \pi/2$	$A_3$
4	$45^\circ$	$-2P_4 + \pi/2$	$A_4$

The angles  $\Psi$  and  $\Delta$  can be related to the complex reflection coefficients of the parallel (p) and perpendicular (s) components of elliptically polarized light according to the following equation [31]:

$$\rho = \frac{R_p}{R_s} = \tan \Psi \exp i\Delta \quad (2.2.1)$$

Here,  $\rho$  is the ratio between the complex reflection coefficients for the p- and s-components,  $R_p$  and  $R_s$ , respectively. This equation holds only for isotropic and homogeneous films of uniform thickness and composition as modelled in the four layers optical model (see figure 2.10) [32]. Equation (2.2.1) relates the angles  $\Psi$  and  $\Delta$  to bulk, surface and substrate properties as  $\rho$  is a function of the (complex) refractive index of the medium, the adsorbed film and the substrate, the thickness of the substrate and adsorbed film and the angle of incidence and wavelength of the light.  $\Psi$  and  $\Delta$  themselves are related to the change in amplitude upon reflection and the change in phase shift, respectively [34].

The ratio  $\rho$ , in equation (2.2.1), reduces to a variable of only four unknowns,  $n_1$ ,  $d_1$ ,  $n_2$  and  $k_2$  (where the refractive index of an absorbing material is given by  $N_2 = n_2 + ik_2$  with  $k$  the extinction coefficient), for a given wavelength and angle of incidence at a clean silica substrate ( $d_f = 0$ ) with a non-absorbing film ( $N_1 = n_1$ ) in a medium with known refractive index ( $N_0$ ). By assuming start values for  $n_2$  and  $k_2$ , the other two parameters can be determined by measuring the nulling angles at different angles of incidence or in different media. The accuracy of multiple media measurements however is found to be higher than those at multiple angles of incidence [35]. Therefore, measurements are performed in air and in the solvent in order to characterize the substrate completely. At the chosen start values, iterations are performed until the thickness of the oxide layer is positive and has a minimal imaginary part [34].

As soon as the substrate properties are completely and accurately determined, the growth of an adsorbing film can be measured *in situ*. A numerical iteration procedure on the values of  $\Psi$  and  $\Delta$  (compared to the substrate) yields the thickness and refractive index of the film using the four layer model (see figure 2.10) [34].

The adsorbed amount or optical thickness can be calculated from the thickness and the refractive index of the adsorbed film by using Feijter's expression [36]:

$$\Gamma = d_f \frac{n_f - n_0}{dn/dc} \quad (2.2.2)$$

Even though small changes in  $\Psi$  and  $\Delta$  can lead to large errors in the values of the refractive index and the thickness, the product of the two, the adsorbed amount, is more accurate, since  $d_f$  and  $n_f$  are co-variant (meaning that a large thickness corresponds to a small refractive index and vice versa) [34].

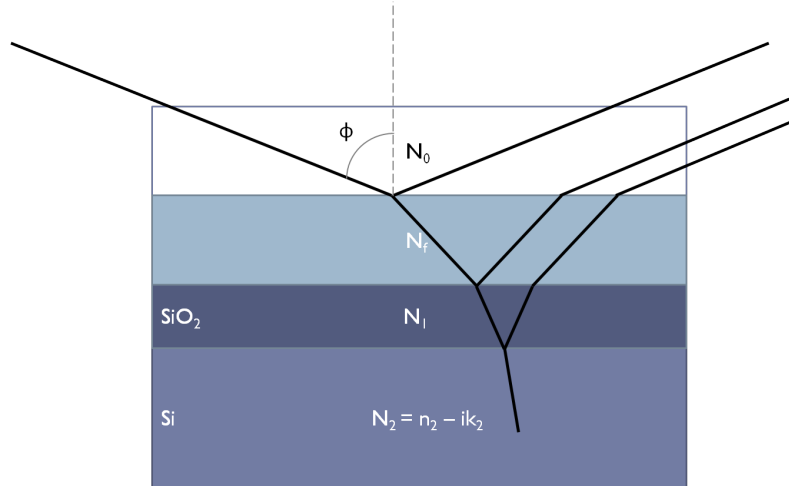


**Figure 2.10:** Optical four layer model. The substrate is assumed to consist of (from bottom to top) bulk silicon with a complex refractive index of  $N_2 = n_2 + ik_2$ , a layer of silica with a refractive index equal to  $N_1$  and thickness  $d_1$ , an adsorbed layer with thickness  $d_f$  and refractive index  $N_f$  and the surrounding transparent medium with refractive index  $N_0$ . The reflection of a light wave is shown schematically at an angle of incidence of  $\phi$ .

# Chapter 3

---

## Experimental

---

### 3.1 Materials

In this section all the commercial materials that were used in the experiments are listed, together with some properties and the suppliers thereof.

**Table 3.1:** Commercial materials.

Name, purity (acronym)	Supplier
Cyclohexane, $\geq 99\%$ (chx)	Sigma-Aldrich
Ethanol, 99.7%	Solveco
Poly(dimethylsiloxane), $M_w = 95000 \frac{g}{mol}$ , $\frac{M_w}{M_n} = 1.9$ (PDMS)	Fluka
Triethyl phosphate, $\geq 99.8\%$ (TEP)	Sigma-Aldrich
Stearyl alcohol / 1-octadecanol, 99% (SA)	Sigma-Aldrich
Toluene, anhydrous	VWR
Octadecyltrichlorosilane, $\geq 90\%$ (OTS)	Sigma-Aldrich
Chloroform, for HPLC $\geq 99.9\%$	Sigma-Aldrich
Silicone oil, for oil baths ( $-50^\circ\text{C}$ to $+200^\circ\text{C}$ )	Sigma-Aldrich
Tetrahydrofuran, for liquid chromatography (THF)	Honeywell Burdick and Jackson
Hydrogen peroxide, 30% by weight $\text{H}_2\text{O}$ ( $\text{H}_2\text{O}_2$ )	Honeywell Burdick and Jackson
Ammonia solution, $\approx 25\%$ ( $\text{NH}_3$ )	Honeywell Burdick and Jackson
Hydrochloric acid, fuming 37% (HCl)	Merck
Hydrofluoric acid, 45-50% solution in $\text{H}_2\text{O}$ (HF)	Acros Organics
Tetraethylorthosilicate, $\geq 99.0\%$ (TEOS)	Sigma-Aldrich
(3-aminopropyl)triethoxysilane, 99% (APS)	Acros Organics
Rhodamine B Isothiocyanate, mixed isomers (RITC)	Sigma-Aldrich
Cyclohexane-d12, 99.5 atom%D	Glaser Lab Kemikalier
Decon 90	Decon Laboratories
Hellmanex III	Hellma
Single-use syringe filters with PTFE membrane, $0.20 \mu\text{m}$	Minisart
Precision cell made of quartz suprasil	HellmaAnalytics

All water used in the experiments was purified by a Milli-Q system. All chemicals were used as received and stored at ambient conditions (except for hydrogen peroxide which was stored in the fridge).

## 3.2 Model System

Silica spheres that were sterically stabilized with 1-octadecanol and dispersed in cyclohexane were used in this research. The particles, code named SD1, were prepared following methods of Stöber [28] and Van Helden [11]. In order to minimize the Van der Waals attraction between the spheres, cyclohexane is chosen as the solvent, which is a good solvent for the octadecyl coating of the spheres and which is refractive index matched with the particles. The spheres were previously used to perform sedimentation experiments [37]. The weight and volume percentages of the stock dispersion SD1 were determined prior to each experiment and were typically found to be in the range 25-31W% and 13-17V% respectively. A protocol for the synthesis of these spheres can be found in Appendix A.

As depletion polymer, poly(dimethyl)siloxane was used. In the current model system, PDMS behaves as an inert molecule and only interacts with the silica spheres and surfaces through depletion interaction [27]. At room temperature the polymer is in a good solvent as the  $\theta$ -temperature of PDMS in cyclohexane is  $-80^{\circ}\text{C}$  [24]. 10 mL stock solutions were prepared with a concentration of  $\approx 100\text{ mg/mL}$  PDMS in cyclohexane. Typically, a fresh PDMS stock solution was prepared once a week.

### 3.2.1 Characterization

Transmission electron microscopy images were taken to determine the size and the morphology of the spheres. The apparent hydrodynamic diameter of the spheres was determined by dynamic light scattering. In order to determine the radius of gyration of PDMS, nuclear magnetic resonance (NMR) diffusion experiments were performed.

#### Transmission Electron Microscopy

Transmission electron microscopy images of SD1 were obtained using a Philips Tecnai 10 microscope. A drop of the diluted dispersion was deposited on a copper grid coated with a formvar support film. The solvent was evaporated by placing the grid under a light bulb. To determine the average particle size and the polydispersity of the particles, the size of at least 100 particles was measured.

#### Dynamic Light Scattering

The apparent hydrodynamic diameter of SD1 was determined by dynamic light scattering using a Malvern Instruments Zetasizer Nano-ZS. A quartz cuvette was filled with 2 mL of a 3V% SD1 dispersion. Prior to use the sample was filtered through a syringe filter. Measurements were performed at  $25^{\circ}\text{C}$  after ten minutes of equilibration at an angle of incidence of  $173^{\circ}$ . The dispersant was cyclohexane with a viscosity of 0.8940 cP and a refractive index of 1.423 at the wavelength of the laser (632.8 nm). The final apparent hydrodynamic diameter obtained was averaged over ten measurements and based on the number of particles present (number mean).

#### Nuclear Magnetic Resonance Diffusion Experiments

NMR diffusion experiments were performed on a Bruker AVII-200 spectrometer operating at 200.13 Mhz for the proton resonance frequency. A DIFF-25 5 mm (1 H) probe was used



to perform the diffusion measurement with the possibility of using a maximum gradient field strength in the z-direction of 9.63 T/m. To determine the diffusion coefficient of the polymer a pulsed gradient stimulated spin echo sequence was utilized. As heating of the sample caused temperature gradients to occur, which in turn generated convection problems during the measurement, the sample was measured at ambient temperature. The effective diffusion time is defined as  $\Delta\text{-}\delta/3$ , where  $\Delta$  is the time between the gradient pulses and  $\delta$  is the length of a gradient pulse. 8 scans and gradients ranging between 0.15 and 9.63 T/m in 64 steps were used to obtain a  $\Delta$  of 103 ms and a  $\delta$  of 0.72 ms. The NMR data analysis was performed in MatLab using an in-house code partially derived from matNMR. The estimated error was derived from a Monte Carlo error estimation [38].

The sample consisted of a solution of  $\approx 5$  mg/mL PDMS in deuterated cyclohexane which was transferred into a glass NMR-tube. The tube was sealed with a cap and excess Teflon tape to prevent evaporation of cyclohexane.

### 3.2.2 Phase Diagram

The phase diagram of SD1 and PDMS was obtained by mixing varying concentrations of the colloidal particles and the polymer. Phase separation was determined by visual inspection of the samples and occurred at sufficiently high concentrations of both colloidal particles and polymer. Phase separation was typically observed within 30 minutes after mixing the two species.

## 3.3 Silica Substrates

The substrates consisted of hydrophobized silica surfaces which were prepared from 4 inch polished silicon wafers (p-type, boron doped, with a resistivity of 1-10  $\Omega\cdot\text{cm}$  and with a thermally oxidized silica layer of around 300  $\text{\AA}$ ) and were purchased from Semiconductor Wafer Inc., Taiwan. The oxidized silicon wafer was cut into small slides with a width of  $\approx 10$  mm and a length of 2-3 cm. Prior to use, the substrates were placed in a slide holder and cleaned in a base mixture of  $\text{NH}_4\text{OH}$ ,  $\text{H}_2\text{O}_2$  and  $\text{H}_2\text{O}$  (volume ratio 3:3:16) at 80°C for 5 minutes after which they were rinsed with water. Subsequently, the substrates were cleaned by an acid mixture consisting of  $\text{HCl}$ ,  $\text{H}_2\text{O}_2$  and  $\text{H}_2\text{O}$  (volume ratio of 3:3:16) at 80°C for 10 minutes after which they were thoroughly rinsed with water and then ethanol. Finally, the substrates were stored in ethanol awaiting further use.

The surface chemistry of the substrates can easily be modified as the silica surface consists of five  $-\text{OH}$  groups per nanometre [39]. To obtain spheres and particles of the same material, the surfaces were hydrophobized. Four methods of surface modification were utilized. Gas-phase silanization with dimethyloctylchlorosilane yielded surfaces modified with  $\text{C}_8$ -chains. Liquid-phase silanization with octadecyltrichlorosilane and esterification in solution and in melt of stearyl alcohol, all yielded  $\text{C}_{18}$  hydrophobized surfaces. Prior to hydrophobization the silica substrates were rinsed with ethanol, dried with nitrogen and plasma cleaned in air for 5 minutes (Harrick Scientific Corp, Model PDC-3XG plasma cleaner) to remove any organic impurities.

### 3.3.1 Gas-Phase Silanization with Dimethyloctyltrichlorosilane

Silica surfaces, hydrophobized with C<sub>8</sub> chains, were prepared by gas-phase silanization of the hydrophilic silica substrates. The cleaned surfaces were placed in a desiccator with around 3 mL dimethyloctylchlorosilane. The desiccator was evacuated with a vacuum pump and left for 14-18 hours at room temperature. The substrates were then sonicated in THF (3×5 min) followed by ethanol (3×5 min) to remove any unreacted material. The substrates were stored in ethanol awaiting further use.

### 3.3.2 Liquid-Phase Silanization with Octadecyltrichlorosilane

Eight 20 mL glass vials were filled with 0.1 mL OTS and 19.9 mL anhydrous toluene (0.5% (v/v)). In each vial, one cleaned surface was immersed in the solution for 24 hours. The substrates were then thoroughly rinsed with chloroform and put in a chloroform bath for 2-3 minutes [40]. Finally, the substrates were sonicated in ethanol for 15 minutes and stored in ethanol awaiting further use.

### 3.3.3 Esterification of the Surface in a Solution of Stearyl Alcohol in Triethyl Phosphate

Esterification of the silica surface by stearyl alcohol in TEP typically proceeded as follows. Eight cleaned surfaces were placed in a solution of 17 g stearyl alcohol in 100 mL TEP in a three-neck flat-bottom flask at a temperature between 150-160 °C, which was maintained with an oil bath, under nitrogen flow (through a Pasteur pipette) and for the duration of four days. A reflux condenser was added to the set-up to prevent the evaporation of the solution and a magnet ensured homogeneous heat distribution throughout the oil (see figure 3.1). As soon as the substrates were removed from solution, they were rinsed by sonication in THF (3×5 min) followed by ethanol (3×5 min) to remove unreacted reagents. The substrates were stored in ethanol awaiting further use.



**Figure 3.1:** Set-up used for the esterification of silica substrates with stearyl alcohol in TEP.

### 3.3.4 Esterification of the Surface in Melt of Stearyl Alcohol

30 grams of stearyl alcohol was quantitatively transferred to a 100 mL two-neck round-bottom flask and heated to 180-200°C. A mechanical stirrer was placed on top to homogenize the melt (see figure 3.2). One silica substrate was placed in the melt for 3-4 hours. The substrate was rinsed three times in pre-heated chloroform ( $\approx 55^\circ\text{C}$ ) and sonicated in ethanol for 15 minutes. The substrate was stored in ethanol awaiting further use.

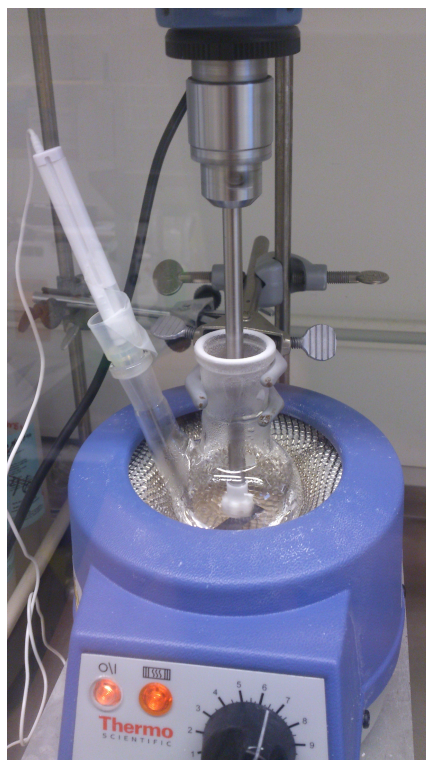


**Figure 3.2:** Set-up used for the esterification of silica substrates in the melt of stearyl alcohol.

### 3.3.5 Characterization

The silica substrates were characterized with atomic force microscopy and by measuring the contact angle of a drop of water on the surface.

#### Atomic Force Microscopy

Atomic force microscopy (AFM) was performed to determine the surface roughness of the silica substrates. The instrument that was used was a scanning probe microscope from Park Systems, model XE-100. Images were obtained in tapping mode using a scanner with a XY scan range of  $50 \times 50 \mu\text{m}$  and a working distance of the Z-scanner of  $12 \mu\text{m}$ . Si-probes were used with a resonance frequency range from 200-400 kHz and a spring constant of 13-77 N/m (manufactured by AppNano). Measurements were performed in air and at room temperature with a scan rate varying from 0.2 to 1 Hz. Images were taken both ways and topography, amplitude and phase images were obtained. Sample preparation consisted of taping the substrate to a magnetic coin with double-sided tape

## Contact Angle Measurements

A Drop and Bubble Shape Tensiometer PAT-1 from Sinterface Technologies was used to accurately determine the contact angle of a drop of water on the hydrophobized silica surfaces. Measurements were performed at room temperature. The contact angles on the C<sub>8</sub>- and TEP-surfaces were determined at one single area by measuring the contact angle from the obtained image of the water droplet. The contact angles on the LPS- and Melt-surfaces were determined by measuring the contact angle of water on three different places on the substrate. In addition, various drop volumes, ranging from 25-80 mm<sup>3</sup> were measured. The contact angle on the LPS-surfaces was averaged over 55 values, obtained in a total of 7 different measurements. For the Melt-substrates, the contact angle was averaged over 15 values, also obtained in a total of 7 measurements.

## 3.4 Surface Adsorption

The adsorption of silica particles from dispersion unto macroscopic silica surfaces was studied with ellipsometry and atomic force microscopy.

### 3.4.1 Single-Wavelength Ellipsometry

A modified, automated Rudolph Research thin-film null ellipsometer, model 43603-200E, was used in order to monitor the adsorbed amount and thickness of adsorbed surface layers in situ. A detailed description of the instrument is given by Tiberg and Landgren [35]. The instrument was equipped with high-precision step motors and controlled with a personal computer. A xenon arc lamp, filtered to a wavelength of 4015 Å, was used as the light source. Measurements were performed at an angle of incidence of 67.87°. The substrate was hanged inside a 7 mL trapezoid cuvette made of optical glass and thermostated to 25°C (see figure 3.3). A magnetic stirrer agitated the sample at  $\approx$  300 rpm. Prior to use, the cuvette and stirrer bean were cleaned in a 5% solution of Decon 90 (by volume in water) overnight, rinsed with warm water and distilled water and then blown dry with nitrogen. The cuvette was equipped with an inlet and an outlet tube connected to a HPLC pump and a multichannel peristaltic pump, respectively. In this way, the solution in the cuvette could be changed without emptying the cuvette. Due to the volatile nature of the solvent, the HPLC pump was also used to maintain a constant sample volume by adding additional cyclohexane every minute.

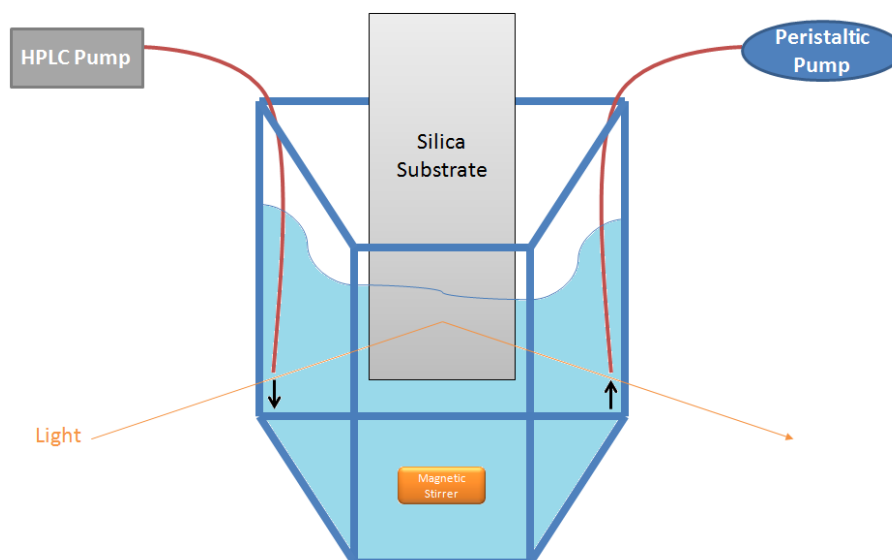


**Figure 3.3:** Cuvette of ellipsometer.

The optical properties of the silica surface, that is the refractive index of the silicon and silicon oxide layer and the thickness of the silica layer, were determined at the start of each experiment to obtain accurate measurements of the thickness and adsorbed amount of the adsorbed surface layer. These properties were determined by measuring the ellipsometric angles  $\Psi$  and  $\Delta$  in two different media. First ethanol, then water, ethanol again and finally cyclohexane were flowed through the cuvette (with a typical flow rate of 5 mL/min for the duration of 5 minutes). Measurements of  $\Psi$  and  $\Delta$  in air and ethanol were used to characterize the substrate. Corrections were made for optical imperfections of the instrument by averaging the ellipsometric angles over four zones.

After characterization of the substrate, the changes in  $\Psi$  and  $\Delta$  were monitored as a function of time. Dispersion SD1 was added to  $\approx 5$  mL of cyclohexane in the cuvette to a final volume percent of 3V%, as soon as a stable baseline was acquired (after at least 100 seconds). Depletion polymer was added before adding the dispersion. After monitoring the ellipsometric angles for a certain time, the cuvette was rinsed from the dispersion by flowing cyclohexane through the cell with a flow rate of 5- 6 mL/min for the duration of five minutes. Measurements of the adsorbed amount and the thickness of the adsorbed layer were performed on gas-phase silanized substrates ( $C_8$  surface layer) and liquid-phase silanized surfaces and esterified surfaces in solution and in the melt ( $C_{18}$  surface layer). The substrates were rinsed with ethanol and dried with nitrogen immediately before use. Samples consisted in all experiments of 3V% SD1 and 0, 2, 4, 6, 8, 10, 12 and 14 mg/mL. In addition, a sample consisting of 3V% SD1 and 1 mg/mL PDMS was measured on a  $C_{18}$ -TEP surface. A HPLC pump with a typical flow rate of 0.01 to 0.025 mL/min, was used to maintain a constant sample volume in the cuvette. In the case of  $C_8$  substrates, measurements were performed until a more or less stable baseline was obtained. Whenever a stable baseline could not be achieved, rinsing started after a significant amount of time had passed. For the  $C_{18}$ -substrates a fixed measurement time was adhered as depicted in table 3.2.

**Table 3.2:** Measurement times (in seconds) of ellipsometry experiments on C<sub>18</sub>-substrates.

Silica Substrate	Before rinsing	After rinsing
C <sub>18</sub> -LPS	5400	1800
C <sub>18</sub> -TEP	13620	3600
C <sub>18</sub> -Melt	5400	1800

The data were analysed using a four-layer model, as explained in detail in section 2.3.1. The substrates were stored in air after use awaiting characterization with AFM.

### Refractive Index

Refractive indices of samples used in the ellipsometry experiments together with the refractive index increment of SD1 and the refractive index of ethanol were necessary to calculate the adsorbed amount, using de Feijter's expression (see section 2.3.1), from the ellipsometric data.

An Abbe 60/ED multi-wavelength refractometer from Bellingham and Stanley Ltd was used to accurately determine the refractive index. This refractometer is equipped with an OSRAM mercury vapour light bulb that allows the measurement of refractive indices at three different wavelengths: 435.8 nm, 546.1 nm and 579.0 nm. Refractive indices were determined at 25°C. By interpolating or extrapolating the measured data, the refractive index of the sample can be determined at any desired wavelength. The refractive index versus wavelength was fitted to a two-term Cauchy equation, given by the following equation:

$$n(\lambda) = A + \frac{B}{\lambda^2} \quad (3.4.1)$$

The fitted values A and B were then used to determine the refractive indices at a wavelength of 401.5 nm (the wavelength of the ellipsometer). The refractive index increment,  $dn/dc$  (in mL/g), was determined by measuring the refractive indices of at least 5 different concentrations of SD1 and fit these values to a line.

### 3.4.2 The Structure of the Layer

After adsorption was measured by ellipsometry the surfaces were studied with AFM to visualize the structure of the adsorbed layer. The same instrument and the same measuring parameters as described in section 3.3.5 were used.

## 3.5 Bulk Aggregation

Bulk aggregation was studied by monitoring two properties of the dispersion with increasing polymer concentration: turbidity and apparent hydrodynamic diameter.

### 3.5.1 Turbidity Measurements

The turbidity was determined by measuring the transmittance of 2 mL samples containing 3V% SD1 and 0, 2, 4, 6, 8, 10, 12 and 14 mg/mL PDMS in cyclohexane in a quartz cuvette thermostated with a water bath at 25°C. The transmittance of pure cyclohexane was measured as well. A Varian Cary WinUV spectrophotometer was used to measure the transmittance. Measurements were performed in the range of wavelengths from 800 to 200 nm with a data interval of 0.500 nm, a scan rate of 300 nm/min, ave time of 0.1 s (time over which data is averaged) and a spectral bandwidth of 2.0 nm.

### 3.5.2 Apparent Hydrodynamic Diameter

The apparent hydrodynamic diameter of the silica spheres with increasing polymer concentration was measured by dynamic light scattering using the same instrument and parameters as described in section 3.2.1. A quartz cuvette was filled with 2 mL samples containing 3V% SD1 and 0, 2, 4, 6, 8, 10, 12 and 14 mg/mL PDMS in cyclohexane. Prior to the measurements, the samples were filtered through a syringe filter. The viscosity of cyclohexane and PDMS was determined separately (see below) and utilized in the size measurements. The final apparent hydrodynamic diameter obtained was based on the number of particles present (number mean).

#### Viscosity

In order to determine the viscosity of solutions of cyclohexane and varying concentration of PDMS, an Ubbelohde Micro-Viscometer 53620 was used (see figure 3.4). The viscometer was filled through the filling tube with 2 mL of sample after which it was hanged in a water bath at 25°C. The venting tube was closed and by applying suction to the capillary tube the liquid was raised up to and above the upper timing mark M1. Suction was then stopped and the venting tube was opened. As the liquid passed the upper timing mark M1, timing was started until the liquid passed the lower timing mark M2. The obtained flow time was averaged over 5 à 6 measurements per sample.

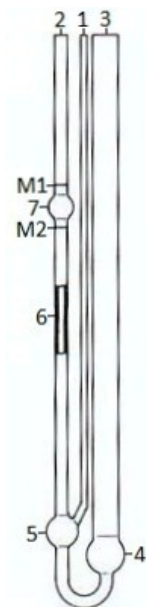


**Figure 3.4:** Ubbelohde micro-viscometer with venting tube (1), capillary tube (2), filling tube (3), reservoir (4), reference level vessel (5), capillary (6), measuring sphere (7), upper timing mark (M1) and lower timing mark (M2). Image taken and adapted from the manual of the viscometer.



---

## Results and Discussion

---

### 4.1 Model System

The silica spheres of dispersion SD1 have an average size of 63.7 nm with a standard deviation of 5.1 nm, as determined with TEM. The apparent hydrodynamic diameter of the particles amounted to  $73.6 \pm 2.85$  nm. The size of the particles as determined with TEM is smaller than the size as determined with DLS due to shrinkage of the particles in the TEM under vacuum and the high-intensity electron beam. In addition, the stearyl layer is invisible in the TEM. Thereby, the size as determined with DLS is an apparent hydrodynamic diameter and takes into account a small layer of solvent molecules around the spheres. A characteristic TEM image of SD1 can be found in figure 4.1. As can be seen, the spheres are not completely spherical. However, the spheres have been used in previous experiments and have shown to be stable for many years [37].

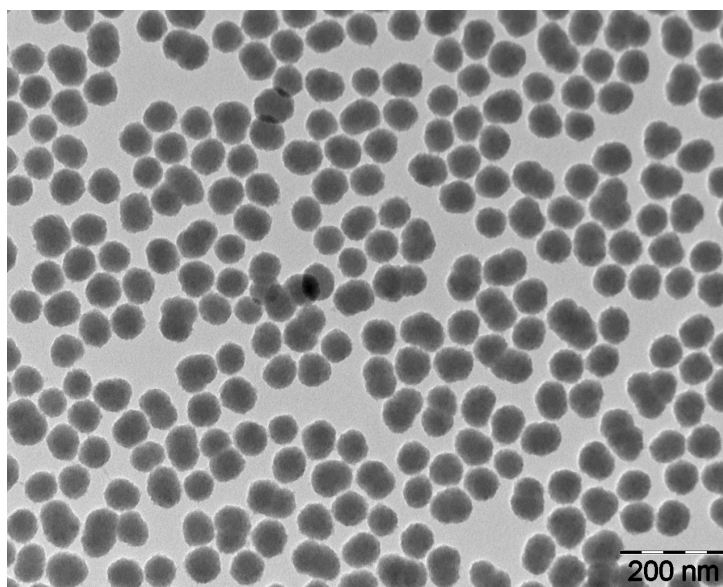


**Figure 4.1:** Typical TEM image of  $C_{18}$ -coated silica particles (SD1) with an average size of 63.7 nm. As can be seen, the spheres are not completely spherical.

The radius of gyration of PDMS, with  $M_w = 95,000$  g/mol, was determined to be 10.1 nm with NMR diffusion. However, a calculation of  $R_g$  yielded a value of 14.4 nm (refer to Appendix E) and literature on PDMS with similar molecular weight and polydispersity index reported a  $R_g$  of 14 nm [26]. Therefore, the radius of gyration of PDMS is taken to be 14 nm.

The phase diagram of SD1 and PDMS can be found in figure 4.2. The phase boundary is drawn schematically as a guide to the eye. The size ratio of the system,  $\frac{R_g}{R_c}$ , is 0.38 for which gas, liquid and solid phase transitions are predicted by theory and computer simulations (see section 2.1.2). In the phase diagram, no solid phases are depicted as these were not observed. This could be due to too large polydispersity of polymer (relative polydispersity in  $R_g$  is 31.6%; refer to Appendix E) and colloids or due to insufficient high concentration of both polymer and colloids to induce crystallization. Experiments were performed with samples containing 3V% SD1 and 0-14 mg/mL PDMS, which can be found in the one phase region of the system (i.e. below the phase boundary).

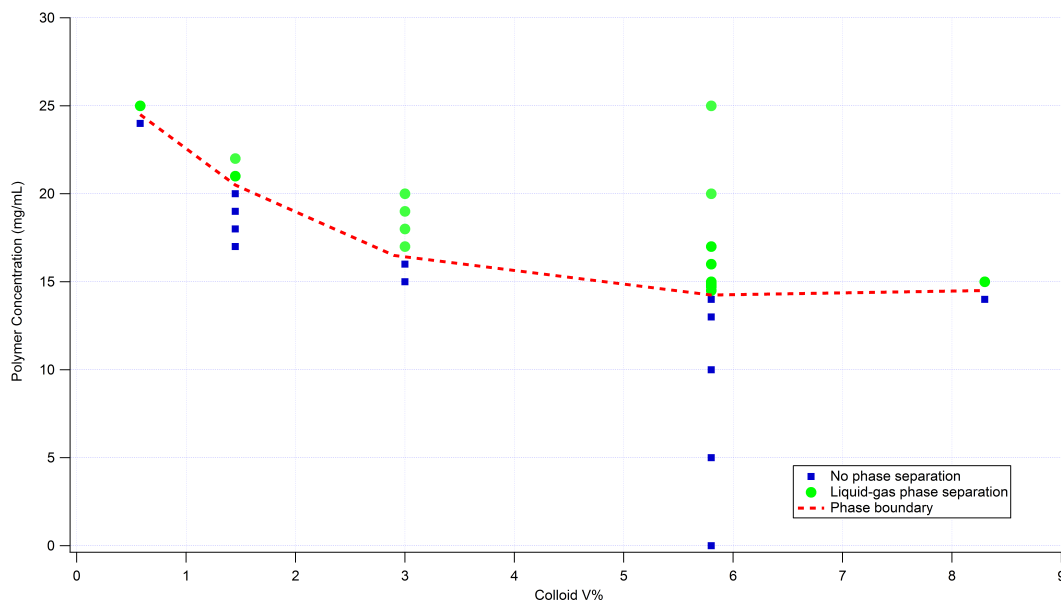


**Figure 4.2:** Experimental phase diagram of mixtures of sterically stabilized silica spheres and PDMS. The blue squares represent compositions that are not phase separated whereas the green circles correspond to compositions that give rise to liquid-gas phase separation. The dotted red line is drawn schematically as a guide to the eye and represents the phase boundary which separates the two-phase region from the one-phase region.

## 4.2 Silica Substrates

To test the model system, initially (ellipsometry) experiments were performed on hydrophobic silica surfaces modified with  $C_8$ -chains. These surfaces were made by a standardized gas-phase silanization procedure which is routinely applied at Lund University. However, the silica particles and the silica surfaces are then not made of exactly the same material. Therefore, silica surfaces modified with  $C_{18}$ -chains had to be made.

The  $C_{18}$  silica substrates were first made by hydrophobization in a solution of 1-octadecanol in TEP. However, it was found that these surfaces were not stable and that the reproducibility of experiments on surfaces made by this hydrophobization procedure proved to be difficult. This was concluded from the fact that surfaces that were stored in ethanol for some time yielded different results in ellipsometry experiments. In addition, performed ellipsometry experiments could not be reproduced within a narrow error margin even on surface from the same wafer and hydrophobized in the same solution. Possibly these effects stem from dissolution of the stearyl layer, making the surface less hydrophobic and less smooth. Furthermore, it is not unlikely that the number density of stearyl chains on the surface was much smaller than the maximal packing fraction of five chains per square nanometre [11], [39]. This could result in bare patches that are essentially still hydrophilic and that might strongly attract the hydrophobic silica spheres. A great number of experimental variations (ranging from different batches of chemicals to new glassware to different reaction times and temperatures) were applied to increase the surface quality, stability and reproducibility of the experiments. Unfortunately, none of these variations could significantly improve the surface properties, so it was decided to change the hydrophobization method.

Gas-phase silanization with dimethyloctylchlorosilane has the advantages that it yields very reproducible surfaces and, not entirely unimportant, that it is easy to apply. Equivalently, silanization with octadecyltrichlorosilane was supposed to yield stable and reproducible surfaces chemically modified with  $C_{18}$ -chains. However, the boiling point of OTS is too high to be able to perform gas-phase silanization at room temperature. Thus, liquid-phase silanization was applied instead. Even though a layer of  $C_{18}$ -chains is chemically bonded to the silica surface with this method, the bonding of the stearyl chains to the silica surface is different for silanized surfaces and esterified surfaces (see figure 4.3).

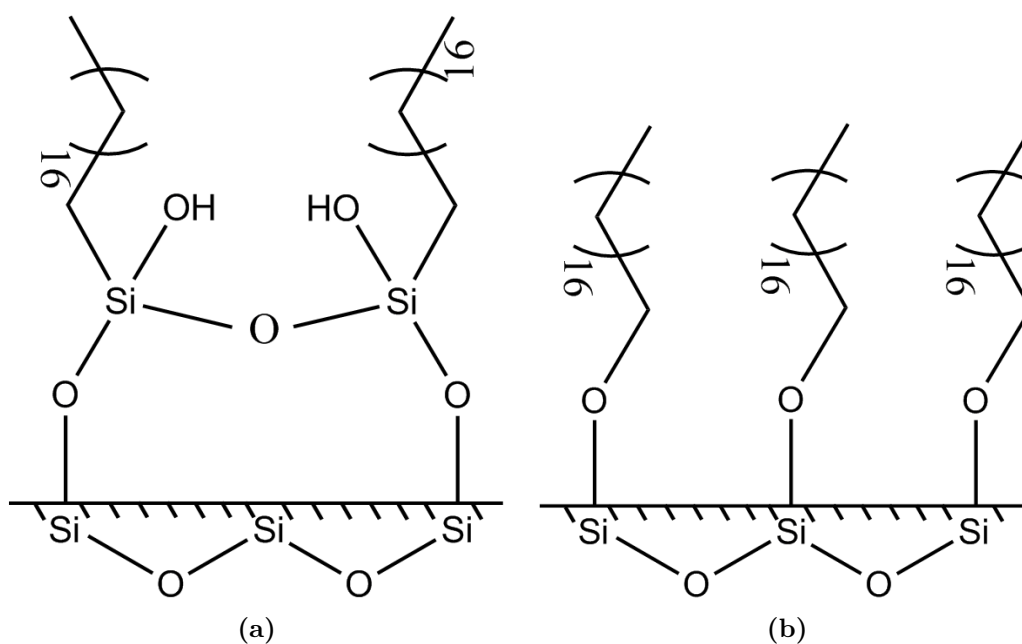


**Figure 4.3:** Chemically bonded  $C_{18}$ -chains to a silica surface arising from different hydrophobization procedures: (a) silanization and (b) esterification.

However, one could argue that the nature of the particles and surfaces differ to begin with and that they could never be exactly the same. To elaborate: the spheres consist of silica with an outer layer of C<sub>18</sub>-chains, whereas the surfaces are made up of a silicon oxide layer on top of a silicon wafer which is then chemically modified to have C<sub>18</sub>-chains on the surface. The idea was then to treat the silica spheres as particles and the silica substrates as surfaces and to decide separately what the best method of surface modification is for either one of these. The best and easiest way to modify the surface chemistry of silica substrates is by silanization, whether it be in liquid-phase or in gas-phase. Esterification of the silica spheres in a melt of stearyl alcohol is mostly applied for sterically stabilizing silica particles.

That being said, another hydrophobization method was applied, namely the esterification of the silica surface in a melt of stearyl alcohol. Even though modifying particles and surfaces in the same way does not guarantee that the particles and surfaces are exactly the same, by this method both particles and surfaces will have the same bonding of stearyl chains to their respective surfaces even though the number of stearyl chains per square nanometre might differ. The original method of coating silica particles is in a melt of 1-octadecanol under nitrogen flow and at 180-200°C. However, practical difficulties were found by applying nitrogen flow to the set-up as the solvent would completely evaporate in due time. The use of a reflux condenser was not an option as the alcohol crystallizes at lower temperatures. Furthermore, using a completely closed flask imposed the risk of building up too much pressure inside. An alternative procedure was thus applied. Instead of a nitrogen flow, of which the main purpose it is thought to be to create a flux inside the melt, a mechanical stirrer was utilized. This stirrer was placed at the top of the melt, slightly submersed into the melt, but high enough to maintain sufficient distance from the surface that was to be hydrophobized. The stirrer was set to a moderate speed of 200-250 rpm. In this way, reproducible and, as far as we could test, stable surfaces were obtained. This was concluded from the fact that surfaces could be stored for some time and still yield the same results in ellipsometry experiments. In addition, performed ellipsometry experiments could be reproduced within a narrow error margin.

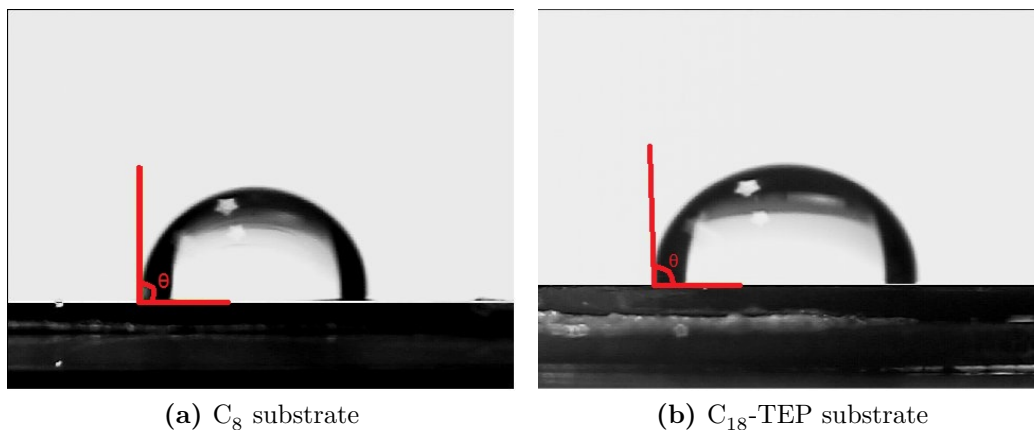
### 4.2.1 Characteristics

The silica substrates were characterized with AFM and by determining the contact angle of water on the substrates. The surface roughness could be determined with AFM and from the contact angle measurements a macroscopic property was used to give an indication of the degree of hydrophobization. Even though four different hydrophobization procedures were applied to produce hydrophobic silica substrates, the resulting substrates show similar contact angles and surface irregularities or lack thereof.

The contact angle of water on the various substrates is summarized in table 4.1. All surfaces are hydrophobic as indicated by the contact angle of water that is larger than 90°. The contact angles are quite close to each other with the exception of C<sub>18</sub>-LPS substrates that show by far the largest contact angle. Two characteristic images of a droplet of water on a hydrophobic surface are shown in figure 4.4.

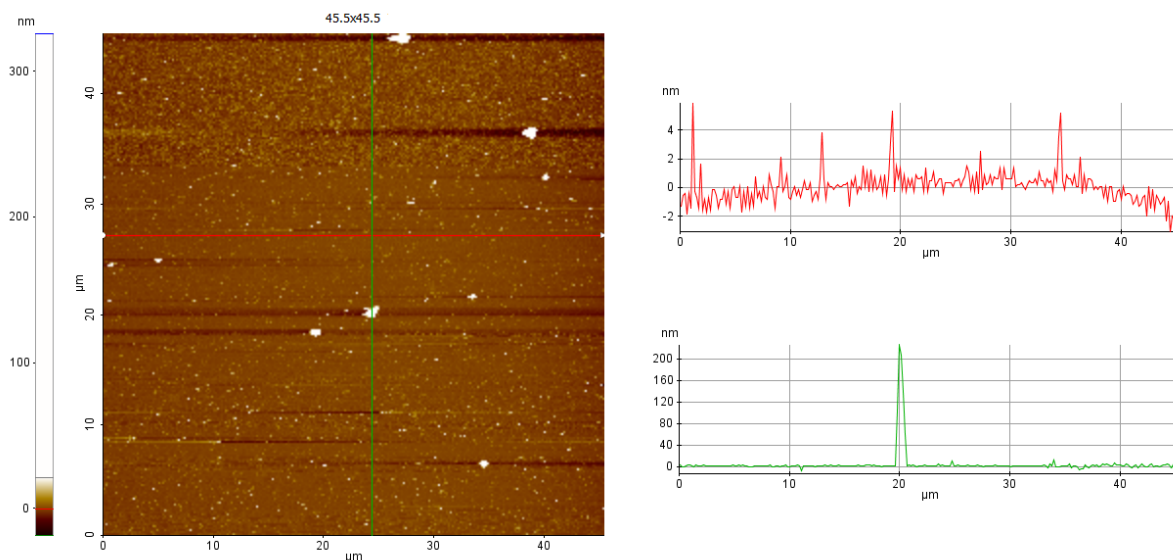
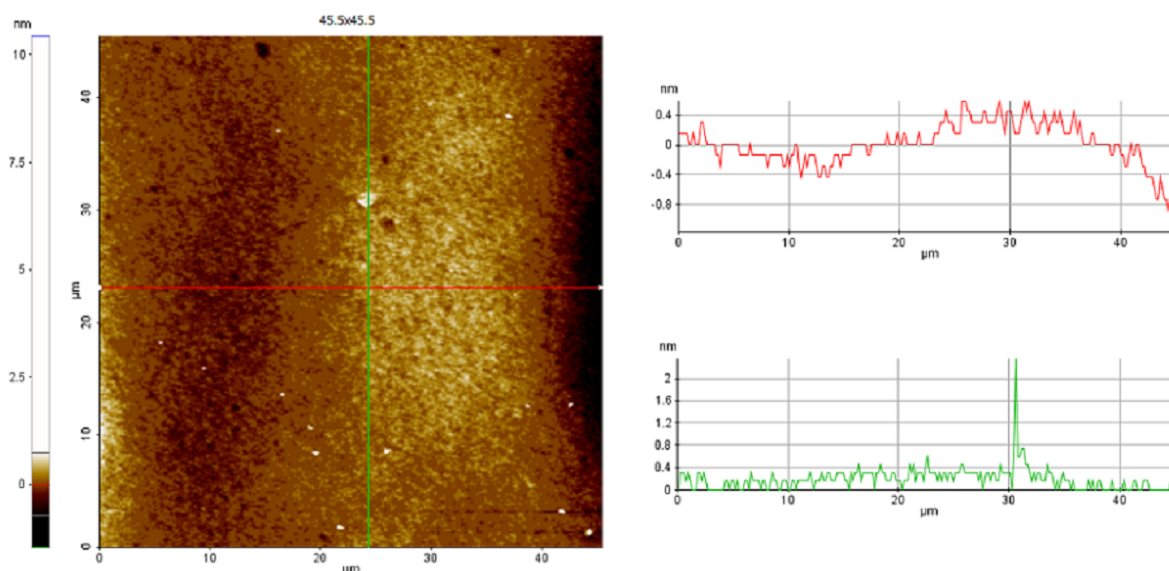
**Table 4.1:** Contact angles of water on the various substrates.

Substrate	Contact Angle
$C_8$	$90.5^\circ$
$C_{18}$ -TEP	$91.0^\circ$
$C_{18}$ -LPS	$97.0^\circ$
$C_{18}$ -Melt	$91.5^\circ$



**Figure 4.4:** (a) Water droplet on a  $C_8$  silica substrate and (b) on a  $C_{18}$ -TEP substrate. The angle  $\theta$  amounts to the contact angle of water on the surface and it has a value of  $90.5^\circ$  and  $91.0^\circ$  respectively.

Where a macroscopic property, i.e. the water contact angle, of the surfaces shows similar values for all surfaces, the surface topologies as investigated by AFM show an equally large resemblance. In figure 4.5, two characteristic AFM images of two different surfaces are shown (typically AFM images of any given prepared hydrophobic substrate look like this). These images show that the surfaces are mainly smooth with irregularities on the order of a couple of nanometres. However, here and there some very large irregularities up to 200 nm can be found. These irregularities are thought to be due to the nature of the hydrophobic surface that attracts impurities (such as dust) and not a result of the hydrophobization procedures. Therefore, the surfaces were stored in ethanol awaiting further use (to prevent the accumulation of impurities on the surfaces).

(a)  $C_8$  Silica Surface -  $45 \times 45 \mu\text{m}$ (b)  $C_{18}$ -TEP Silica Surface -  $45 \times 45 \mu\text{m}$ 

**Figure 4.5:** Characteristic AFM images of hydrophobic silica substrates. An area of  $45 \times 45 \mu\text{m}$  was imaged. (a)  $C_8$  silica surface. The surface is mainly smooth with irregularities of a couple of nanometres as can be seen along the red line. The green line profile shows that here and there irregularities up to 200 nm can be found. (b)  $C_{18}$ -TEP silica surface. The surface is mainly smooth with irregularities in the order of a nanometre.

### 4.3 Surface Adsorption

Surface adsorption was studied with ellipsometry and AFM. With ellipsometry the particle deposition was monitored *in situ* by means of the changes in the ellipsometric angles  $\Psi$  and  $\Delta$  which translate to the adsorbed amount and the thickness of the adsorbed layer. In order to obtain a closer look on the structure of the adsorbed layer, AFM was performed on the surfaces after ellipsometry experiments.

### 4.3.1 Ellipsometry

At the start of each experiment the optical properties of the silicon substrate had to be characterized in order to accurately measure the thickness and adsorbed amount of the adsorbed layer. To do this, zone measurements had to be performed in two different media. Usually, zone measurements are then performed in air and the solvent in which the measurements of the adsorbed layer are performed. However, the data calculation is based on experiments that are performed in water or ethanol, as is usually the case. Thus, it proved to be impossible to analyse the data with the available software using zone measurements in air and cyclohexane, the solvent that was used. Instead, zone measurements performed in ethanol were utilized to determine the optical properties of the substrate. When handling a hydrophobic substrate it is good practice to first introduce ethanol in the cuvette and slowly exchange it with the solvent (or buffer solution) to minimize bubble formation on the surface. We introduced first ethanol, then water, ethanol again and finally cyclohexane in the cuvette before adding the silica particles. This procedure was found to yield data that could be analysed with standard calculation software. Zone measurements were performed in every medium but only the data from air and ethanol were used to characterize the substrate. The complex refractive index of the bulk silicon substrate had a typical value of  $N_2 = 5.5 - 0.3j$  and the refractive index of the silicon oxide layer was typically in between 1.47 and 1.49. The thickness of the silica layer amounted to  $300 \pm 20 \text{ \AA}$ . These three values are sufficient to completely characterize the substrate.

A four-layer model (as discussed in detail in chapter 2) was applied to the studied system. This model is used both for hydrophilic substrates and for hydrophobic substrates. The hydrophobic layer is thin compared to the silica layer and its refractive index is expected not to differ too much from it. The optical properties as determined for the silicon oxide layer thus also take into account the hydrophobic layer.

The cuvette of the ellipsometer could not be completely closed as it did not have a lid of any kind. As a result, evaporation of cyclohexane (which is very volatile) and the subsequent concentrating of the sample were a practicality to be overcome. In order to maintain a constant sample volume and concentration a HPLC pump which could flow at extremely low flow rates was used. Every minute, a very small amount of cyclohexane was added drop wise to the cuvette to counter the volatility of the solvent and maintain similar experimental conditions throughout the measurements.

When the adsorption from the particle dispersion in the presence of PDMS was monitored, first PDMS was added to the cuvette and only until a more or less stable baseline was obtained, the dispersion would be added subsequently. This was done to avoid adding the dispersion and the polymer at the same time and to limit any other competing (kinetic) effects that could arise. Additionally, the polymer did not adsorb to the surface and as such it did not really matter if it was or was not added prior to addition of the silica spheres.

The refractive index of the measured samples and the refractive index increment of

the dispersion were needed to calculate the adsorbed amount using de Feijter's expression (see chapter two). The values of the refractive indices of ethanol, cyclohexane and samples containing 3V% SD1 and 0-14 mg/mL PDMS together with the refractive index increment at a wavelength of 4015 Å, are summarized in table 4.2.

**Table 4.2:** Refractive indices for ethanol, cyclohexane and the samples used in the ellipsometer together with the refractive index increment at a wavelength of 4015 Å, that were used to calculate the ellipsometric data. The digit after SD1 indicates the concentration of added polymer (in mg/mL).

Sample	RI
Ethanol	1.3694
Cyclohexane	1.4367
dn/dc	0.00973
SD1 0	1.4386
SD1 2	1.4383
SD1 4	1.4377
SD1 6	1.4378
SD1 8	1.4373
SD1 10	1.4375
SD1 12	1.4370
SD1 14	1.4375

A typical example of the adsorbed amount (in  $mg/m^2$ ) and thickness (in Å) that result from an ellipsometry experiment is shown in figure 4.6. The thickness and adsorbed amount are shown as a function of time. The silica dispersion is added at a time of zero seconds after which adsorption is monitored for some time. Rinsing is then started, indicated by the green arrow, by exchanging the sample completely for the solvent and measurements continue for some additional time. At the start of rinsing a spike or peak upwards can be found which is common and is an artefact of the measurements. Measurements were performed on C<sub>8</sub>- and C<sub>18</sub>-substrates (TEP, LPS and melt surfaces) of which the obtained data are discussed below.



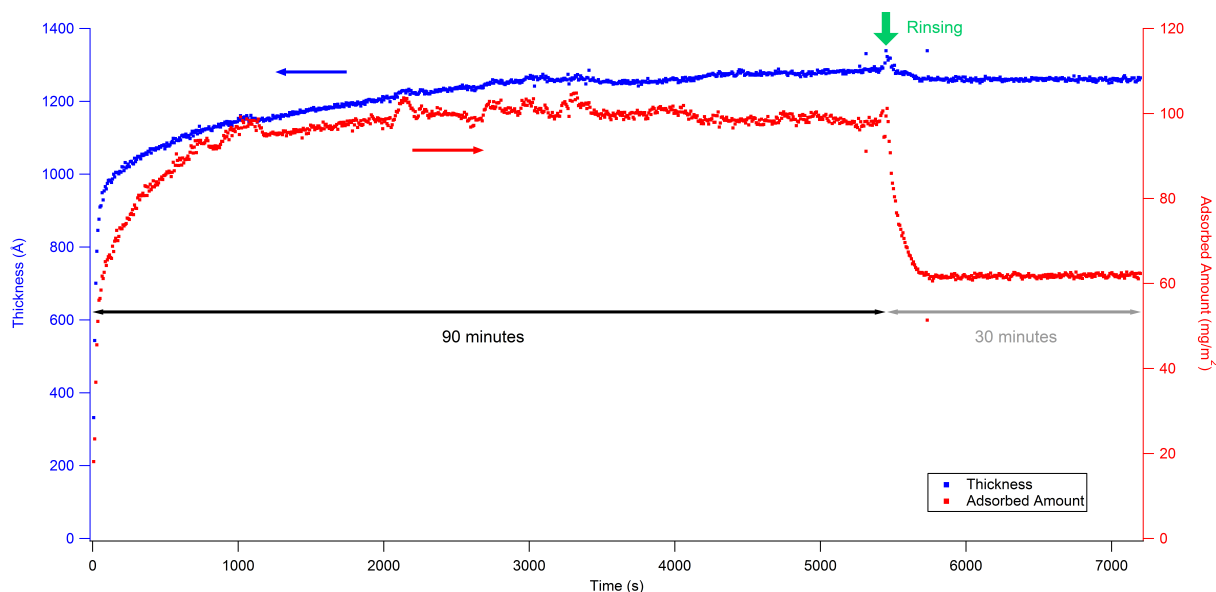


**Figure 4.6:** Typical example of ellipsometry data. Adsorption from 3V% silica dispersion in the presence of 10 mg/mL PDMS on a melt surface. The thickness and adsorbed amount are shown as a function of time. At zero seconds the silica dispersion is added. Particle deposition is then monitored for 5400 s seconds after which rinsing is started (indicated by the green arrow) and monitoring continues for an additional 1800 s seconds.

It is good to keep in mind that generally, the adsorbed amount is the value that is the most reliable from ellipsometry measurements. This is due to the fact that small changes in  $\Psi$  and  $\Delta$  could lead to large errors in thickness and refractive index. However, as the adsorbed amount contains the product of both the thickness and refractive index (it is thus often referred to as an optical thickness) and these values are covariant, the error in adsorbed amount is minimized.

### Gas-phase Silanization with Dimethyloctyltrichlorosilane

In figures 4.7 and 4.8 the thickness per particle diameter and adsorbed amount on  $C_8$  substrates of the different samples containing 3V% SD1 and 0-14 mg/mL PDMS are shown all together.

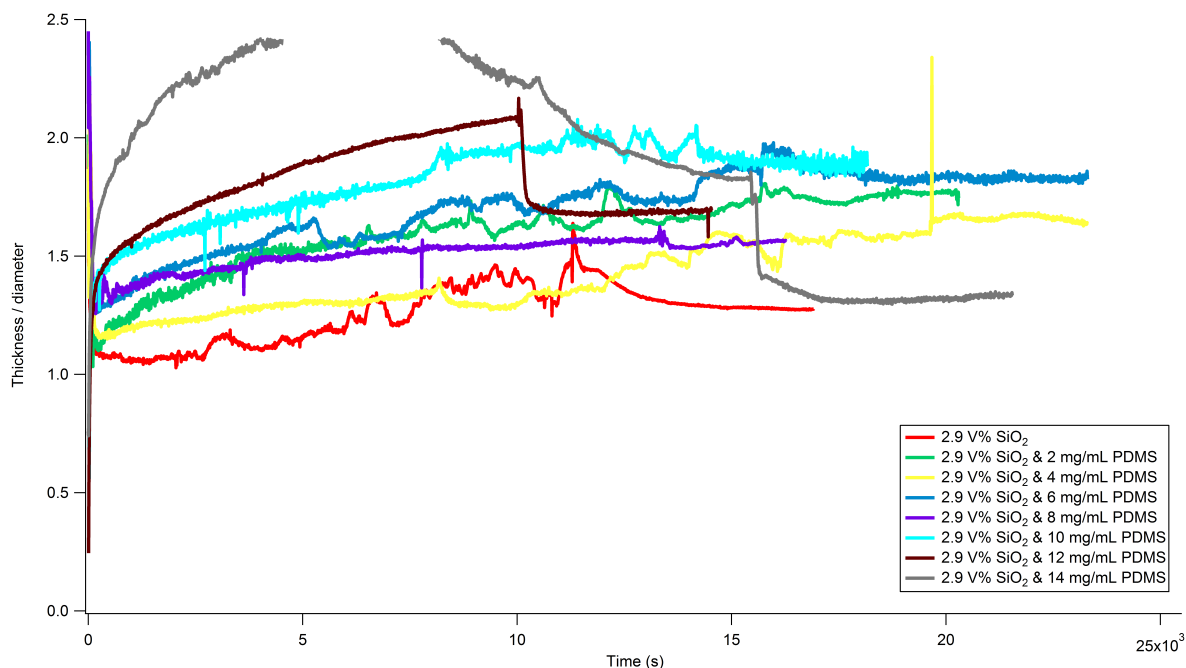
Figures 4.7 and 4.8 show individual curves that exhibit quite some fluctuations which could be a temperature or kinetic effect but of which the true cause is yet unknown. For this system, no fixed measurement time was adhered. Therefore, addition of silica spheres does occur at zero seconds but rinsing starts at a different time for each curve. Eventually, a number of curves, but not all, more or less acquire a plateau value. The missing points in the curve depicting 3V% SD1 and 14 mg/mL PDMS are due to the inability to measure the values of  $\Psi$  and  $\Delta$  due to possibly a too turbid sample and consequently a too low light intensity reaching the detector.

Figure 4.7 shows the thickness per particle diameter as a function of time. From the moment that the dispersion is added (zero seconds) up to the start of rinsing, the thickness per particle diameter lies between 1 and 1.5 for 0-8 mg/mL PDMS. At 0 mg/mL PDMS the least thick adsorbed layer appears and in the range 2-8 mg/mL PDMS a significant

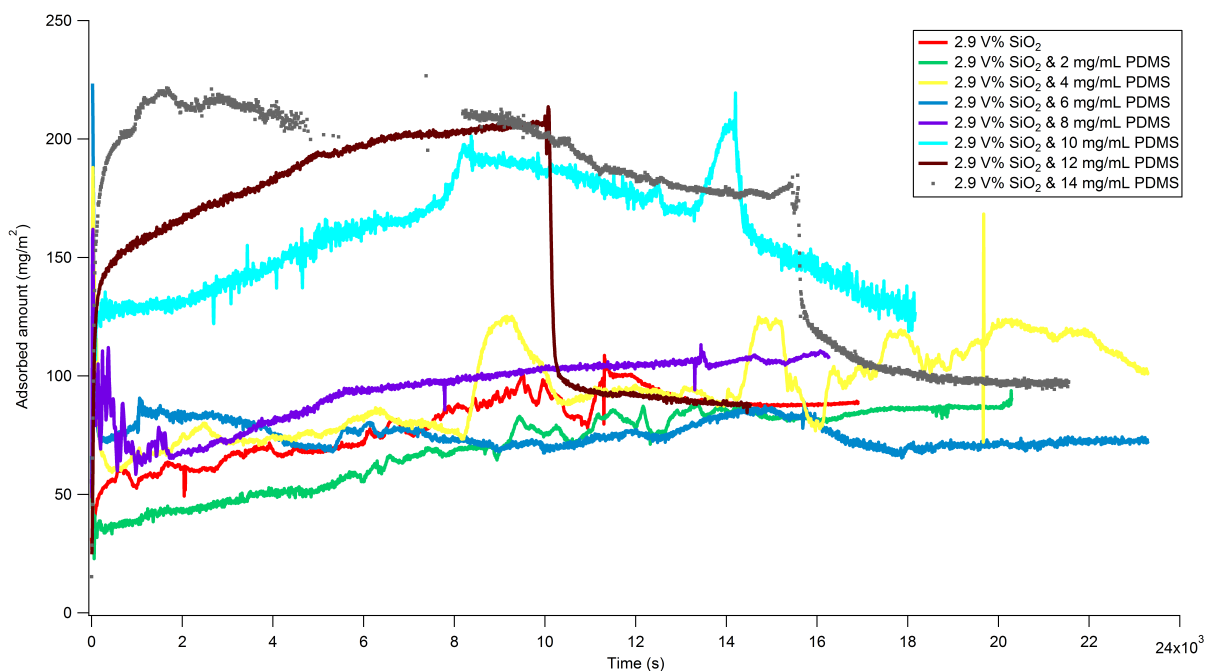
difference in this value cannot be found. However, at the addition of 10 mg/mL and more, an increasing thickness becomes apparent.

Figure 4.8 gives us the adsorbed amount in units of  $mg/m^2$ . Curves of the adsorbed amount in the range 0-8 mg/mL PDMS are quite close to each other in values and as the polymer concentration increases the adsorbed amount does not increase significantly. Upon addition of 10 mg/mL PDMS, a sudden increase in the adsorbed amount can be observed. This increase is maintained when even more polymer is added (12 and 14 mg/mL PDMS concentration).

To obtain a better overview of the thickness and adsorbed amount, these values were singled out at two specific times of 8250 seconds and at 3600 seconds after rinsing (at the end). In our opinion, most of the curves of both thickness and adsorbed amount show a more or less stable value in this region. By plotting these values versus polymer concentration one can obtain a better understanding of the influence of the depletion polymer and hence the increase in attraction between the particles in the presence of a surface. Figures 4.9 and 4.10 show that up to 8 mg/mL PDMS, the thickness and adsorbed amount vary slightly, but mainly fluctuate around a constant value; around 1.5 for the thickness per particle diameter and around  $80 mg/m^2$  for the adsorbed amount. An increase in both properties can be seen starting from the addition of 10 mg/mL PDMS and more. At the end, the curves do not show a general trend; the values of thickness and adsorbed amount are generally lower than before rinsing but that is all that can be said. At this point it might be a good reminder that we are still within the one phase region, that is, below the phase boundary.



**Figure 4.7:** Thickness normalized to particle diameter of adsorption from a 3V% silica particle dispersion and 0-14 mg/mL PDMS on  $C_8$  surfaces. Rinsing started at a different time for each experiment.



**Figure 4.8:** Adsorbed amount in  $mg/m^2$  of adsorption from a 3V% silica particle dispersion and 0-14 mg/mL PDMS on  $C_8$  surfaces. Rinsing started at a different time for each experiment.

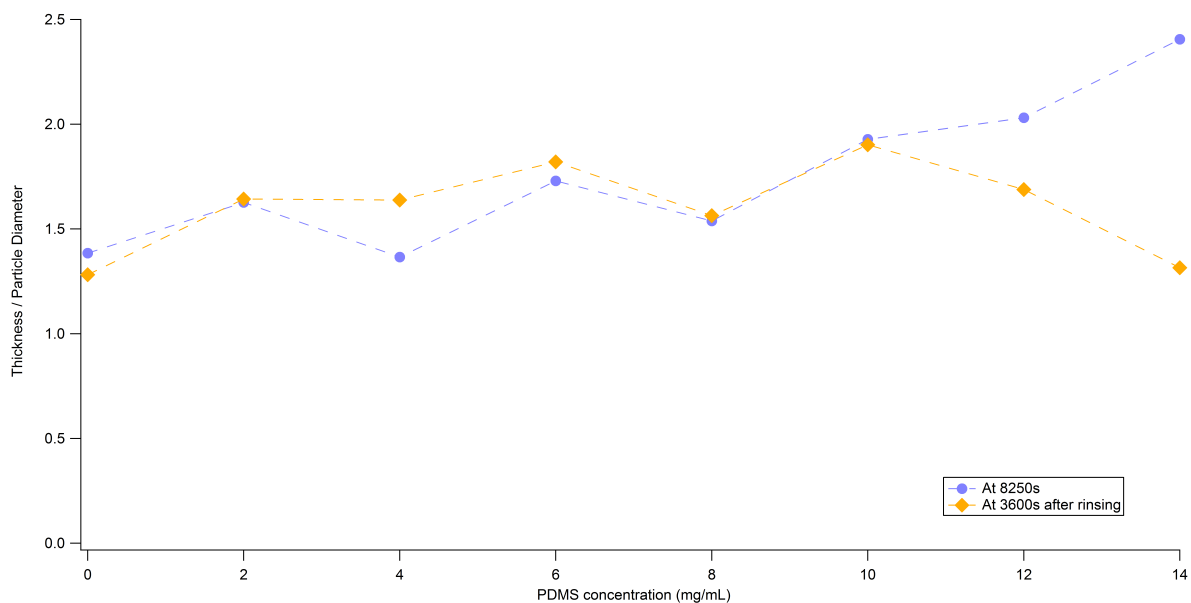


**Figure 4.9:** Thickness per particle diameter of adsorption from a 3V% silica particle dispersion and 0-14 mg/mL PDMS versus polymer concentration evaluated at 8250 seconds and at 3600 seconds after rinsing on  $C_8$  surfaces.

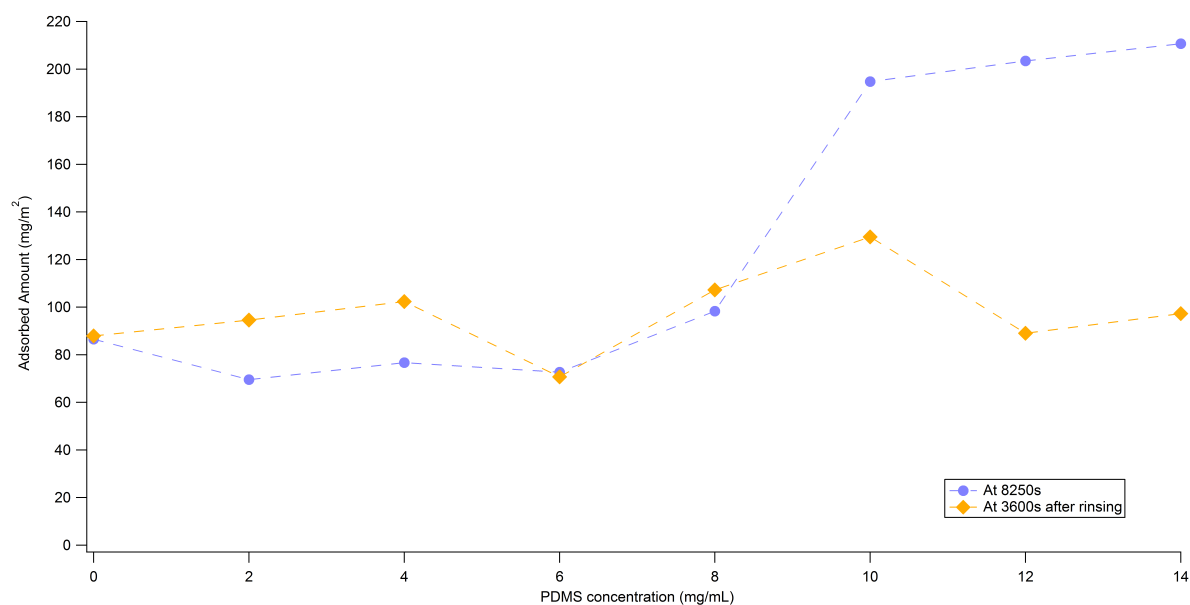


**Figure 4.10:** Adsorbed amount of adsorption from a 3V% silica particle dispersion and 0-14 mg/mL PDMS versus polymer concentration evaluated at 8250 seconds and at 3600 seconds after rinsing on  $C_8$  surfaces.

### Esterification of the Surface in a Solution of Stearyl Alcohol in Triethyl Phosphate

As discussed in section 4.2, problems were found with the reproducibility and stability of surfaces made by esterification in a solution of stearyl alcohol in TEP. Ellipsometry experiments on different batches of TEP-surfaces yielded significantly different results that could not be ascribed to the error margin. In addition, surfaces from the same batch behaved differently as well. Nevertheless, the results from the TEP-surfaces are discussed below as they represent a large part of the research performed in this work.

Figures 4.11 and 4.12 show the thickness per particle diameter and the adsorbed amount in  $mg/m^2$  versus time. For this system a fixed measurement time of 13620 seconds before rinsing and 3600 seconds after rinsing was adhered. These curves show some fluctuations but seemingly a fewer number than with the gas-phase silanized substrates. On the other hand, some fluctuations, as can be seen best in figure 4.12, extend over a long time. Again, we can only speculate about the origin of these fluctuations.

The thickness per particle diameter has a value in the range 1-1.5 for 0-8 mg/mL PDMS, similar to the  $C_8$ -surfaces. However, in this case, all curves show a thickness smaller than in the absence of depletion polymer. Again, for 10 mg/mL PDMS and higher concentrations a (sudden) increase in thickness can be observed.

The adsorbed amount, figure 4.12, shows some interesting behaviour. Upon addition of 1 mg/mL PDMS, an increase in the adsorbed amount occurs already. From 2-10 mg/mL PDMS the values of the adsorbed amount are quite close to each other, ranging from 130-160  $mg/m^2$  with a slightly higher value of 170-180  $mg/m^2$  at a PDMS concentration of 8 mg/mL. Finally, at 12 mg/mL PDMS concentration the highest value is measured. Admittedly, 14 mg/mL PDMS would most probably give an even higher value for the

adsorbed amount but again it was not possible to measure this sample for a sufficient amount of time to be able to judge this properly.

An overview of thickness per particle diameter and adsorbed amount versus PDMS concentration instead of time is given in figures 4.13 and 4.14. These curves were evaluated at 8000 seconds and 3600 seconds after the start of rinsing. Figure 4.13 shows a similar trend as was seen before in figure 4.9; a more or less stable thickness up to 10 mg/mL PDMS, at which point an increase in the value is observed. The adsorbed amount on the other hand, figure 4.14, shows a sharp increase up to 2 mg/mL PDMS after which the values remain stable up to and including 10 mg/mL PDMS, with the exception of 8 mg/mL PDMS which has a slightly higher peak value. Eventually, 12 mg/mL PDMS has the highest value and a decrease can be seen in the adsorbed amount with 14 mg/mL PDMS. By comparing the adsorbed amount and thickness we see that as the thickness remains constant for some time, the adsorbed amount increases almost constantly. This indicates that a more densely covered layer is being formed. It must be noted that these curves in particular, are extremely time-dependent. Evaluated at any other time they do not show a trend at all.

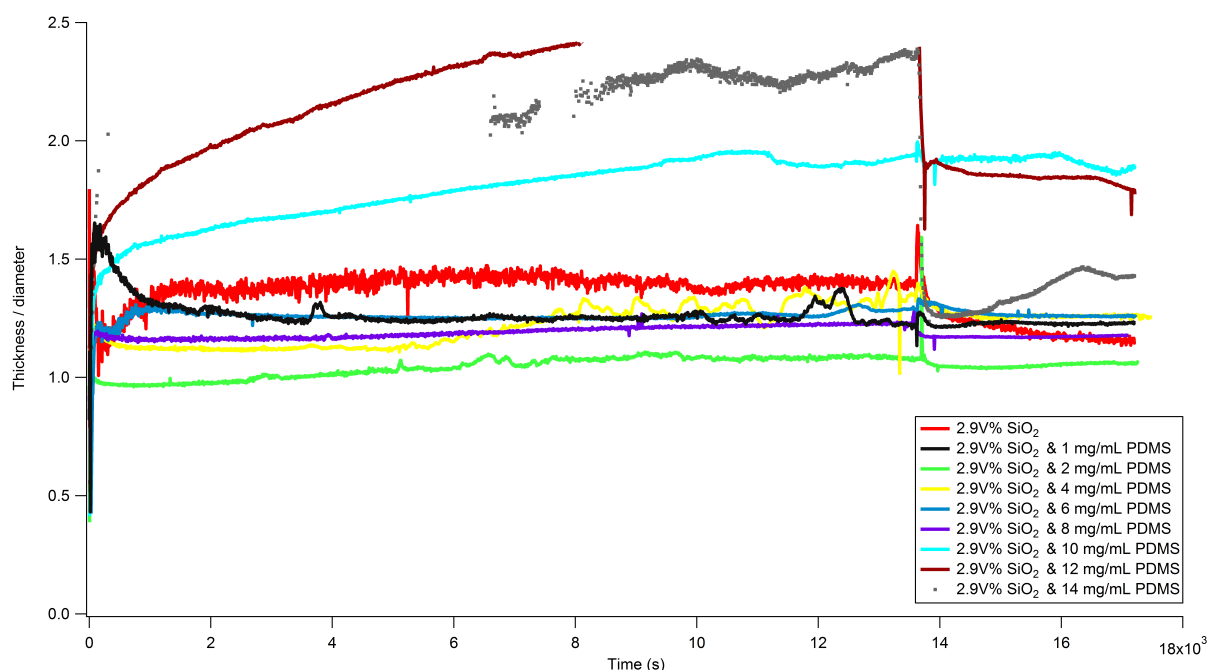


**Figure 4.11:** Thickness normalized to the particle diameter versus time of adsorption from a 3V% silica particle dispersion and 0-14 mg/mL PDMS on C<sub>18</sub>-TEP surfaces. Rinsing started at 13620s.

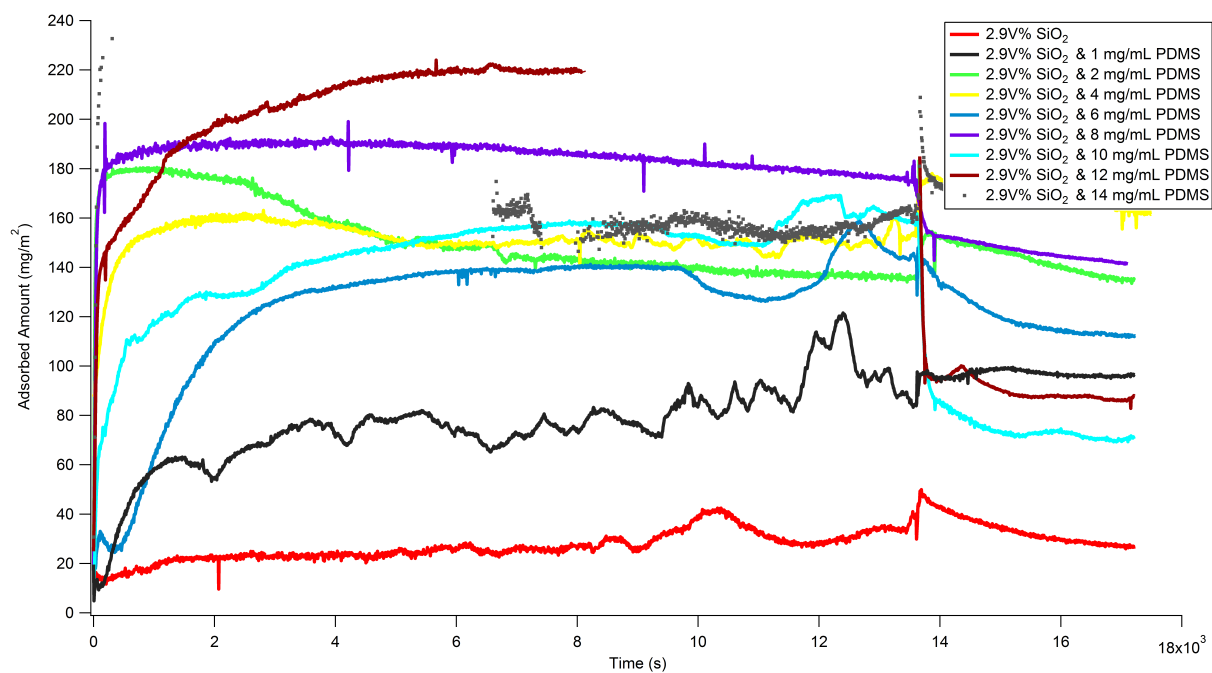


**Figure 4.12:** Adsorbed amount versus time of adsorption from a 3V% silica particle dispersion and 0-14 mg/mL PDMS on C<sub>18</sub>-TEP surfaces. Rinsing started at 13620s.

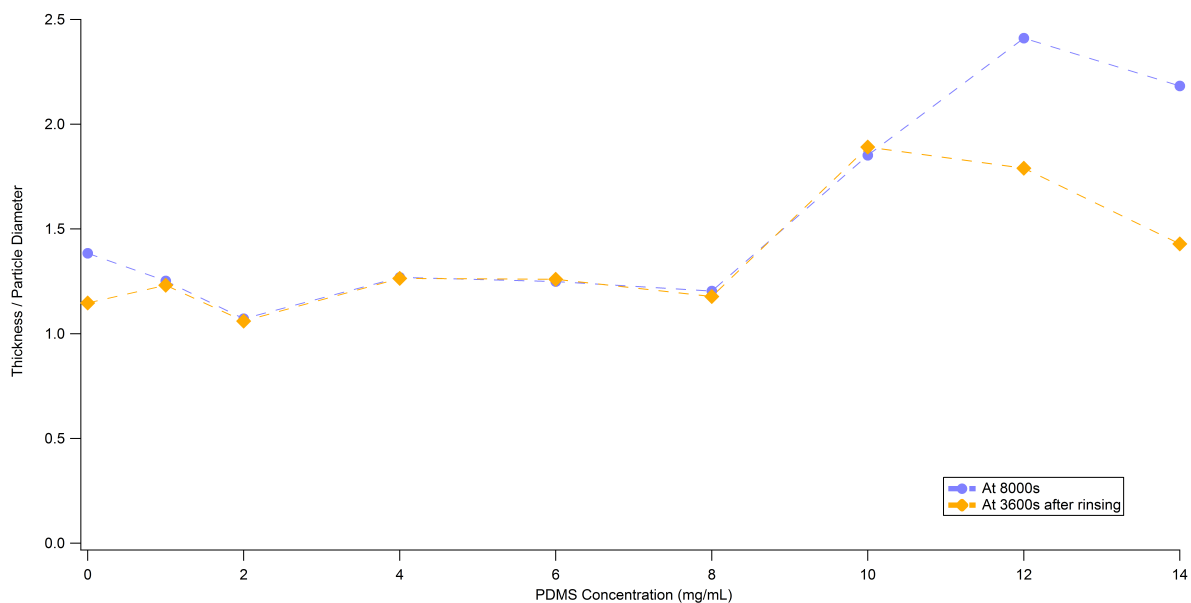


**Figure 4.13:** Thickness per particle diameter of adsorption from a 3V% silica particle dispersion and 0-14 mg/mL PDMS versus PDMS concentration evaluated at 8000s and 3600s after the start of rinsing on C<sub>18</sub>-TEP surfaces.

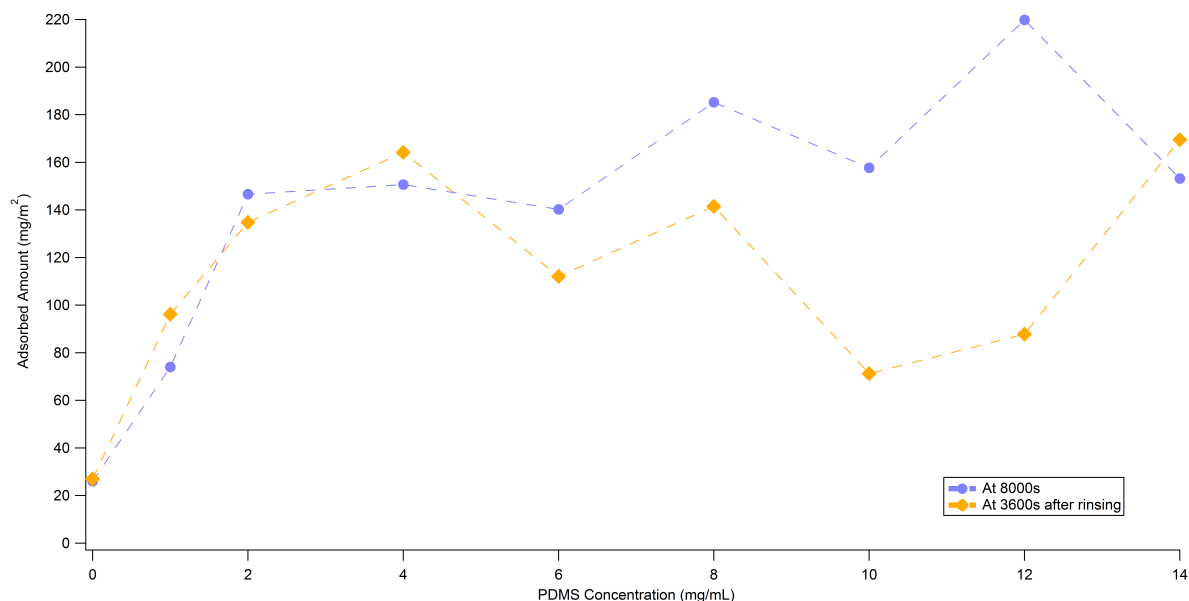


**Figure 4.14:** Adsorbed amount of adsorption from a 3V% silica particle dispersion and 0-14 mg/mL PDMS versus PDMS concentration evaluated at 8000s and 3600s after the start of rinsing on  $C_{18}$ -TEP surfaces.

### Liquid-phase Silanization with Octadecyltrichlorosilane

The thickness per particle diameter and adsorbed amount versus time on  $C_{18}$ -LPS surfaces of adsorption from a 3V% silica dispersion and 0-14 mg/mL PDMS are shown in figures 4.15 and 4.16. A fixed measurement time of 5400 seconds before and 1800 seconds after rinsing was adhered for curves with 2-12 mg/mL PDMS. The two extremes, 0 and 14 mg/mL PDMS, were measured first and with a longer time of more than 8000 seconds before rinsing and almost 3000 seconds after rinsing. Based on these first two curves it was determined not to be necessary to measure for more than 2 hours in total (as the curves achieve more or less a plateau within this time) and therefore the measurement time was decreased for the subsequent measurements. These curves do show far fewer fluctuations than have been seen up until now. Note that some points are missing from the curve depicting 10 mg/mL PDMS due to a short-time malfunction of the ellipsometer during which no angles could be measured.

Curves of the thickness per particle diameter, as depicted in figure 4.15, do show an almost continuous increase versus time that do not always reach a stable value. The reason for this is hard to pinpoint but could be due to the intrinsic larger errors in the thickness. Immediately upon addition of depletion polymer an increase in the value of the thickness can be observed. The thickness of 2-10 mg/mL PDMS lie quite close to each other whereas an increase in the thickness arises upon addition of 12 and 14 mg/mL PDMS.

The adsorbed amount on the other hand, figure 4.16, shows a consistent increase upon addition of more and more polymer. This stepwise increase can be observed over the whole range of depletion polymer concentration. In addition, the curves of the adsorbed amount do not show an endless increase versus time but in almost all cases do reach a plateau within the measurement time.

Figures 4.17 and 4.18 again give an overview of the thickness per particle diameter and the adsorbed amount versus polymer concentration instead of time in order to obtain a clearer grasp on the effect of the depletion polymer. The thickness and adsorbed amount are evaluated at three different times: twice in the measurement time before rising and once after rinsing for half an hour. From the evaluations at 3200 and 5300 seconds it can be said that they match closely. Whereas evaluations for the  $C_{18}$ -TEP or  $C_8$ -surfaces depend heavily on the chosen evaluation time, here there is not such a strong dependence; the following trends can be seen at any given time. The thickness increases upon addition of 2 mg/mL PDMS, then stays constant up to and including 10 mg/mL after which it increases once more. The adsorbed amount on the other hand, increases with every extra addition of PDMS and, going from 4 to 6 mg/mL PDMS, the largest increase can be observed. The fact that the thickness remains constant while the adsorbed amount increases indicates that a more densely packed layer is being formed. After rinsing there is, as usual, not a definite trend any more, but the values are lower than before rinsing with just a few exceptions.

In addition, figures 4.17 and 4.18 clearly show that the thickness and adsorbed amount increase upon addition of merely 2 mg/mL PDMS. This corresponds with the calculated polymer concentration needed to overcome the thermal energy (a derivation hereof can be found in chapter 5 and leads to values ranging from 1.25 to 1.73 mg/mL PDMS).

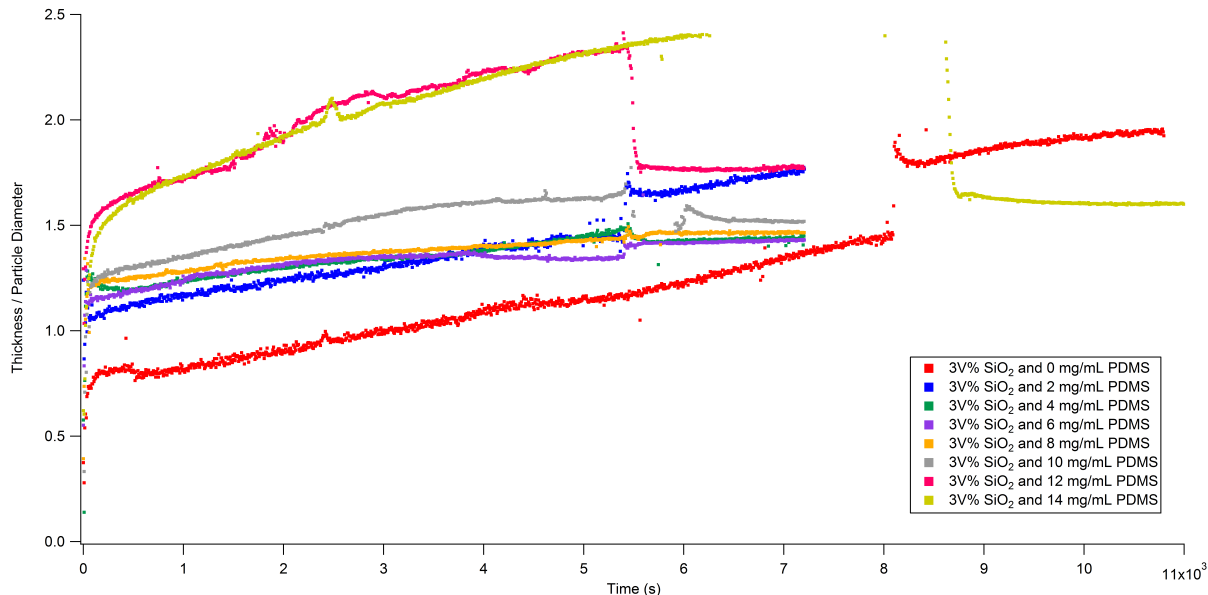


**Figure 4.15:** Thickness per particle diameter versus time of adsorption from a 3V% silica particle dispersion and 0-14 mg/mL PDMS on  $C_{18}$ -LPS surfaces. Rinsing started after 5400s of measurements for all experiments except for 0 and 14 mg/mL PDMS. Here, rinsing started respectively at 8100s and 8563s.



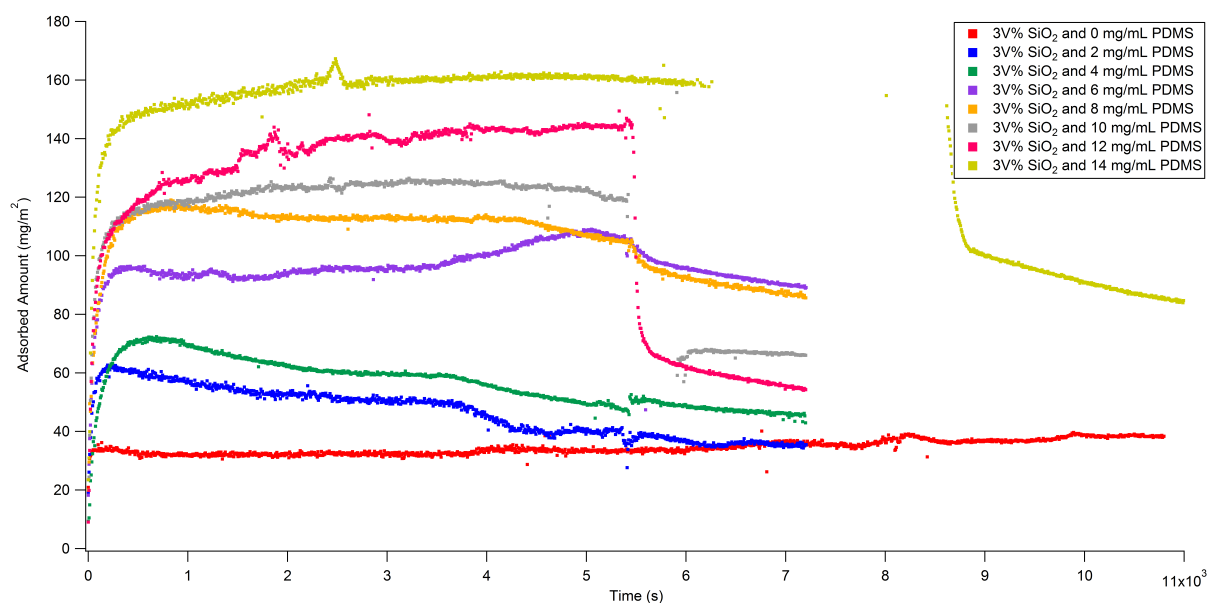


**Figure 4.16:** Adsorbed amount in  $\text{mg}/\text{m}^2$  of adsorption from a 3V% silica particle dispersion and 0-14  $\text{mg}/\text{mL}$  PDMS on  $\text{C}_{18}$ -LPS surfaces. Rinsing started after 5400s of measurements for all experiments except for 0 and 14  $\text{mg}/\text{mL}$  PDMS. Here, rinsing started respectively at 8100s and 8563s.

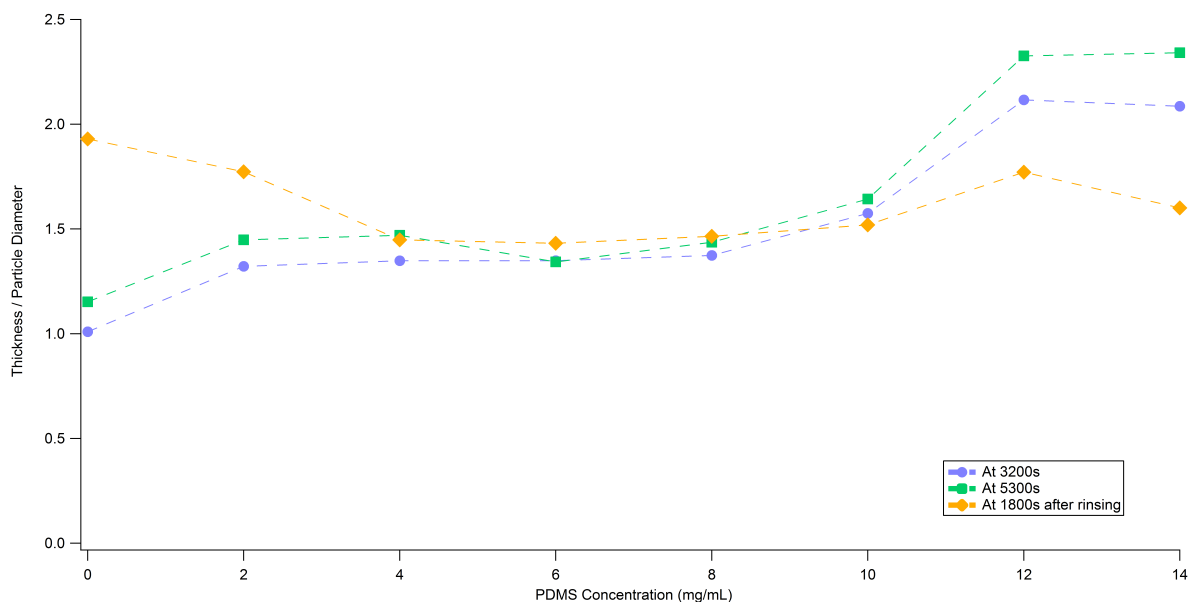


**Figure 4.17:** Thickness per particle diameter of adsorption from a 3V% silica particle dispersion and 0-14  $\text{mg}/\text{mL}$  PDMS versus PDMS concentration on  $\text{C}_{18}$ -LPS surfaces, evaluated at various times: 3200s, 5300s and 1800s after the start of rinsing. Addition of merely 2  $\text{mg}/\text{mL}$  PDMS is sufficient for the depletion interaction to overcome the thermal energy as indicated by an increase in the thickness.

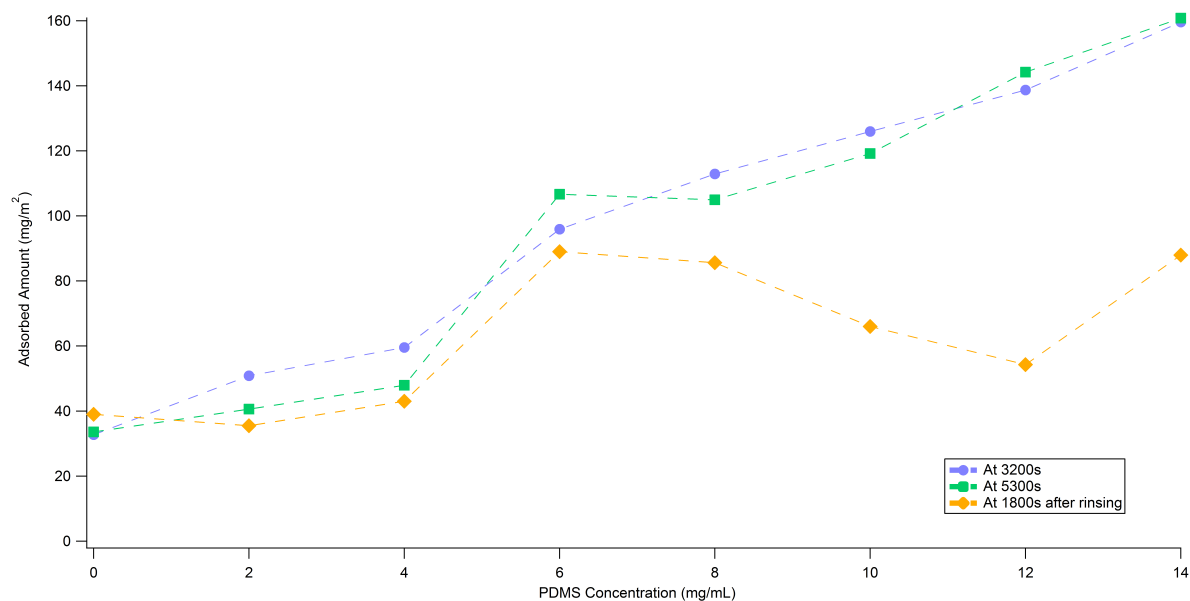


**Figure 4.18:** Adsorbed amount in  $mg/m^2$  of adsorption from a 3V% silica particle dispersion and 0-14 mg/mL PDMS versus PDMS concentration on  $C_{18}$ -LPS surfaces, evaluated at various times: 3200s, 5300s and 1800s after the start of rinsing. Addition of merely 2 mg/mL PDMS is sufficient for the depletion interaction to overcome the thermal energy as indicated by an increase in the adsorbed amount.

### Esterification of the Surface in Melt of Stearyl Alcohol

Last but not least, the ellipsometry results of the thickness per particle diameter and adsorbed amount versus time of adsorption from a 3V% silica dispersion and 0-14 mg/mL PDMS on  $C_{18}$ -Melt surfaces are shown in figures 4.19 and 4.20. As with the experiments on  $C_{18}$ -LPS surfaces, a fixed measurement time of 5400 seconds before and 1800 seconds after rinsing was adhered for curves with 2-12 mg/mL PDMS. The two extremes, 0 mg/mL and 14 mg/mL PDMS, were measured first and with a longer time of more than 8000 seconds before rinsing and almost 3000 seconds after rinsing. Based on these first two curves it was determined not to be necessary to measure for more than 2 hours in total (as the curves achieve more or less a plateau within this time) and therefore the measurement time was decreased for the subsequent measurements. These curves are similar to those discussed above, namely the  $C_{18}$ -LPS surfaces. These curves show much less fluctuations in comparison with the  $C_{18}$ -TEP and  $C_8$  surfaces and in most cases a plateau values is obtained. Another similarity with the  $C_{18}$ -LPS surfaces can be found in the fact that the thickness displays a continuous increase in the values versus time which rarely stabilizes. Again, only speculations can be made on the cause of this. Then again, the adsorbed amount does reach stable values and even maintains these in most cases.

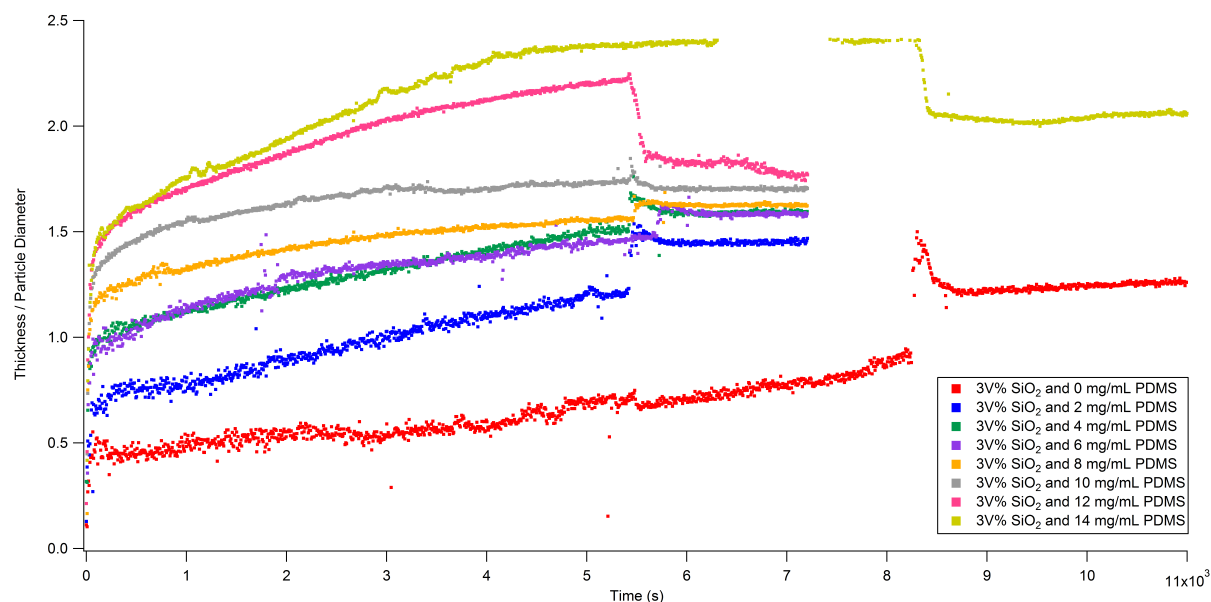
The thickness per particle diameter, figure 4.19, shows an immediate increase upon addition of 2 mg/mL PDMS. Upon a higher concentration of PDMS, the thickness keeps increasing. However, the values of the thickness of 4 and 6 mg/mL PDMS almost overlap over the whole time range.

Figure 4.20 shows that the curves of the adsorbed amount increase with increasing

polymer concentration. The values of the adsorbed amount of 2 and 4 mg/mL PDMS correspond greatly whereas every extra addition of polymer results in an increased adsorbed amount on the surface. The steps in the increase also seem to become larger when going to higher PDMS concentrations. At the end, after rinsing, all curves seem to have obtained equilibrium indicated by the stable values.

The thickness after rinsing is not always lower than before as can be seen clearly in figure 4.21 and any signs of a trend cannot really be observed either. For the adsorbed amount, the values after rinsing are lower than before as depicted in figure 4.22. Both these figures show in addition the values of these two properties at two additional times: 3200 and 5300 seconds. As was mentioned before, here the evaluation is not time dependent as both times show a similar trend. A relatively slow increase can be observed in the adsorbed amount at lower PDMS concentration whereas the rate of the increase rapidly rises from 6 to 12 mg/mL PDMS after which it decreases again. The thickness shows a fast increase up to 4 mg/mL PDMS after which a more or less stable value is maintained from 4 to 10 mg/mL PDMS, until finally an increase is detected again.

Moreover, figures 4.21 and 4.22 show (similarly to figures 4.17 and 4.18) that addition of 2 mg/mL PDMS is sufficient for the depletion interaction to overcome the thermal energy which corresponds well with performed calculations (refer to chapter 5).



**Figure 4.19:** Thickness per particle diameter versus time of adsorption from a 3V% silica particle dispersion and 0-14 mg/mL PDMS on C<sub>18</sub>-Melt surfaces. Rinsing started after 5400s of measurements for all experiments except for 0 and 14 mg/mL PDMS. Here, rinsing started respectively at 8264s and 8325s.

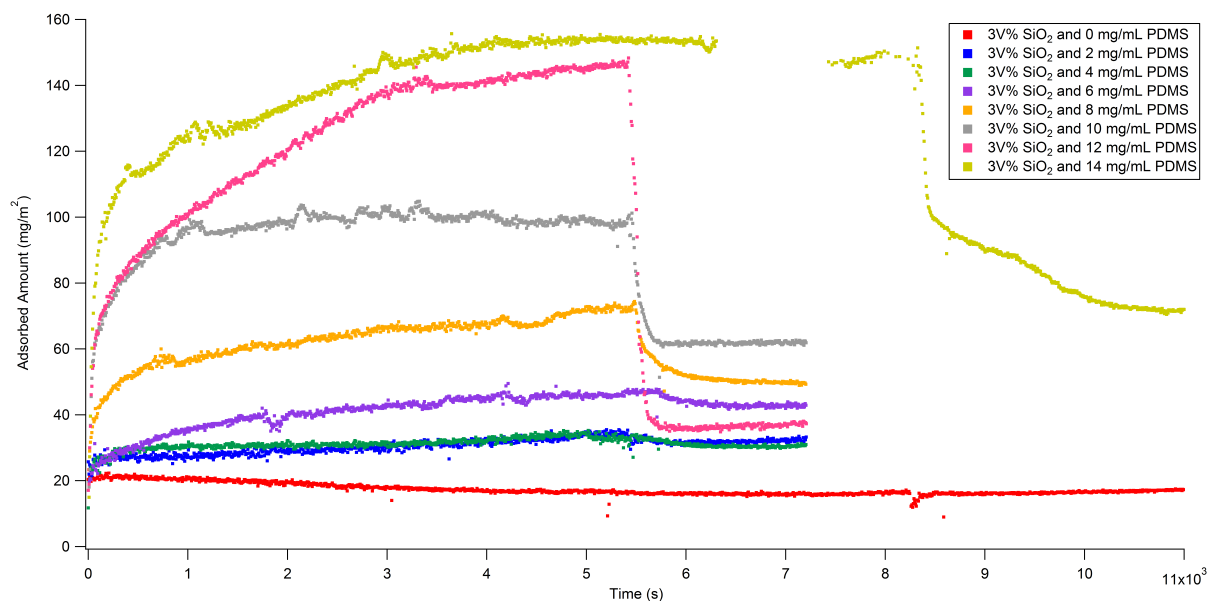


**Figure 4.20:** Adsorbed amount versus time of adsorption from a 3V% silica particle dispersion and 0-14 mg/mL PDMS on  $C_{18}$ -Melt surfaces. Rinsing started after 5400s of measurements for all experiments except for 0 and 14 mg/mL PDMS. Here, rinsing started respectively at 8264s and 8325s.

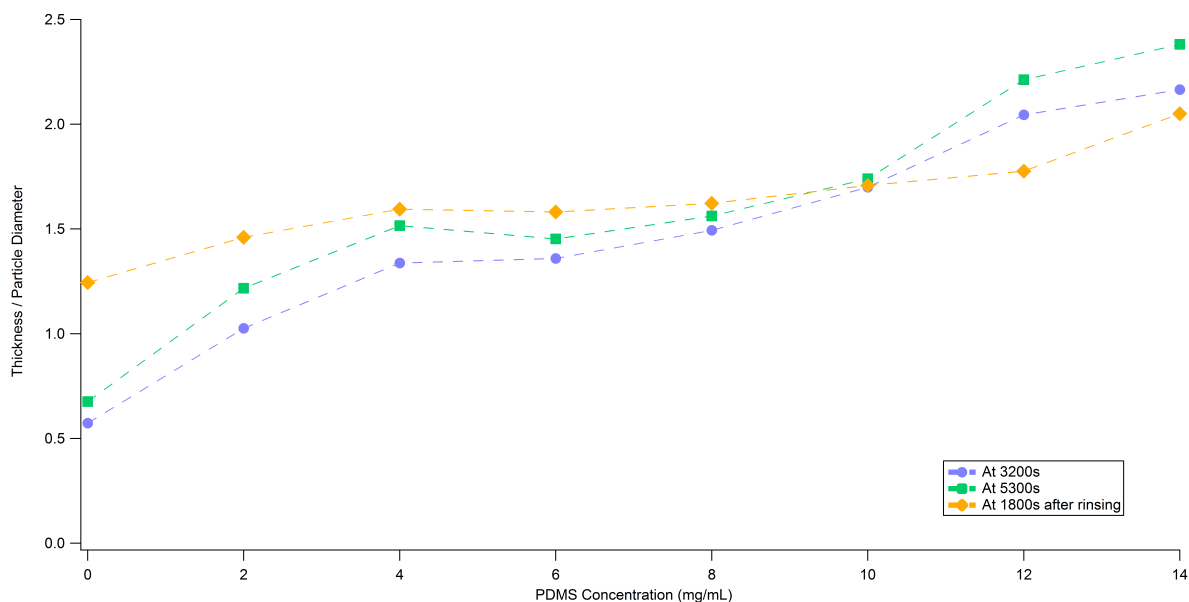


**Figure 4.21:** Thickness per particle diameter of adsorption from a 3V% silica particle dispersion and 0-14 mg/mL PDMS versus PDMS concentration on  $C_{18}$ -Melt surfaces, evaluated at various times: 3200s, 5300s and 1800s after the start of rinsing. Addition of merely 2 mg/mL PDMS is sufficient for the depletion interaction to overcome the thermal energy as indicated by an increase in the thickness.

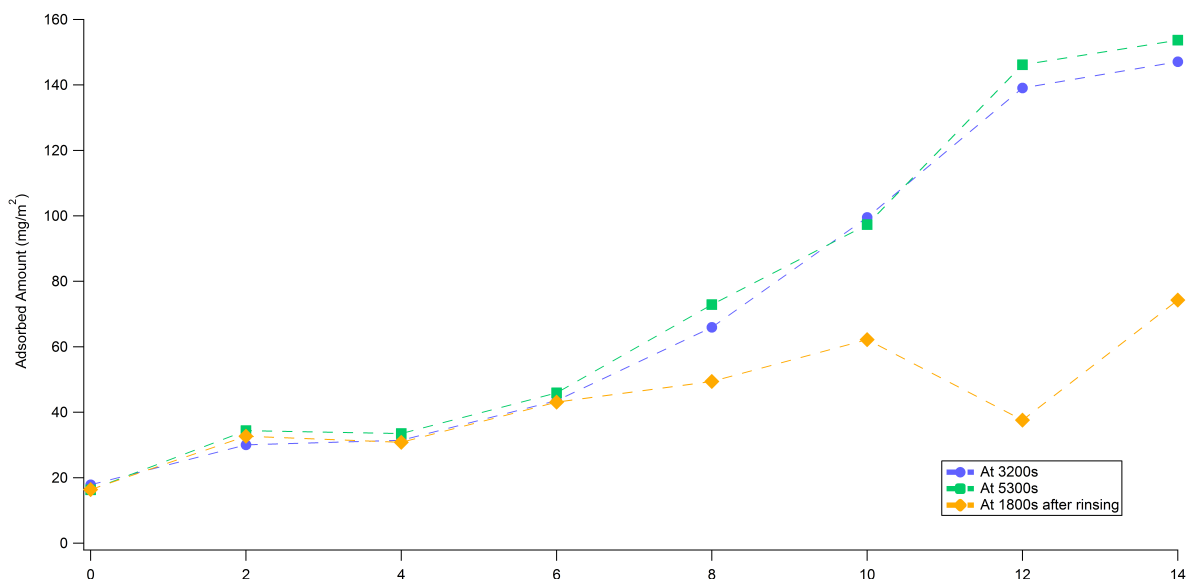


**Figure 4.22:** Adsorbed amount of adsorption from a 3V% silica particle dispersion and 0-14 mg/mL PDMS versus PDMS concentration on  $C_{18}$ -Melt surfaces, evaluated at various times: 3200s, 5300s and 1800s after the start of rinsing. Addition of merely 2 mg/mL PDMS is sufficient for the depletion interaction to overcome the thermal energy as indicated by an increase in the adsorbed amount.

### Comparison of Melt and LPS surfaces

To conclude this section, an overview is given with the results of single-wavelength ellipsometry experiments on  $C_{18}$ -Melt and  $C_{18}$ -LPS surfaces. As discussed above, these surfaces show quite some similarities and as explained in section 4.2 the  $C_{18}$ -LPS and  $C_{18}$ -Melt substrates are of the best quality. Thus, the thickness per particle diameter and adsorbed amount at 3200 seconds on both  $C_{18}$ -Melt and  $C_{18}$ -LPS surfaces are plotted versus PDMS concentration in figures 4.23 and 4.24 respectively. In addition, the evaluations of these values at 5300 seconds are depicted in figures 4.25 and 4.26. All four figures show that the  $C_{18}$ -LPS and  $C_{18}$ -Melt surfaces correspond well in the adsorbed amount and thickness of the surface layer. An increase in both values upon increasing polymer concentrations is also apparent for both systems. Between 0 and 2 mg/mL a turning point is observed where the depletion interaction overcomes the thermal energy and adsorption increases (refer to chapter 5). Generally speaking it can be said that both systems follow the same trends. Interesting differences can be found in the adsorbed amount (figures 4.25 and 4.26). Typically, the adsorbed amount on  $C_{18}$ -LPS surfaces is higher than that on  $C_{18}$ -Melt surfaces for the same PDMS concentration. This is most notably apparent for 6 and 8 mg/mL PDMS concentrations. In addition, it is striking that the adsorbed amount in the absence of depletion polymer (incidentally, the same holds for the thickness) is lower on  $C_{18}$ -Melt surfaces than on  $C_{18}$ -LPS surfaces. Aside from the fact that simulations of Linse and Wennerström [1] predict no adsorption in the absence of increasing attraction between the particles, i.e. in the absence of depletion polymer, we find different values of adsorbed amount depending on the surfaces (this applies by the way to all studied surfaces:  $C_8$ ,  $C_{18}$ -TEP,  $C_{18}$ -Melt and  $C_{18}$ -LPS surfaces). In chapter 5 we will discuss in detail how it is possible that surface adsorption occurs in the absence of

depletion polymer. At the moment it might suffice to say that it is related to the chemical nature of the surfaces, see e.g. figure 4.3, which in turn affects the interactions between particles and surfaces (e.g. Van der Waals interactions).

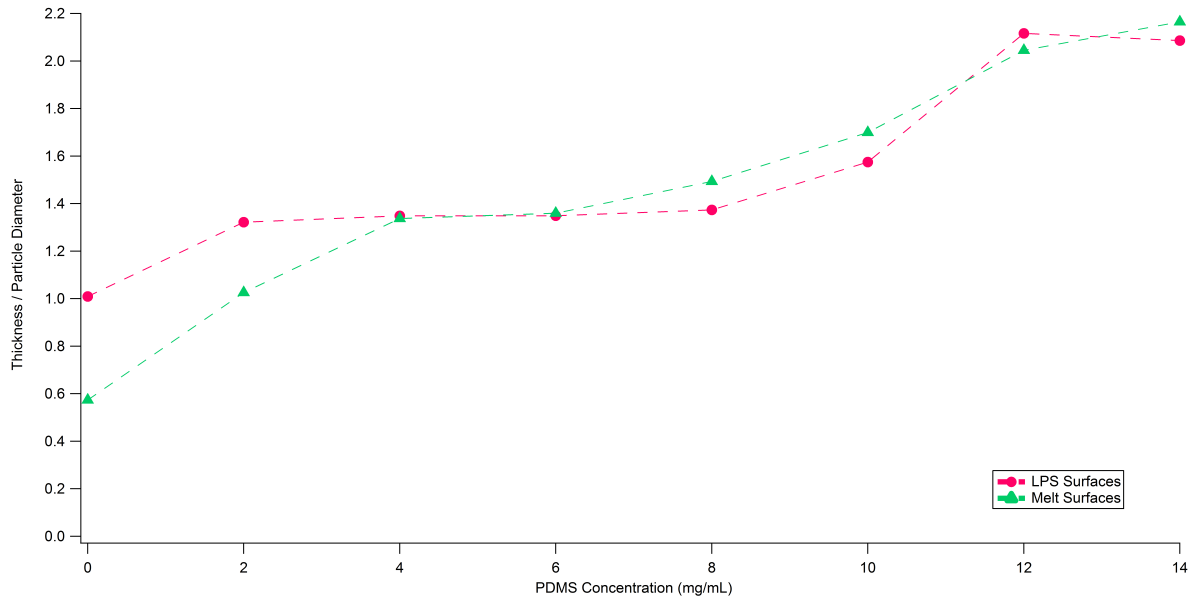


**Figure 4.23:** Thickness per particle diameter of adsorption from a 3V% silica particle dispersion and 0-14 mg/mL PDMS on LPS and Melt surfaces evaluated at 3200s.

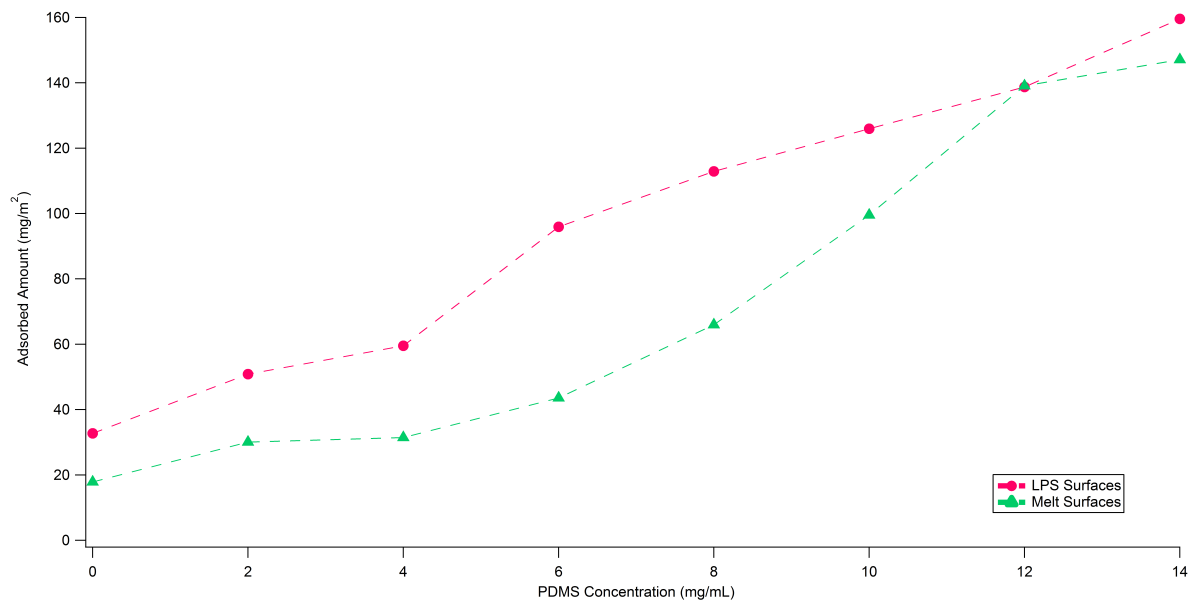


**Figure 4.24:** Adsorbed amount of adsorption from a 3V% silica particle dispersion and 0-14 mg/mL PDMS on LPS and Melt surfaces evaluated at 3200s.

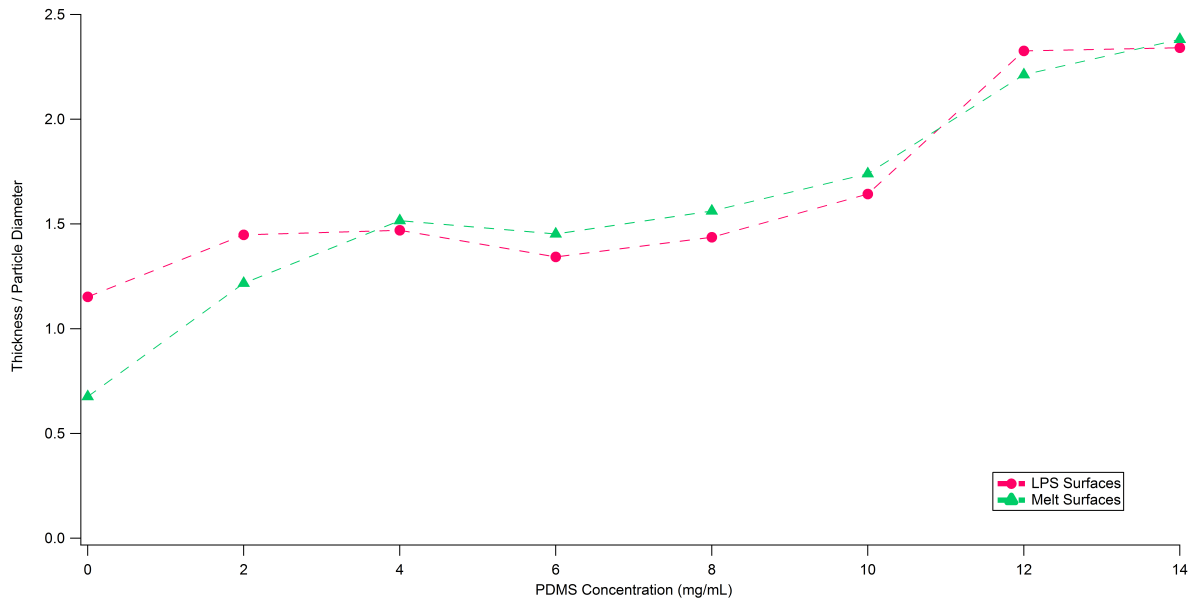


**Figure 4.25:** Thickness per particle diameter of adsorption from a 3V% silica particle dispersion and 0-14 mg/mL PDMS on LPS and Melt surfaces evaluated at 5300s.

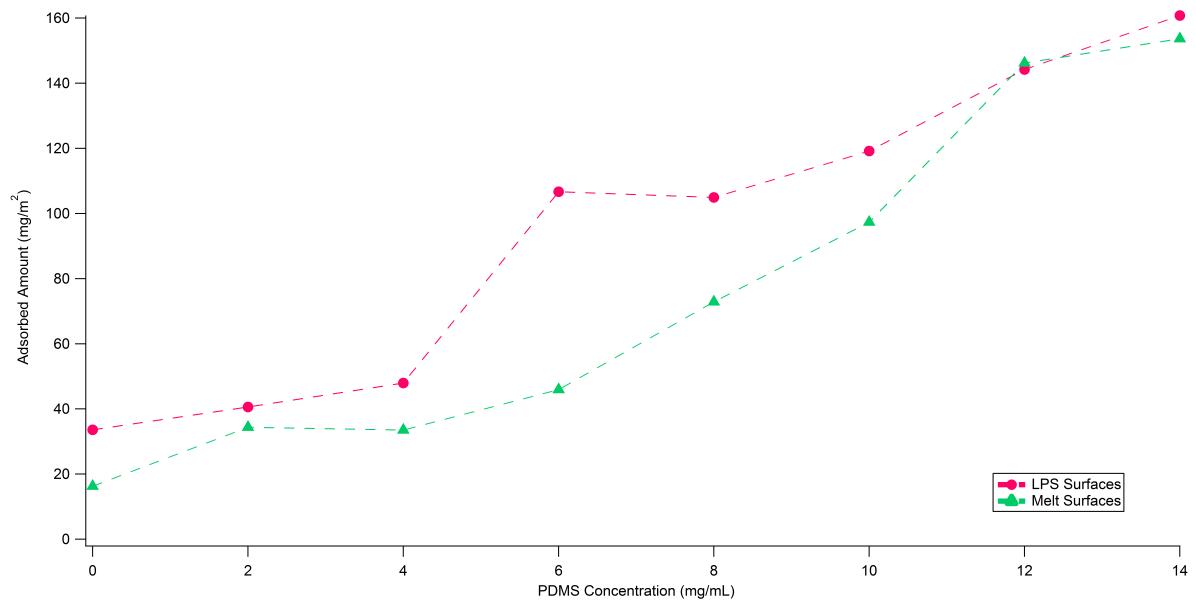


**Figure 4.26:** Adsorbed amount of adsorption from a 3V% silica particle dispersion and 0-14 mg/mL PDMS on LPS and Melt surfaces evaluated at 5300s.

### 4.3.2 The Structure of the Layer

The  $C_{18}$  silica substrates (TEP, Melt and LPS) on which ellipsometry was performed, as discussed in section 4.3.1, were investigated afterwards with AFM in order to observe the structure of the adsorbed layer. AFM was utilized as a means of confirming the results from the ellipsometer and in addition, we were curious to find out if the effect of the depletion polymer could be seen with AFM as with ellipsometry. It must be taken into account that the effects of drying cannot be predicted and can have a large influence. For example, while taking the surface out of the solvent (after rinsing), additional spheres could have been deposited on the surface (a process known as convective assembly). The eventual obtained dry substrate with silica spheres might not be the same as the substrate in dispersion as was measured with ellipsometry in terms of the adsorbed amount (and of course thickness) and spatial arrangement.

#### TEP Substrates

AFM images of adsorption from a 3V% silica particle dispersion in the presence of 0 and 6 mg/mL PDMS on  $C_{18}$ -TEP surfaces can be found in figure 4.27. Figure 4.27b and 4.27d show a zoom in of 4.27a and 4.27c respectively where the separate silica spheres can be distinguished. Figure 4.27a is imaged over a large area of  $45 \times 45 \mu\text{m}$  and shows areas covered with patches of spheres next to bare surface area. At a higher concentration of polymer, figure 4.27c, we observe that the surface is more densely covered with particles and that the bare surface area has decreased significantly. This is not only in accordance with the fact that a larger concentration of depletion polymer drives more particles to the surface but also with the values measured with ellipsometry. The adsorbed amount in the absence of polymer is only 30 mg/mL whereas in the presence of 6 mg/mL PDMS it corresponds to a much higher value of  $\approx 110$  mg/mL.

#### LPS Substrates

AFM images of  $C_{18}$ -LPS substrates are shown of adsorption from a 3V% silica particle dispersion in the absence of PDMS and upon addition of 8 mg/mL PDMS in figure 4.28. In the absence of depletion polymer (figure 4.28a), the imaged surface area shows regions that are completely free from silica particles. Places that are covered with particles have either one or multiple layers of spheres on top of each other on the surface as can be seen clearly in figure 4.28b. At higher concentrations of polymer the surface seems less covered with particles. Figure 4.28c, for example, gives a pattern-like adsorption on the surface. A closer look on parts of this pattern, as in figure 4.28d, reveals that the particles are arranged in complete disorder while completely filling a small surface area. This is a specific phenomenon that is found on all  $C_{18}$ -LPS surfaces with adsorption from a particle dispersion with a high concentration of PDMS. There is not a straightforward explanation for this. The only thing that must not be forgotten is the fact that the  $C_{18}$ -LPS surfaces are by far the most hydrophobic as shown for instance by their water contact angle (see table 4.1). The consequence of this might be that drying (or other unknown) effects are more prone to occur.



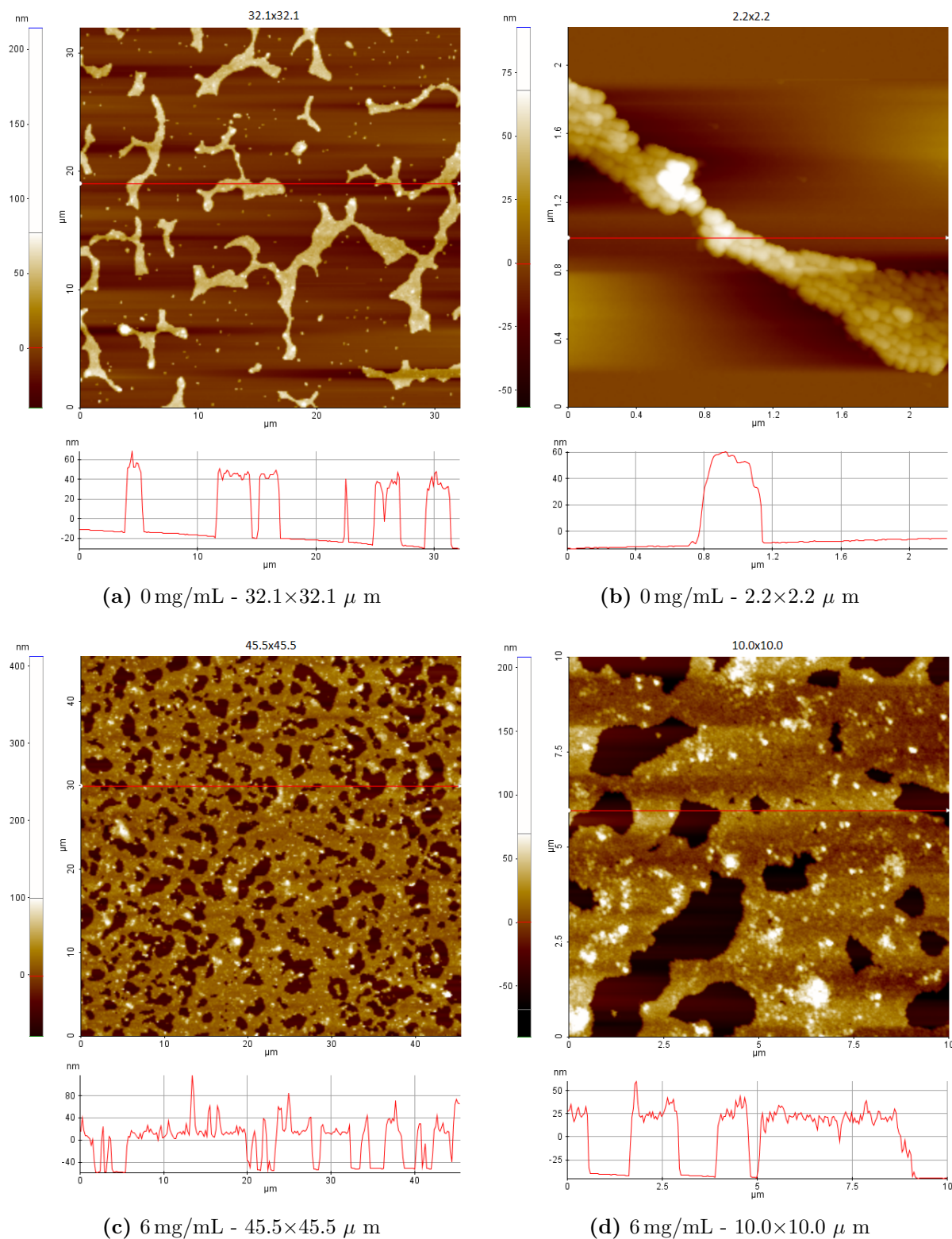


**Figure 4.27:** (a,b) AFM images of adsorption from a 3V% silica particle dispersion in the absence of depletion polymer on  $C_{18}$ -TEP surfaces. (b) is a zoomed in image of (a). (c,d) AFM images of adsorption in the presence of 6 mg/mL PDMS on  $C_{18}$ -TEP surfaces. (d) is a zoomed in image of (c). The area that was scanned to obtain the image is depicted under each figure. The graph under each topography image corresponds with the line profile of the red line that is drawn through the image.

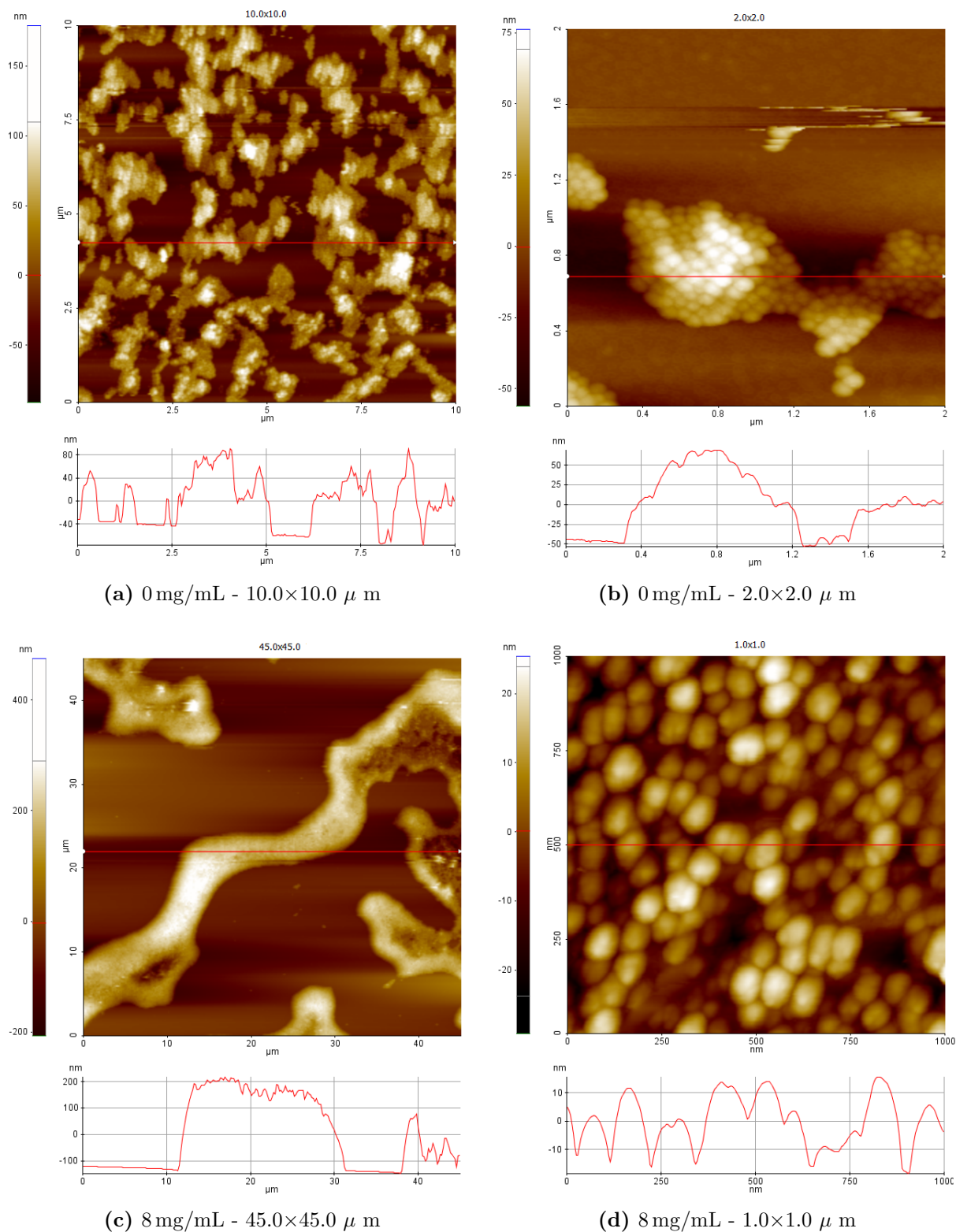


**Figure 4.28:** (a,b) AFM images of adsorption from a 3V% silica particle dispersion in the absence of depletion polymer on  $C_{18}$ -LPS surfaces. (b) is a zoomed in image of (a). (c,d) AFM images of adsorption in the presence of 8 mg/mL PDMS on  $C_{18}$ -LPS surfaces. (d) is a zoomed in image of (c). The area that was scanned to obtain the image is depicted under each figure. The graph under each topography image corresponds with the line profile of the red line that is drawn through the image.

## Melt Substrates

AFM images of  $C_{18}$ -Melt substrates are shown of adsorption from a 3V% silica particle dispersion in the presence of 4 mg/mL PDMS and upon addition of 8 mg/mL PDMS in figure 4.29. On an equal surface area, there are more particles adsorbed on the  $C_{18}$ -Melt surface in the case of adsorption in the presence of 8 mg/mL PDMS than in the presence of 4 mg/mL PDMS concentration. In addition, this corresponds well with the measured ellipsometry values. Where 4 mg/mL PDMS yields an eventual adsorbed amount (after rinsing) of  $\approx 30 \text{ mg/m}^2$ , a doubling of the polymer concentration almost doubles the adsorbed amount as well. In the AFM images this is translated in much less bare surface area, and thus more particles adsorbed on the surface, in the case of the higher PDMS concentration.

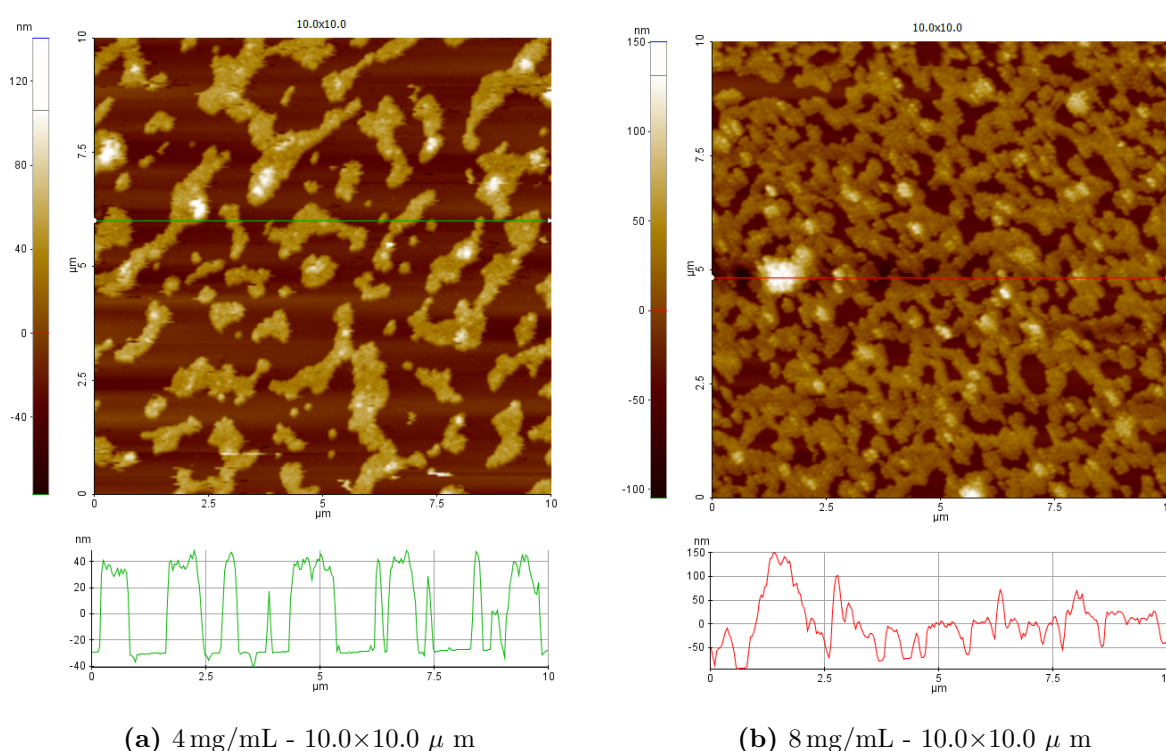


**Figure 4.29:** (a) AFM image of adsorption from a 3V% silica particle dispersion in the presence of 4 mg/mL depletion polymer on  $C_{18}$ -Melt surfaces. (b) AFM image of adsorption in the presence of 8 mg/mL PDMS on  $C_{18}$ -Melt surfaces. Both images show an equal surface area of  $10.0 \times 10.0 \mu\text{m}$  as depicted under each image. The graph under each topography image corresponds with the line profile of the red and green line that is drawn through the image.

In conclusion, it can be stated that AFM indeed does confirm the results of the ellipsometry experiments. A higher adsorbed amount on the ellipsometer corresponds with more spheres on the surfaces as imaged with AFM and equivalently a smaller area of bare surface.

## 4.4 Bulk Aggregation

Surface adsorption of hydrophobic silica particles has been experimentally studied for samples in the one-phase region in the presence of a surface of the same material. Consequently, the competitive phenomenon, bulk aggregation, is studied for the same samples in the absence of a surface.

### 4.4.1 Turbidity Measurements

In order to determine the turbidity of the samples, with turbidity being an indication of the occurrence of bulk aggregation, the transmittance was measured. The transmittance of the samples was then related to the relative turbidity according to equation 4.4.1:

$$\text{Relative turbidity} = \frac{T_{\text{solvent}} - T_{\text{sample}}}{T_{\text{sample}}} \quad (4.4.1)$$

The transmittance of the samples was measured at a broad range of the electromagnetic spectrum, but only the value at 401.5 nm, that is the wavelength of the ellipsometer, is of interest. In figure 4.30 the turbidity of a 3V% silica particle dispersion versus concentration of PDMS in cyclohexane is plotted. The value of the relative turbidity remains constant almost over the whole range, fluctuating around a fixed value of  $\approx 0.5$ . Only at very high polymer concentration of 14 mg/mL, close to the phase boundary, a slight increase of the turbidity can be observed.

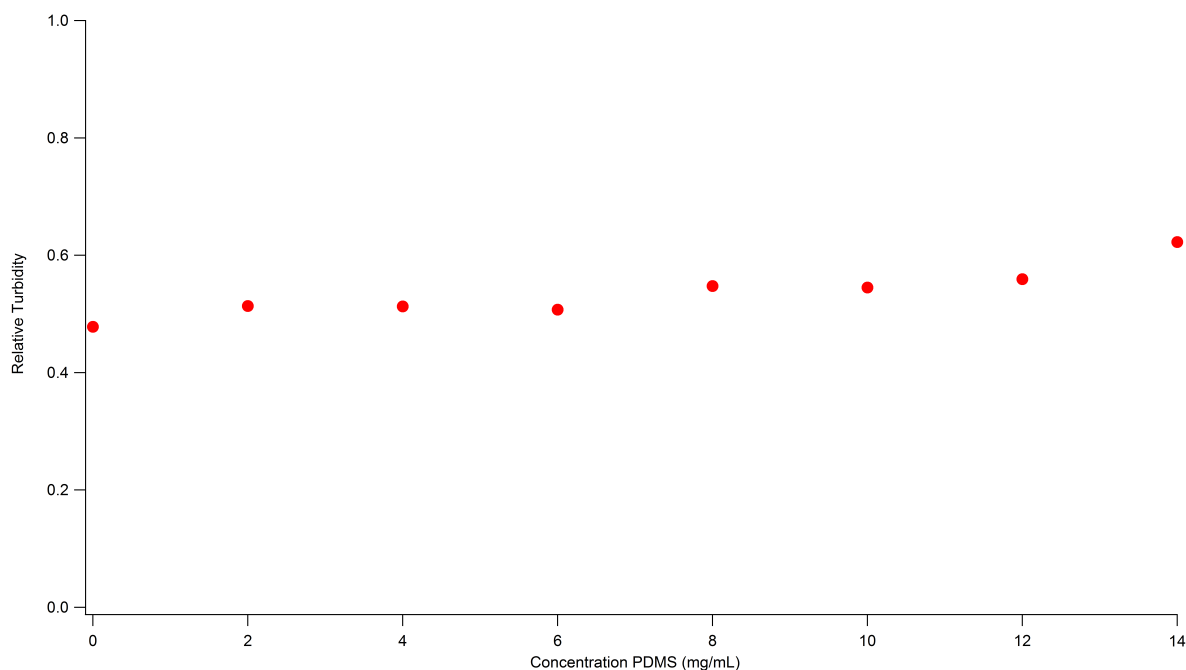


**Figure 4.30:** Relative turbidity of 3V% SiO<sub>2</sub> particle dispersion versus concentration of PDMS in cyclohexane. Recorded @ 401.5 nm.

### 4.4.2 Apparent Hydrodynamic Diameter

Initial measurements of the apparent hydrodynamic diameter as a function of polymer concentration resulted in an almost linear increase of the particle size up to almost twice the particle diameter (figure 4.31). In our opinion, this increase was not due to actual bulk

aggregation. Instead, an increase in the viscosity of the medium might as well explain this increase of the apparent hydrodynamic diameter. The fact is that the apparent hydrodynamic diameter is the product of the viscosity of the medium and the size of the particles according to the Stokes-Einstein equation for diffusion of spherical particles:

$$D = \frac{k_B T}{6\pi\eta R} \quad (4.4.2)$$

In equation 4.4.2 the product of  $\eta$  and  $R$  is the value that is obtained by dynamic light scattering as the apparent hydrodynamic diameter. As the molecular weight of PDMS is quite high (95,000 g/mol), it is not unthinkable that the viscosity of cyclohexane increases in proportion as the amount of dissolved PDMS increases. Therefore, the relative viscosity of the medium, that is that is cyclohexane and 0-14 mg/mL PDMS, was experimentally determined. The relative viscosity,  $\eta_{rel}$  is defined according to equation 4.4.3:

$$\eta_{rel} = \frac{\eta}{\eta_{solvent}} = \frac{t_{flow_{solution}}}{t_{flow_{solvent}}} \quad (4.4.3)$$

Assuming a literature value of the dynamic viscosity of cyclohexane of 0.8940 cP, the corresponding viscosities of the media were determined. The values are summarized in table 4.3.

**Table 4.3:** Flow times, relative viscosity and dynamic viscosity of the medium.

Chx and X mg/mL PDMS	$t_{flow}$	$\eta_{relative}$	$\eta_{dynamic}$ (cP)
0	12.72	1	0.894
2	13.96	1.10	0.981
4	15.17	1.19	1.066
6	16.60	1.30	1.166
8	18.33	1.44	1.288
10	19.45	1.53	1.367
12	21.11	1.66	1.484
14	21.19	1.67	1.489

Remeasuring the apparent hydrodynamic diameter of the samples and correcting the values for the viscosity of cyclohexane to that of the viscosity of the medium (as depicted in table 4.3), particle sizes were obtained that are shown in figure 4.32 as a function of PDMS concentration. As can be seen in figure 4.32, the size of the particles is quite constant over the whole range of polymer concentrations, fluctuating around a value of 70 nm only showing a slight increase at the last measured concentration of 14 mg/mL PDMS (this also indicates that PDMS does not adsorb unto the silica spheres).

From both the turbidity and apparent hydrodynamic diameter measurements it can be concluded that, below the phase boundary, the bulk is not affected by aggregation of any kind.

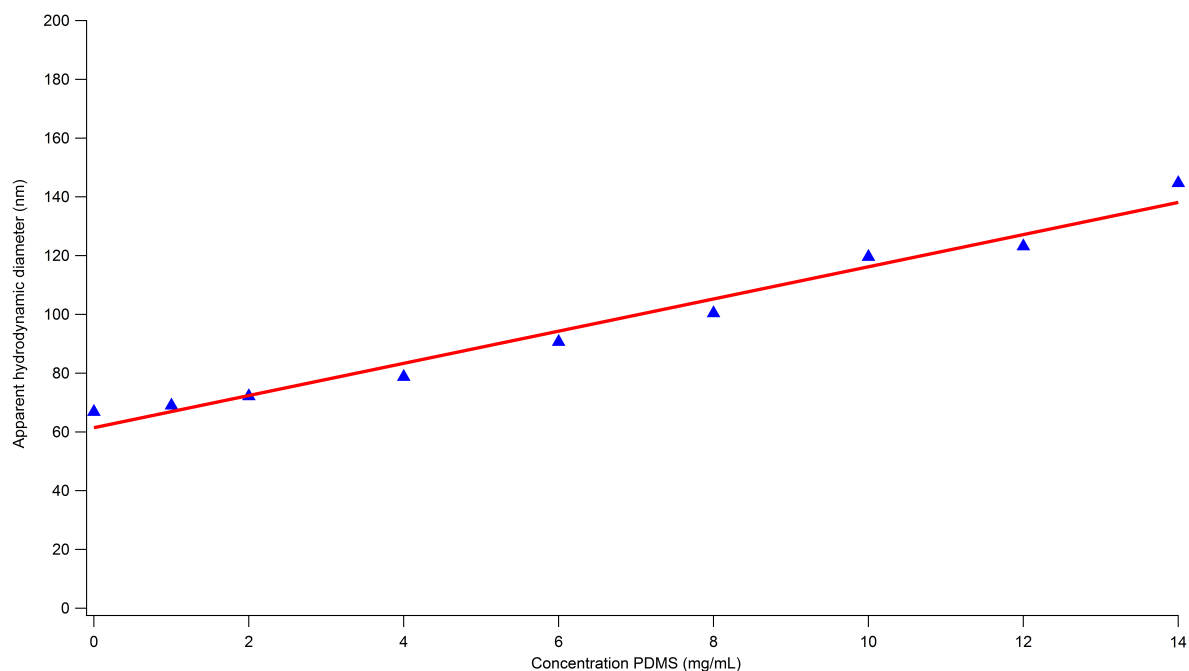


**Figure 4.31:** Apparent hydrodynamic diameter of 3V% SiO<sub>2</sub> particle dispersion versus concentration of PDMS in cyclohexane as measured with DLS. An almost linear increase of the particle size can be observed as no corrections were made for the increase in sample viscosity due to increasing concentration of the polymer.

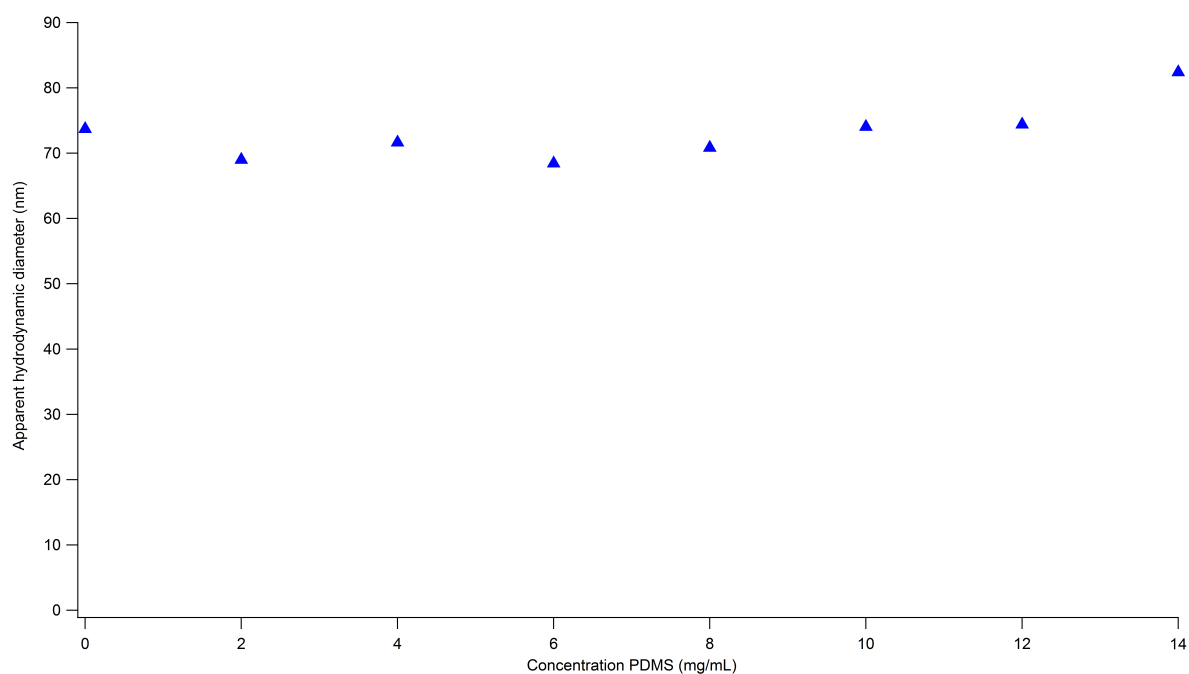


**Figure 4.32:** Apparent hydrodynamic diameter of 3V% SiO<sub>2</sub> particle dispersion versus concentration of PDMS in cyclohexane as measured with DLS. Corrections are made for the increase in sample viscosity due to increasing concentration of the polymer.

## Van der Waals Attraction and Depletion Interaction

---

### 5.1 Van der Waals Attraction

The results, as discussed in chapter 4, have shown that surface adsorption of particles increases with increasing polymer concentration and thus with increasing attraction between the particles. In other words, surface adsorption occurs before bulk aggregation as Linse and Wennerström predicted [1]. However, it was also found that surface adsorption occurs even in the absence of depletion polymer, thus without inducing additional attraction between the particles, contradicting the findings of Linse and Wennerström. What could be the cause of this adsorption in the absence of depletion polymer? We argue that this is a consequence of the Van der Waals attraction.

The Van der Waals attraction  $V(h)$  between two unequal spheres of radii  $a_1$  and  $a_2$  at a small separation  $h$  between the surfaces of the particles, is given by [41]:

$$V(h) = -\frac{A}{6} \left[ \frac{a_1 a_2}{h(a_1 + a_2)} \right] \text{ for } h < a_1, a_2 \quad (5.1.1)$$

Here  $A$  is the Hamaker constant. For identical spheres with radius  $a$ , a sphere-sphere Van der Waals attraction  $V_{ss}(h)$  is obtained:

$$V_{ss}(h) = -\frac{A}{12} \left[ \frac{a}{h} \right] \text{ for } h < a \quad (5.1.2)$$

By substitution of  $a_1 = a$  in equation (5.1.1) and taking the limit of  $a_2 \rightarrow \infty$ , the sphere-wall attraction,  $V_{sw}(h)$  is obtained:

$$V_{sw}(h) = -\frac{A}{6} \left[ \frac{a}{h} \right] \text{ for } h < a \quad (5.1.3)$$

Comparison of (5.1.2) and (5.1.3) leads to the conclusion that the sphere-wall attraction is twice as large as the sphere-sphere attraction, provided that the separation  $h$  is small compared to the radius of the particles. The stronger attraction between spheres and walls could easily elongate the life time  $\tau$  of spheres on the wall, whereas in bulk the

life time is still too short to notice dimers. This can be illustrated by the (approximate) formula for the life time:

$$\tau \approx \tau_0 \exp \left[ \frac{|V(h = \delta)|}{kT} \right] \quad (5.1.4)$$

Here,  $\tau_0$  is a typical diffusion time for free, unrestricted diffusion of a sphere over a certain distance and  $V(h = \delta)$  is the Van der Waals attraction at a separation of  $\delta$ . Substitution of the Van der Waals attraction between spheres ((5.1.2)) and between a wall and a sphere ((5.1.3)), yields a life time of wall-sphere particles that is  $e^2$  larger than that of sphere-sphere particles.

### 5.1.1 Van der Waals Attraction Between Stearyl-Coated Silica

Now that we have derived the formulae for sphere-sphere and sphere-wall Van der Waals attraction, we can calculate the Van der Waals attraction in the studied system: stearyl silica in cyclohexane. The Hamaker constant of stearyl silica in cyclohexane is equal to 0.15 kT at a temperature of 298 K [20]. The derived equations for the sphere-sphere and the sphere-wall attractions then become:

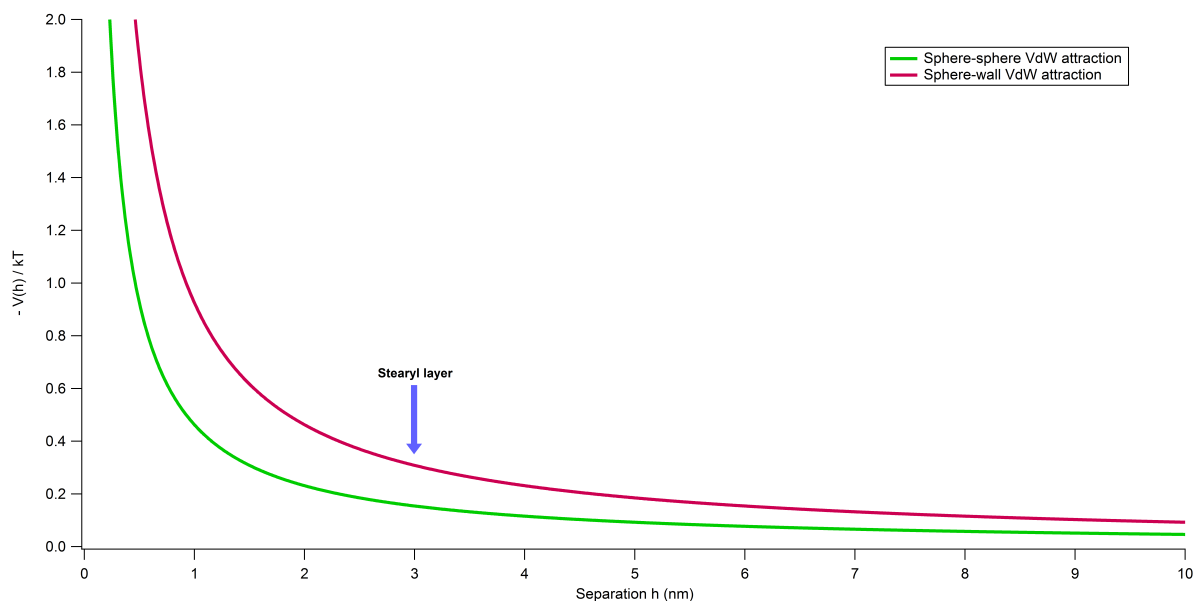
$$\frac{V_{ss}(h)}{kT} = -\frac{0.15}{12} \left[ \frac{a}{h} \right] \quad (5.1.5)$$

$$\frac{V_{sw}(h)}{kT} = -\frac{0.15}{6} \left[ \frac{a}{h} \right] \quad (5.1.6)$$

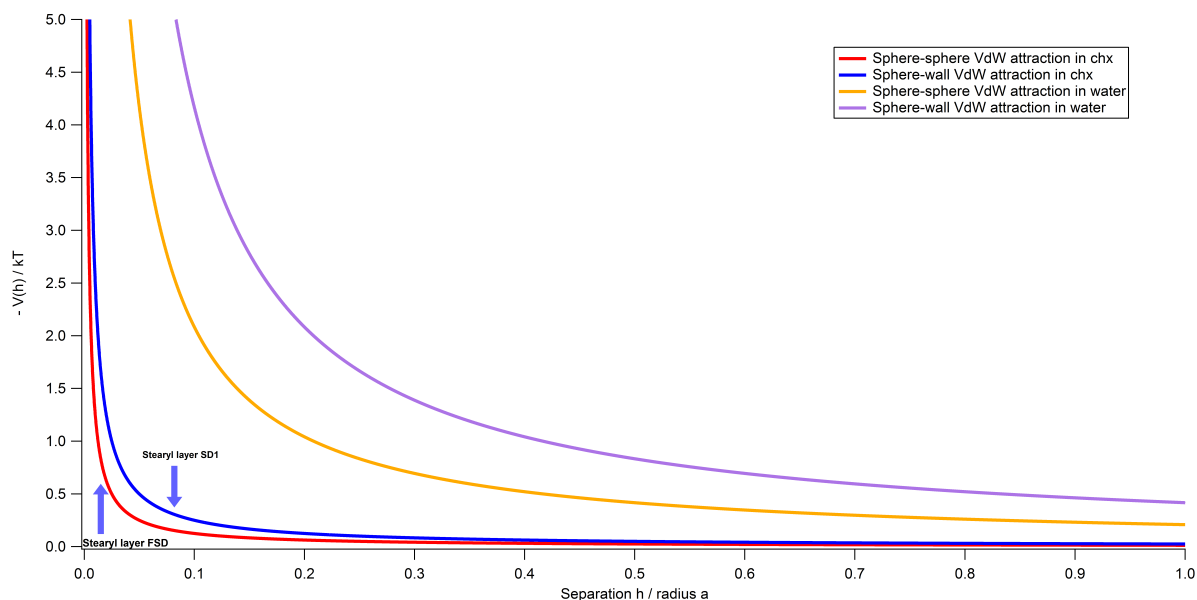
For spheres with a radius  $a$  of 37 nm (dispersion SD1),  $V_{ss}(h)/kT$  and  $V_{sw}(h)/kT$  are presented graphically as a function of the separation  $h$  in figure 5.1. The separation as defined by the stearyl layer is indicated by an arrow. A stearyl chain extends 1.5 nm in cyclohexane from the surface of the silica particle [20]. The minimum separation between two stearyl silica spheres (or one stearyl silica sphere and a stearyl silica wall) is thus 3 nm. For dispersion SD1, the sphere-sphere Van der Waals attraction has a value of 0.154 kT at  $h = 3$  nm. The sphere-wall Van der Waals attraction is twice as strong and has a value of 0.308 kT.

Figure 5.2 depicts general curves of the Van der Waals attraction, now as a function of separation per radius of the particles. The stearyl layer of dispersion SD1 is indicated with an arrow as well as that of dispersion FSD (see Appendix B). The Van der Waals attraction of large particles increases to significant values and we predict that the larger the particles the more surface adsorption will occur without enhancing the attraction. In addition, the Van der Waals attraction of silica in water is graphically depicted in figure 5.2; a Hamaker constant of 1.5 kT was used [41]. In water, the Van der Waals attraction is much larger than in cyclohexane; to use a water-based system, the Debye length must be regulated by controlling the ionic strength of the system.





**Figure 5.1:** Sphere-sphere and sphere-wall Van der Waals attraction (in terms of  $kT$ ) versus separation  $h$  of stearyl silica spheres dispersed in cyclohexane with a diameter of 74 nm. An arrow indicates the (maximal) separation as a result of the stearyl layer.



**Figure 5.2:** Sphere-sphere and sphere-wall Van der Waals attraction (in terms of  $kT$ ) as a function of separation per radius of the particles. The potentials for both stearyl silica in cyclohexane and silica in water are depicted. An arrow indicates the separation as a result of the stearyl layer for dispersion SD1 and FSD.

Even though the sphere-wall Van der Waals attraction of  $0.308 kT$  for dispersion SD1 is not sufficient to overcome the thermal energy ( $kT$ ), it must be kept in mind that the calculated Van der Waals attraction is a minimum value. In the derivation above, we assumed a system of perfectly spherical particles and perfectly flat spheres. In reality, such a system does not exist. Thus, surface roughness of both particles and walls will most definitely increase the Van der Waals attraction and consequently increase the life time  $\tau$  of dimers on the wall as given in (5.1.4). Not completely spherical spheres (that have one or more sides that are flat) will have an increased attraction between wall and spheres due to the enlarged sphere-wall contact area. In addition, the presence of a cavity will strongly enhance the Van der Waals attraction as given in (5.1.3) also due to the increase in sphere-wall contact area. Size polydispersity of the spheres will add to this as each sphere might find its optimum cavity that yields a perfect fit. Furthermore, in the derivation above, the Van der Waals attraction between the stearyl chains themselves is neglected. If all these effects would in fact be taken into account, the Van der Waals attraction would significantly increase and could certainly exceed  $kT$  (especially for the sphere-wall interaction).

As mentioned in chapter 4, the adsorbed amount in the absence of depletion polymer is lower for  $C_{18}$ -Melt surfaces than for  $C_{18}$ -LPS surfaces. It follows that in order for more adsorption to occur, the Van der Waals attraction of spheres and surfaces must be larger in the case of Melt surfaces than in the case of LPS surfaces. This could be explained by the different bonding of the stearyl chains to the surface as illustrated in figure 4.3. The less dense packing of stearyl chains on LPS surfaces might lead to smaller interparticle separation (due to possible interpenetration of the chains) and thus an increase in the Van der Waals potential.

## 5.2 Depletion Interaction

The polymer concentration that is needed to overcome the thermal energy is derived below by using the expression of the depletion potential between a sphere and a contacting flat surface. The relevant equations were taken from the book *Colloids and the Depletion Interaction* by Henk Lekkerkerker and Remco Tuinier [14].

### 5.2.1 Depletion Interaction due to Penetrable Hard Spheres

The depletion interaction between a sphere and a flat surface,  $W_{sp}(h)$ , due to penetrable hard spheres is given by:

$$\frac{W_{sp}(h)}{n_b kT} = -\frac{1}{3}\pi(\sigma - h)^2 \left(3R + \frac{\sigma}{2} + h\right) \quad \text{for } 0 \leq h < \sigma \quad (5.2.1)$$

Here,  $n_b$  is the bulk number density of penetrable hard spheres,  $k$  is the Boltzmann constant,  $T$  is the temperature,  $\sigma$  is the diameter of the penetrable hard spheres,  $h$  is the separation between a sphere and a flat surface and  $R$  is the radius of the spheres. At contact  $h = 0$  and equation (5.2.1) becomes:

$$\frac{W_{sp}(0)}{n_b kT} = -\frac{1}{3}\pi\sigma^2 \left(3R + \frac{\sigma}{2}\right) \quad (5.2.2)$$

In order for the depletion potential to overcome the thermal energy,  $\frac{W}{kT} \geq 1$  and thus:

$$\frac{W_{sp}}{kT} = 1 = -\frac{n_b \pi \sigma^2}{3} \left( 3R + \frac{\sigma}{2} \right) \quad (5.2.3)$$

Which gives an expression for  $n_b$ :

$$n_b = \frac{3}{\pi \sigma^2 \left( 3R + \frac{\sigma}{2} \right)} \quad (5.2.4)$$

Substituting  $R = 37 \times 10^{-9}m$  and  $\sigma \approx 28 \times 10^{-9}m$  and dividing by Avogadro's number, the number of moles penetrable hard spheres per cubic metre is obtained:

$$n = \frac{3}{N_{AV} \pi \sigma^2 \left( 3R + \frac{\sigma}{2} \right)} = 16 \frac{mmole}{m^3} \quad (5.2.5)$$

Multiplying  $n$  with the molecular weight of the PDMS that was used ( $M_w = 95000 \text{ g/mol}$ ), the concentration of polymer needed to overcome the thermal energy is obtained:

$$c_{pol} = 1.54 \frac{mg}{mL} \quad (5.2.6)$$

Alternatively, using the approximation  $R \gg \sigma$ , equation (5.2.1) simplifies to:

$$W_{sp}(h) = -n_b kT \pi R (\sigma - h)^2 \quad (5.2.7)$$

Substituting for the known values of  $R$  and  $\sigma$ , a value for the polymer concentration is obtained equal to  $1.73 \text{ mg/mL}$ .

## 5.2.2 Depletion Interaction due to Ideal Polymers

The expression for the depletion potential between two spheres,  $W_{ss}(h)$ , due to ideal polymers is given by equation (5.2.8), in the Derjaguin approximation:

$$W_{ss}(h) = -n_b kT R R_g^2 \left( 4\pi \ln 2 - 4\sqrt{\pi} \frac{h}{R_g} + \frac{\pi h^2}{2 R_g^2} \right) \quad (5.2.8)$$

Assuming that the sphere-surface potential,  $W_{sp}(h)$ , is equal to twice the sphere-sphere potential, the expression for a sphere and a contacting surface ( $h = 0$ ) becomes:

$$W_{sp}(0) = -n_b kT R R_g^2 8\pi \ln 2 \quad (5.2.9)$$

Thereby,

$$\frac{W_{sp}}{kT} = 1 = -n_b R R_g^2 8\pi \ln 2 \quad (5.2.10)$$

Which leads to

$$n_b = \frac{1}{R R_g^2 8\pi \ln 2} \quad (5.2.11)$$

Substituting  $R$  and  $R_g$  by numerical values and dividing by Avogadro's number, a value of  $13 \text{ mmole/m}^3$  polymer is obtained which corresponds to a concentration of  $1.25 \text{ mg/mL}$ .



## Chapter 6

---

# Why These Results Could Be Published

---

The research, as described in this thesis, presents the results of an experimental study of surface adsorption versus bulk aggregation of particles and surfaces of exactly the same material. The experiments were performed in order to test the new predictions from theory and simulations that were made by Linse and Wennerström [1]. The results that were found, confirm the predictions that were made to a large extent. However, prior to our research, experimental evidence already hinted to the validity of these predictions.

Wijting et al. [25] studied the wetting behaviour in a similar system of organophilic silica spheres in cyclohexane with PDMS as depletant. At sufficiently high concentrations of both colloids and polymers a gas-liquid phase separated system was obtained. The contact angle of the gas-liquid interface on various substrates, among others a silica rod, was measured. Upon approach of the critical point from the two-phase region, the contact angle decreased from large values (partial wetting) to zero (complete wetting).

Furthermore, fluid-solid transitions on walls were studied by Dinsmore et al. [42]. It was found that in binary hard-sphere mixtures a fluid monolayer of large spheres forms at a hard wall at concentrations below the phase boundary. Upon an increase of the concentration of the depletant spheres, the wall-fluid becomes a wall-solid in coexistence with the bulk fluid. The system consisted of charge-stabilized large (413 nm) and small polystyrene spheres with an extremely small size ratio of 0.084 that were dispersed in a density-matched mixture of H<sub>2</sub>O and D<sub>2</sub>O. The Debye length was screened to  $\approx 5$  nm so that the particles effectively behaved like hard spheres. The wall was a negatively charged glass surface that acted like a hard wall. The wall-fluid and wall-solid phases were observed with optical microscopy. In addition, the experimental observations were compared to a theoretical model.

In what manner does our research distinguish itself from the ones mentioned above? First and foremost, we did use the same system as Wijting et al., but we did not enter the two-phase region. Instead, we approached the binodal by increasing the depletant concentration. Our results could thus be seen as complementary to those of Wijting et al..

Secondly, whereas Dinsmore et al. did investigate the increase of surface adsorption upon increase of depletant concentration they used a different system and they only obtained qualitative results. On the other hand, we used a system in which the particles were not charged (to prevent any electrostatic effects), not too large (to limit sedimentation at least on the time scale of the experiments) and we used exactly the same particles and surfaces (where Dinsmore et al. settled for simply negatively charged particles and substrates). In addition, we also studied the occurrence of bulk aggregation. Furthermore, our results could be directly compared to the new predictions from simulations and theory made by Linse and Wennerström. We have also found that the assumption that adsorption does not arise unless the interaction strength is increased does not hold in practice (as adsorption does occur in the absence of depletant) of which we have provided a theoretical explanation. Last but not least, we present quantitative and qualitative results by means of ellipsometry experiments and AFM confirmation.

In conclusion it can be said that we present the interested reader with a complete set of quantitative and qualitative experiments that can be compared to the latest predictions from theory and computer simulations regarding the competition between surface adsorption and bulk aggregation of particles and surfaces of exactly the same material.

## Conclusions and Outlook

---

### 7.1 Conclusions

The competition between surface adsorption and bulk aggregation of particles and surfaces of the same material was experimentally studied in a system of stearyl silica spheres dispersed in cyclohexane and hydrophobic silica surfaces. As the attraction between the particles in the presence of a surface was increased, by means of depletion interaction due to the polymer PDMS, surface adsorption occurred. Ellipsometry experiments showed that surface adsorption occurred at concentrations far below the bulk phase boundary. An increase of the depletant concentration resulted in an increase in the adsorbed amount. Surface adsorption was found to arise even in the absence of depletant and was explained on the basis of Van der Waals attraction. The minimal polymer concentration needed to overcome the thermal energy was calculated and was consistent with the observed concentrations. The ellipsometry results were confirmed with AFM measurements which also revealed the structure of the adsorbed layer. Bulk aggregation was investigated by means of turbidity and viscosity measurements and was found not to occur in the window of the interaction strength where surface adsorption occurs.

The obtained results correspond well with the predictions from theory and simulations by Linse and Wennerström. In the limit of perfectly hydrophobic spheres and flat surfaces, theory predicts that no adsorption should occur in the absence of depletion polymer.

### 7.2 Outlook

For further research, the following experiments on systems of organophilic silica spheres in cyclohexane could be considered:

- Spectroscopic ellipsometry.  
Throughout this thesis, results from single-wavelength ellipsometry experiments are reported. This technique has some severe limitations, among others the fact that it is difficult to measure the thickness and adsorbed amount of systems with large particles (exceeding 100 nm). Spectroscopic ellipsometry, on the other hand, does not have this limitation and it can give more detailed information on the adsorbed layer.

- System with a smaller size ratio.

The phase diagram of colloid and polymer mixtures depends sensitively on the size ratio of polymer to colloids. In our research, we used a system with a size ratio larger than 0.3 resulting in gas-liquid phase separation (and in theory also a solid phase could be observed). Therefore, it could be interesting to study a system with a size ratio smaller than 0.3 for which only liquid-crystal coexistence is observed.

- Confocal microscopy.

The adsorption of fluorescently labelled silica particles from dispersion unto a macroscopic surface can be visualized and followed through time with confocal microscopy. In this manner, it could be possible to see how the particles adsorb on a surface. Preliminary experiments with a fluorescent silica dispersion were already performed and the results of these are reported in Appendix B.

Apart from performing additional experiments with a similar system as the one studied, we propose to study a water-based system. By using water as a solvent, many practical difficulties that arose with cyclohexane as a solvent can be avoided. Furthermore, supplementary techniques can be used to study the system. Thereby, a study in a completely different medium would confirm the generality of the observed effects. It might also be easier to prevent the surface adsorption of particles in the absence of depletant by tuning the ionic strength. Last but not least, water is by far a more relevant medium for applications. We propose the following experiments (in conjunction with the ones mentioned above and those that were already performed):

- AFM in liquid phase.

Whereas it was not possible to perform AFM in liquid phase with cyclohexane as a solvent (the cell was made out of plastic), this will cease to be a problem with water as a solvent. By performing AFM in liquid the adsorption process could be visualized in situ.

- QCM-D.

QCM-D experiments were performed with the studied system (see Appendix C), but cyclohexane damaged the coarse crystals that are used as silica substrates and no reliable results could be obtained. QCM-D can yield complementary results to ellipsometry, as with the former the wet mass is determined (solvent molecules that couple to the substrate are taken into account), while the latter yields the dry mass.

- Cubic particles.

Linse and Wennerström predicted that *in the limit of cubic particles, no adsorption would occur* [1]. To test this prediction, cubic particles could be used in similar experiments. In addition, it is very interesting to study the build-up of surface layers of cubic particles.

In addition, it is interesting to evaluate the effect of colloid and polymer polydispersity on the minimal polymer concentration needed to overcome the thermal energy. Finally, additional computer simulations could be interesting to perform. For instance, the Van der Waals attraction could be taken into account to determine if this indeed is the cause of the adsorption in the absence of polymer.



---

# Acknowledgements

---

As I have reached the end of this thesis, I would like to take the time to thank a number of people as I could never have performed this research on my own.

First of all I would like to thank my supervisors: Albert, Lennart and Tommy. Albert, my tutor, I cannot thank you enough for offering me this project at a time when I was not sure where I wanted to perform the research for my Master Thesis. To be honest, I wanted to stay at *FCC*, but having already done two projects at your department I was encouraged to go elsewhere (and righteously so). Then you brought this project to my attention that was to be performed at Lund University in Sweden. This was completely unexpected as I had never considered going abroad for my Master Thesis. However, the more I learned about this project, the harder it was for me to walk away from it. So I packed my belongings and I was soon on my way to Lund. And that is where I met you, Lennart and Tommy. I could not have wished for two better, kinder and more welcoming supervisors during my eleven months in Lund. I have enjoyed my stay more than I had ever imagined and that is not in the least thanks to you. Lennart, you were always around to help me with any questions that I had and you were ever so interested to hear about any progress that I had made. The first weeks that I was there you made sure that I felt right at home and that I had everything that I needed. As we continued down the road you gave me the freedom to perform the experiments that I wanted to do, but you made sure that I did not drift too far away in my enthusiasm. Tommy, sometimes it was hard to track you down, due to your very busy travelling schedule, but when I did manage to track you down you always gave me all the help and time I needed and I thank you for that. I learned a lot from you about the ellipsometer; a technique that I had never worked with before. Your enthusiasm (even when things went wrong) and laughter are contagious and your presence always brings about a nice atmosphere thanks to your funny jokes and positive attitude. Furthermore, Albert, thank you for paying me a visit during my stay in Lund, for attending my seminar and for always keeping in touch. I greatly appreciate the fact that your door is always open for me.

Of course, there are many other people that helped me during my stay at Lund. Tobias, thank you so much for teaching me how to use the ellipsometers (Rudolph and Horiba), the AFM, the tensiometer and basically all the equipment that I have used. Moreover, thank you for always being ready to help me with the same equipment when it failed to do what it was supposed to do. I would like to thank Marianna for showing me around the lab and always helping me to find the things I needed (especially in the beginning). Maria S and Christopher, you have helped me out more times than I could

have counted and without your help, many things would have been impossible; your help was truly indispensable. Ruiyu, thank you for helping me to measure the contact angles on the hydrophobic surfaces. Maria W, your knowledge about the AFM is astonishing and thank you for assisting me to obtain even better images. Solmaz, thank you for your help with the light scattering and turbidity measurements. Sanna, thank you so much for the NMR measurements and especially for your patience and perseverance to make sure we obtained that diffusion coefficient. Karin, thank you so much for advice on light scattering related questions and more importantly for your always friendly and warm character and for showing genuine interest in me and everybody around you. Additionally, I would like to thank Per Linse and Håkan Wennerström as without your work I could not have done mine.

Finally, I would like to thank my officemates, first Norah, then Marta. You made my time in *our* office filled with joy and laughter and I really enjoyed your company. I would like to thank the whole Physical Chemistry and also the Theoretical Chemistry department for the nice atmosphere, the great working environment and of course for the *fika*. In particular, I would like to thank my dear friends: Anil, Dat, Fei, Hongduo, Jessie, Steven, Tiny and Weimin. Thank you so much for your company, the excursions, the dinners, the parties and all the other things (too many to name them all).

Last but most certainly not least, I would like to thank my parents. Mijn lieve, lieve ouders. Zonder jullie onvoorwaardelijke hulp en steun zou ik nergens zijn. Ik kan mij geen betere ouders voorstellen dan jullie. Ik dank jullie uit de grond van mijn hart voor alles. *Shukran!*

---

# Bibliography

---

- [1] P. Linse and H. Wennerström. Adsorption versus aggregation. Particles and surface of the same material. *Soft Matter*, 8:2486–2493, 2012.
- [2] R.J. Hunter. *Foundations of Colloid Science*. Oxford University Press, Oxford, 2nd edition, 2001.
- [3] A. Adamczyk. *Adsorption of Particles: Theory in Encyclopedia of Surface and Colloid Science*. Taylor & Francis, 2nd edition, 2006.
- [4] P. Jiang, J.F. Bertone, K.S. Hwang, and V.L. Colvin. Single-Crystal Colloidal Multilayers of Controlled Thickness. *Chemistry of Materials*, 11(25):2132–2140, 1999.
- [5] J. Kleinert, S. Kim, and O.D. Velev. Electric-field-assisted convective assembly of colloidal crystal coatings. *Langmuir : the ACS journal of surfaces and colloids*, 26(12):10380–5, 2010.
- [6] H. Okudera and A. Hozumi. The formation and growth mechanisms of silica thin film and spherical particles through the stober process. *Thin Solid Films*, 434(1):62–68, 2003.
- [7] H. Okudera and Y. Yokogawa. Formation of tio<sub>2</sub> thin films by hydrolysis of ti-tetraethoxide in ethanol: kinetics, surface morphology, constituent phases and their formation mechanism. *Thin Solid Films*, 401(1):124–130, 2001.
- [8] H. Shin, M. Agarwal, M.R. De Guire, and A.H. Heuer. Deposition mechanism of oxide thin films on self-assembled organic monolayers. *Acta Materialia*, 46(3):801 – 815, 1998.
- [9] P. Lipowsky, S. Jia, R.C. Hoffman, and N.Y. Jin-Phillip. Thin film formation by oriented attachment of polymer-capped nanocrystalline ZnO. *International Journal of Materials Research*, 97(5), 2006.
- [10] P. Lipowsky, N. Hedin, J. Bill, R.C. Hoffmann, A. Ahniyaz, F. Aldinger, and L. Bergstrom. Controlling the assembly of nanocrystalline zno films by a transient amorphous phase in solution. *The Journal of Physical Chemistry C*, 112(14):5373–5383, 2008.
- [11] A.K. Van Helden, J.W. Jansen, and A. Vrij. Preparation and characterization of spherical monodisperse silica dispersions in nonaqueous solvents. *Journal of Colloid and Interface Science*, 81(2):354–368, 1981.

- [12] N.A.M Verhaegh, D. Asnaghi, and H.N.W Lekkerkerker. Transient gels in colloid-polymer mixtures studied with fluorescence confocal scanning laser microscopy. *Physica A: Statistical Mechanics and its Applications*, 264(1-2):64–74, 1999.
- [13] E.H.A de Hoog, L.I. de Jong-van Steensel, M.M.E. Snel, and H.N.W. Lekkerkerker. Preparation of a Colloidal Crystal at a Wall Characterized with AFM. *Langmuir*, 17(18):5486–5490, 2001.
- [14] H.N.W. Lekkerkerker and R. Tuinier. *Colloids and the Depletion Interaction*, volume 833. Springer, 1st edition, 2011.
- [15] N.V. Dziomkina and G.J. Vancso. Colloidal crystal assembly on topologically patterned templates. *Soft Matter*, 1:265–279, 2005.
- [16] W.C.K. Poon. The physics of a model colloid-polymer mixture. *Journal of Physics: Condensed Matter*, 14:R859–R880, 2002.
- [17] P.N. Pusey and W. van Megen. Phase behaviour of concentrated suspensions of nearly hard colloidal spheres. *Nature*, 320:340–342, 1986.
- [18] A. Vrij, J.W. Jansen, J.K.G. Dhont, C. Pathmamanoharan, and H.M. Fijnaut. Light Scattering of Colloidal Dispersions in Non-polar Solvents at Finite Concentrations Silica Spheres as Model Particles for Hard-sphere Interactions. *Faraday Discussions of the Chemical Society*, 76:19–35, 1983.
- [19] A. Vrij, M.H.G.M. Penders, P.W. Rouw, C.G. de Kruif, J.K.G. Dhont, C. Smits, and H.N.W. Lekkerkerker. Phase-transition phenomena in colloidal systems with attractive and repulsive particle interactions. *Faraday Discussions of the Chemical Society*, 90:31, 1990.
- [20] J.W. Jansen, A. Vrij, and C.G. de Kruif. Attractions in sterically stabilized silica dispersions: I. Theory of phase separation. *Journal of Colloid and Interface Science*, 114(2):471–480, 1986.
- [21] M.M. Kops-Werkhoven. Dynamic light scattering and sedimentation experiments on silica dispersions at finite concentrations. *The Journal of Chemical Physics*, 74(3):1618, 1981.
- [22] C.G. de Kruif, P.W. Rouw, J.W. Jansen, and A. Vrij. Hard sphere properties and crystalline packing. *Journal de Physique*, 46(3), 1985.
- [23] N.A.M. Verhaegh, J.S. van Duijneveldt, J.K.G. Dhont, and H.N.W. Lekkerkerker. Fluid-fluid phase separation in colloid-polymer mixtures studied with small angle light scattering and light microscopy. *Physica A: Statistical Mechanics and its Applications*, 230(3-4):409–436, 1996.
- [24] N.A.M. Verhaegh, D. Asnaghi, H.N.W. Lekkerkerker, M. Giglio, and L. Cipelletti. Transient gelation by spinodal decomposition in colloid-polymer mixtures. *Physica A: Statistical Mechanics and its Applications*, 242:104–118, 1997.
- [25] W. Wijting, N. Besseling, and M.A. Cohen Stuart. Wetting in a Colloidal Liquid-Gas System. *Physical Review Letters*, 90(19):17–20, 2003.

- 
- [26] E.H.A. de Hoog. *Interfaces and Crystallization in Colloid-Polymer Suspensions*. PhD thesis, Utrecht University, 2001.
- [27] A.P. Philipse. Private communication.
- [28] W. Stöber and A. Fink. Controlled Growth of Monodisperse Silica Spheres in the Micron Size Range. *Journal of Colloid and Interface Science*, 26:62–69, 1968.
- [29] R.M.A Azzam and N.M. Bashara. *Ellipsometry and Polarized Light*. Elsevier B.V., 1st edition, 1987.
- [30] H. Tompkins and E.A. Irene. *Handbook of ellipsometry*. William Andrew Publishing & Springer Germany, 2005.
- [31] T. Nylander and T. Arnebrant. Ellipsometry as a tool for in situ studies of adsorption (manuscript), 1987.
- [32] Y. Samoshina. *Polyelectrolytes on Surfaces and their Complexes with Surfactants, Thermodynamics versus kinetics*. PhD thesis, Lund University, 2004.
- [33] H.G. Tompkins and W.A. McGahan. *Spectroscopic Ellipsometry and Reflectometry - A User's Guide*. John Wiley & Sons, Inc., 1999.
- [34] T. Halthur. *Multilayer Structures for Biomaterial Applications: Biomacromolecule-based Coatings*. PhD thesis, KTH Royal Institute of Technology, 2005.
- [35] F. Tiberg and M. Landgren. Characterization of thin nonionic surfactant films at the silica/water interface by means of ellipsometry. *Langmuir : the ACS journal of surfaces and colloids*, 9(4):927–932, 1993.
- [36] J.A. De Feijter, J. Benjamins, and F.A. Veer. Ellipsometry as a tool to study the adsorption behavior of synthetic and biopolymers at the air-water interface. *Biopolymers*, 17(7):1759–1772, 1978.
- [37] D.M.E. Thies-Weesie. *Sedimentation and Liquid Permeation of Inorganic Colloids*. PhD thesis, Utrecht University, 1995.
- [38] J.S. Alper and R.I. Gelb. Standard errors and confidence intervals in nonlinear regression: comparison of Monte Carlo and parametric statistics. *Journal of Physical Chemistry*, 94(11):4747, 1990.
- [39] D.P. Chang, M. Jankunec, J. Barauskas, F. Tiberg, and T. Nylander. Adsorption of lipid liquid crystalline nanoparticles on cationic, hydrophilic, and hydrophobic surfaces. *ACS applied materials & interfaces*, 4(5):2643–51, 2012.
- [40] A.W. Sonesson, U.M. Elofsson, H. Brismar, and T.H. Callisen. Adsorption and mobility of a lipase at a hydrophobic surface in the presence of surfactants. *Langmuir : the ACS journal of surfaces and colloids*, 22(13):5810–7, 2006.
- [41] J. Lyklema, editor. *Fundamentals of Interface and Colloid Science - Volume I: Fundamentals*. Academic Press, 1991.

- [42] A.D. Dinsmore, P.B. Warren, W.C.K. Poon, and A.G. Yodh. Fluid-solid transitions on walls in binary hard-sphere mixtures. *EPL (Europhysics Letters)*, 40(3):337–342, 1997.
- [43] N.A.M. Verhaegh and A. Van Blaaderen. Dispersions of Rhodamine-Labeled Silica Spheres : Synthesis, Characterization, and Fluorescence Confocal Scanning Laser Microscopy. *Langmuir : the ACS journal of surfaces and colloids*, 10(5):1427–1438, 1994.
- [44] A. Van Blaaderen and A. Vrij. Synthesis and Characterization of Colloidal Dispersions of Fluorescent , Monodisperse Silica Spheres. *Langmuir : the ACS journal of surfaces and colloids*, 8(12):2921–2931, 1992.
- [45] E.A.G. Jamie, G.J. Davies, M.D. Howe, R.P.A. Dullens, and D.G.A.L. Aarts. Thermal capillary waves in colloid-polymer mixtures in water. *Journal of Physics: Condensed Matter*, 20(49):494231, 2008.
- [46] M.H. Lee, F.L. Beyer, and E.M. Furst. Synthesis of monodisperse fluorescent core-shell silica particles using a modified Stober method for imaging individual particles in dense colloidal suspensions. *Journal of colloid and interface science*, 288:114–23, 2005.
- [47] A. M. Nechifor, A. P. Philipse, F. de Jong, and J.P.M. van Duynhoven. Preparation and Properties of Organic Dispersions of Monodisperse Silica Receptor Colloids Grafted with Calixarene Derivatives or Alkyl Chains. *Langmuir : the ACS journal of surfaces and colloids*, 12(16):3844–3854, 1996.
- [48] F. Höök, B. Kasemo, T. Nylander, C. Fant, K. Sott, and H. Elwing. Variations in coupled water, viscoelastic properties, and film thickness of a Mefp-1 protein film during adsorption and cross-linking: a quartz crystal microbalance with dissipation monitoring, ellipsometry, and surface plasmon resonance study. *Analytical chemistry*, 73(24):5796–804, 2001.
- [49] T. Nylander, R.A Campbell, P. Vandoolaeghe, M. Cárdenas, P. Linse, and A.R. Rennie. Neutron reflectometry to investigate the delivery of lipids and DNA to interfaces (Review). *Biointerphases*, 3(2):FB64, 2008.
- [50] B. Vincent. The calculation of depletion layer thickness as a function of bulk polymer concentration. *Colloids and Surfaces*, 50:241–249, 1990.
- [51] B. Vincent, J. Edwards, S. Emmett, and R. Croot. Phase separation in dispersions of weakly-interacting particles in solutions of non-adsorbing polymer. *Colloids and Surfaces*, 31:267–298, 1988.
- [52] A.P. Philipse. Particulate Colloids: Aspects of Preparation and Characterization. In J. Lyklema, editor, *Fundamentals of Colloids and Interface Science - Volume IV*. Elsevier, 2005.

# Appendices





# Appendix A

---

## Protocol for the Synthesis of Silica Spheres Coated with Stearyl Alcohol

---

This protocol for the synthesis of sterically stabilized silica spheres was composed according to the following references [11] and [20].

There are different methods to prepare silica dispersions. The protocol as described below is based on Stöber [28] and consists of the hydrolysis of a silicon containing compound (TES in this case). The advantages of Stöber silica are, among others, that monodisperse spherical particles dispersed in ethanol can easily be obtained and that the particle size can be effectively tuned as desired. The reaction equation for the formation of silica in this way, can be found in figure A.1. The presence of ammonia has been found to be essential for the formation of spherical particles. The resulting sol is electrostatically stabilized due to the negatively charged  $\text{OH}^-$  groups that are adsorbed onto the particle surface. The negatively charged silica particles are made hydrophobic by esterification of the silanol groups with an alcohol, stearyl alcohol in this case. The corresponding reaction equation is portrayed in figure A.2. The maximum number of alcohols on the surface is determined mostly by the size and shape of the reacting alcohol. For example, a single chain alkane covers an area of  $37 \text{ \AA}^2$ . However, due to sterical hindrance, not every silanol group will eventually react with an alcohol. Nevertheless, the hydrophobization is assumed to be complete as the bare silanol groups will be overshadowed by the hydrophobic alkyl chains that are bound to the surface.

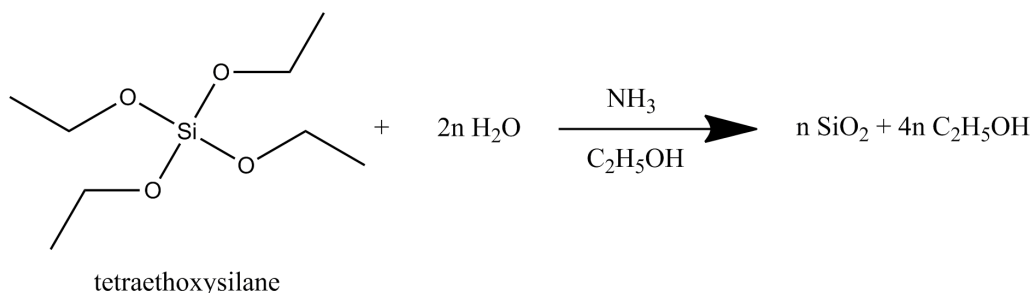


**Figure A.1:** The complete reaction equation for the formation of silica from a silicon containing precursor (TES).

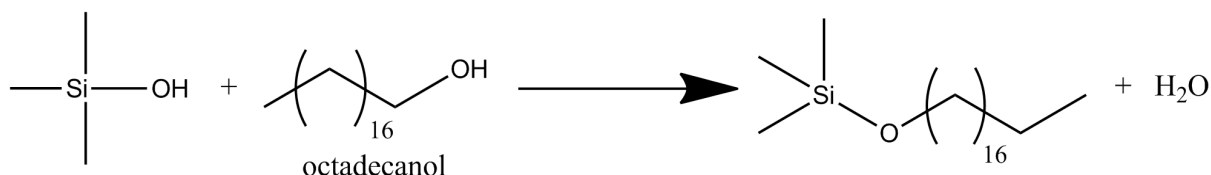


**Figure A.2:** The esterification of the silanol groups on the surface of the silica spheres to produce stearyl silica, proceeds according to this reaction equation at elevated temperature.

The size of the silica particles is determined by the amounts of ammonia, water, TES and ethanol present. Under the condition that the amounts of ammonia and water are not too large, the size can be roughly predicted by the following equation:

$$a \approx 0.74 \frac{[\text{NH}_3] \times [\text{H}_2\text{O}]}{[\text{TES}]^2} \text{ nm}$$

By using the densities of TES and ammonia, this equation can be rewritten as:

$$a \approx 19 \left(\frac{x}{y}\right)^2 \text{ nm}$$

With  $x$  being the amount of concentrated ammonia (25%) en  $y$  the amount of TES (in mL). The exact volume of ethanol is not important as long as the concentration of TES remains approximately 0.17 mol/L. In order to synthesize particles with a diameter of  $\pm 70$  nm, the required volumes are: 1055 mL ethanol, 40 mL TES and 76 mL concentrated ammonia (25%).

The protocol to synthesize monodisperse silica spheres in ethanol followed by their hydrophobization with stearyl alcohol is described in the following two sections.

## A.1 Monodisperse Silica Spheres in Ethanol

In order to synthesize monodisperse particles, the glassware must be as clean as possible and the reagents must be as pure as possible. Therefore, clean all glassware thoroughly before use in a 8% HF-solution.

While stirring with a mechanical stirrer, transfer quantitatively 76 mL concentrated ammonia (25%) to 1055 mL ethanol in a 2 L three-neck round-bottom flask by a funnel under the solution surface. Then add 40 mL TES by a funnel under the solution surface to the reaction mixture under severe mechanical stirring ( $\approx 1000$  rpm). After approximately ten minutes, the reaction mixture becomes turbid and the stirring speed should be decreased to  $\approx 200$  rpm. The reaction is complete after 12-16 hours.

## A.2 Hydrophobization with Stearyl Alcohol

The hydrophobization of the silica surface with stearyl alcohol is performed in a melt of stearyl alcohol at a temperature of 180-200°C. First, add a solution of 50 g of stearyl alcohol in 160 mL ethanol to the alcosol. The ethanol and water are then removed either by (azeotropic) distillation or through the use of a rotatory evaporator. After

all the ethanol and water are removed from the dispersion, transfer the residue to a two-neck round-bottom flask and heat the flask to 100-120°C with an oil bath while stirring with a magnetic stirrer. Apply a weak nitrogen flow to the reaction mixture to remove the last amount of ethanol and water still present. After approximately one hour no ethanol is distilled any more. Now, raise the temperature to 180-200°C and maintain this temperature for (at least) 3 hours.

Finally, purify the stearyl silica by vacuum distillation (at a pressure <1.3 mbar) followed by sedimentation in an analytical ultracentrifuge. Remove the supernatant and redisperse the sediment in cyclohexane. Repeat this at least three times at  $\approx 40,000$  g for the duration of 30 minutes per centrifugation round.



# Appendix B

---

## Fluorescent Silica Dispersion

---

### B.1 Synthesis of Fluorescent and Hydrophobic Silica Spheres

Fluorescent, hydrophobic silica spheres were synthesized based on a protocol that was composed according to the following references [11], [20], [43], [44], [45], [46] and [47].

#### B.1.1 Fluorescent, Hydrophilic Silica Spheres

Prior to use, all the glassware was cleaned with a 8% hydrofluoric acid solution for 15-30 minutes in order to remove nucleation sites. Subsequently, the acid was removed by rinsing with cold, hot and distilled water and finally with ethanol.

A 25 mL erlenmeyer that was dried for 3 hours at 120 °C was covered with aluminium foil. 0.0938 g of APS was added to a solution of 0.1178 g RITC in 10 mL anhydrous ethanol in the erlenmeyer. The solution was then stirred on a magnetic stirring plate in the dark for 40 hours.

While stirring with a magnetic stirrer (up to 1500 rpm), 51 mL of ammonium hydroxide (1 M NH<sub>3</sub> and 2.8 M H<sub>2</sub>O) was added to 335 mL of ethanol by a funnel under the solution surface in a 2 L three-neck round-bottom flask. Secondly, a mixture of 335 mL ethanol, 28.3 mL TES and the dye solution were added by a funnel under the solution surface to the reaction mixture under severe magnetic stirring ( $\approx$  1000 rpm). As soon as the mixture became turbid the stir rate was decreased to  $\approx$  200 rpm and the mixture was stirred for ten hours in the dark.

0.7 mL TES was added to the reaction mixture, under magnetic stirring, followed by 50 mL of TES and at least 50 mL of water with intervals of 2 hours until a total of 253 mL of TES and at least 250 mL of water had been added (water was added regularly to keep the molar ratio of water:TES at least 10:1).

The final reaction mixture was centrifuged three times at 200 g for 2 hours. Every time the supernatant was removed and the sediment was washed in ethanol. Finally, the

particles were redispersed in ethanol.

### B.1.2 Hydrophobization

An amount of the alcocol containing  $\approx 15$  g of silica was dispersed in 180 mL triethyl phosphate. The ethanol was removed from the mixture using a rotatory evaporator at  $60^\circ\text{C}$  and 175 mbar and with a  $\Delta P$  equal to 18 mbar. As soon as all the ethanol was evaporated, the mixture was transferred to a 1 L three-neck round-bottom flask. 21.6 g of 1-octadecanol was added to the flask and the mixture was heated to  $150^\circ\text{C}$  using an oil bath. The flask was placed under a nitrogen flow as soon as the 1-octadecanol had dissolved (at  $\approx 75^\circ\text{C}$ ). The temperature of the reaction mixture was maintained constant at  $150^\circ\text{C}$  and proceeded for the duration of 4 days while stirring. The final reaction mixture was centrifuged three times at 200 g for two hours. Every time the supernatant was removed and the sediment was washed in cyclohexane. Finally, the particles were redispersed in cyclohexane. The dispersion was labelled FSD.

## B.2 Results

### B.2.1 Size and Morphology

The apparent hydrodynamic diameter of FSD was determined with DLS and amounted to  $421.6 \text{ nm} \pm 4.136 \text{ nm}$ . The dispersion was not filtered prior to the measurement as there were no available hydrophobic syringe filters with the appropriate pore diameter. In addition, an average was taken over only three measurements as the sample sediments quite fast. A characteristic TEM image of the fluorescent spheres can be seen in figure B.1. The spheres are spherical and very monodisperse as can be seen directly from the spontaneous ordering of the particles on the TEM grid.

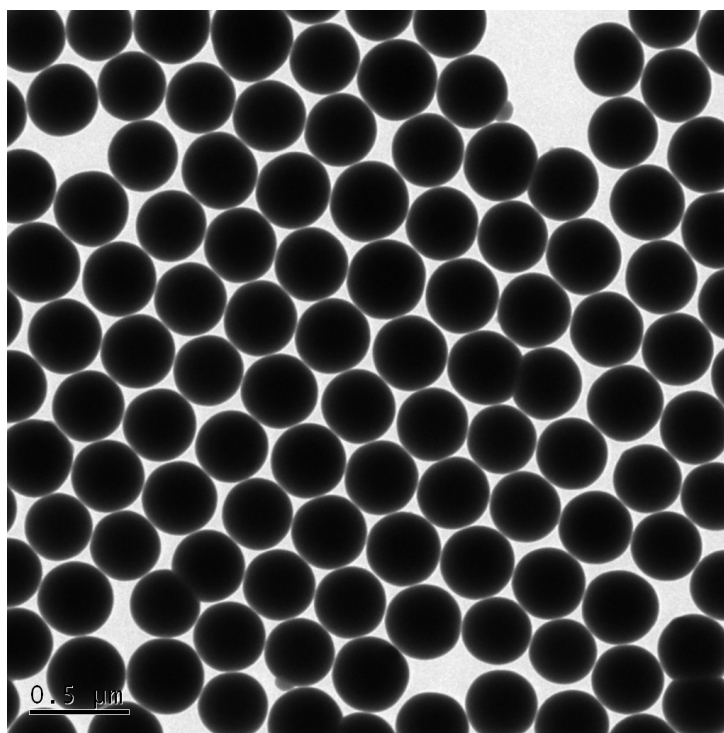


**Figure B.1:** Characteristic TEM image of dispersion FSD.

## B.2.2 Confocal Microscopy

Confocal micrographs of fluorescent and hydrophobic silica spheres on a C<sub>18</sub>-TEP hydrophobic silica substrate were obtained with a Leica CLSM SP5 microscope. Measurements were performed with a HeNe laser at an excitation wavelength of 543 nm. A non-resonant scanner (1400 lines/second) and a glycerol immersion objective with a magnification of 63× and a numerical aperture of 1.30 were used. Images were taken at a temperature of 25°C in the dispersion of the silica spheres. Some confocal images (of the substrate) can be found in figures B.2 to B.5.

## B.2.3 AFM

AFM was used to determine the structure of the adsorbed fluorescent silica spheres on the (dried) silica surface. The studied surface was made by hanging the C<sub>18</sub>-TEP silica substrate in a 3V% SD1 dispersion for two hours and eventually rinsing with cyclohexane. The substrate was slowly removed from the solvent, dried and taped to a magnetic coin in order to be examined with AFM. Some characteristic AFM images are shown in figures B.6 to B.9.

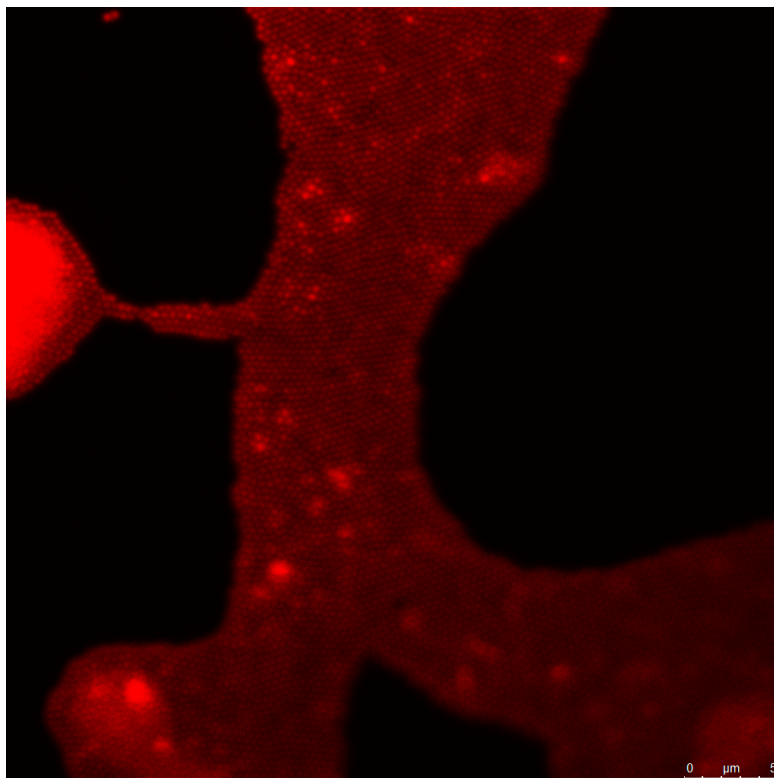


**Figure B.2:** A number of spheres adsorb to the surface. Here and there multiple layers of spheres can be seen. The spheres pack quite closely and show short-range ordered structures.

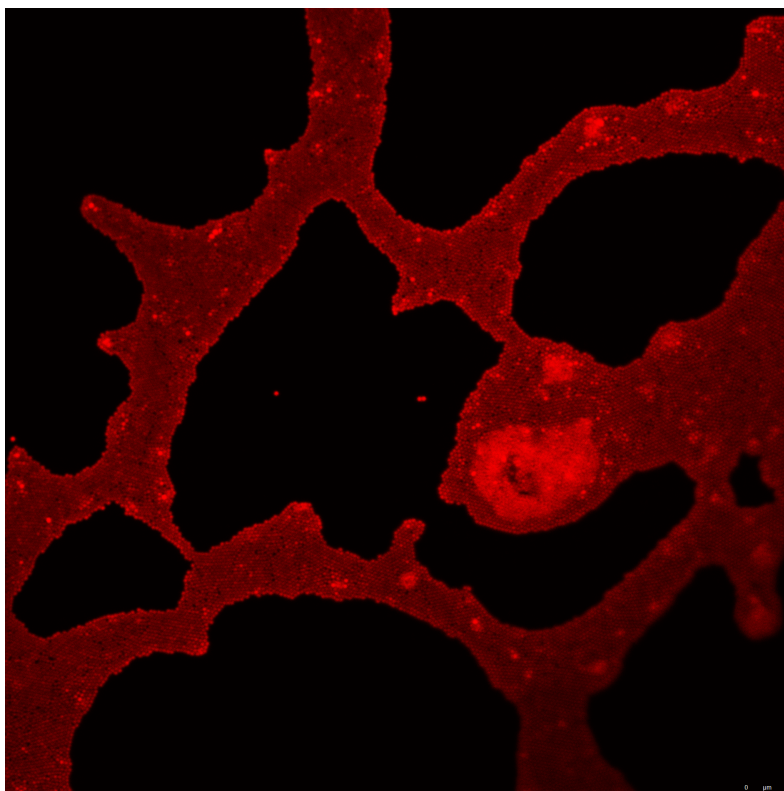


**Figure B.3:** At some places a network of patches of spheres can be found. Again, there is close packing of the spheres with some local ordering.



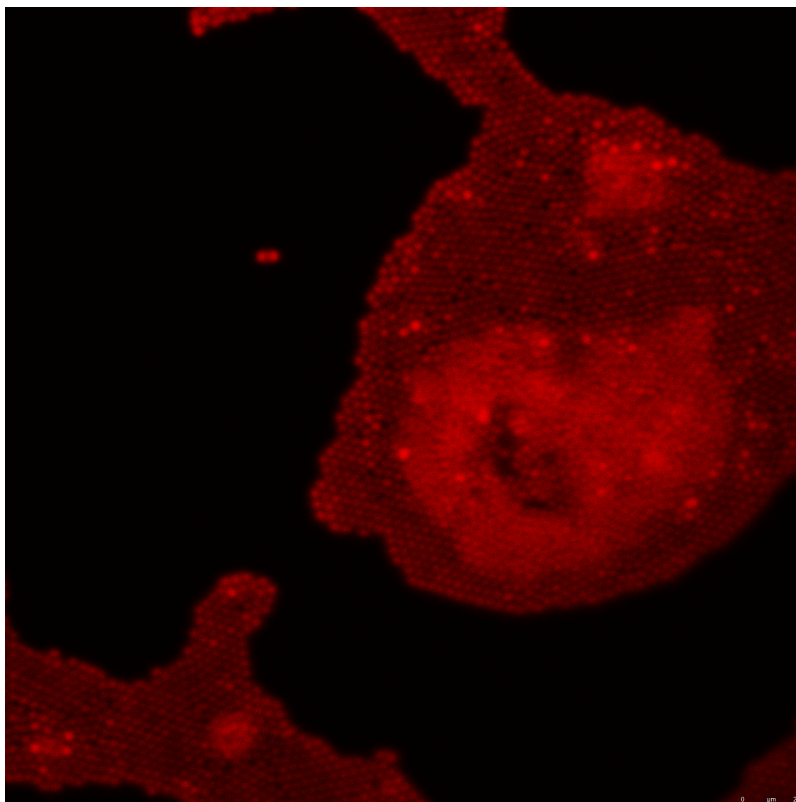


**Figure B.4:** A zoom in of figure B.3. The spheres can be more clearly distinguished as well as the multiple layers of spheres.

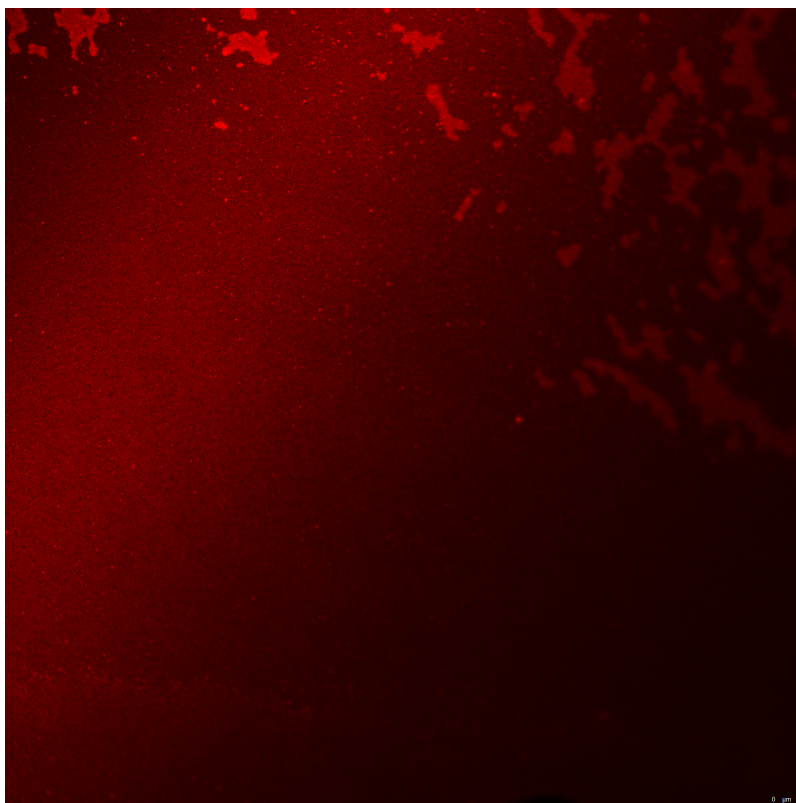


**Figure B.5:** Other areas are completely covered with spheres as can be seen here.

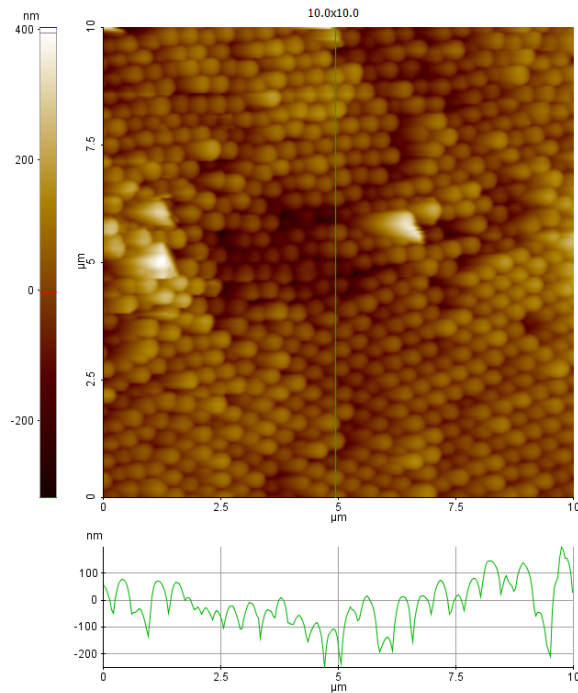


**Figure B.6:** AFM image over an area of  $10 \times 10 \mu\text{m}$ . The silica spheres can clearly be distinguished from each other and many spheres are adsorbed to the surface. There seems to be some short-range ordering and the spheres are closely packed. The profile of the vertical green line is shown below the topography image.

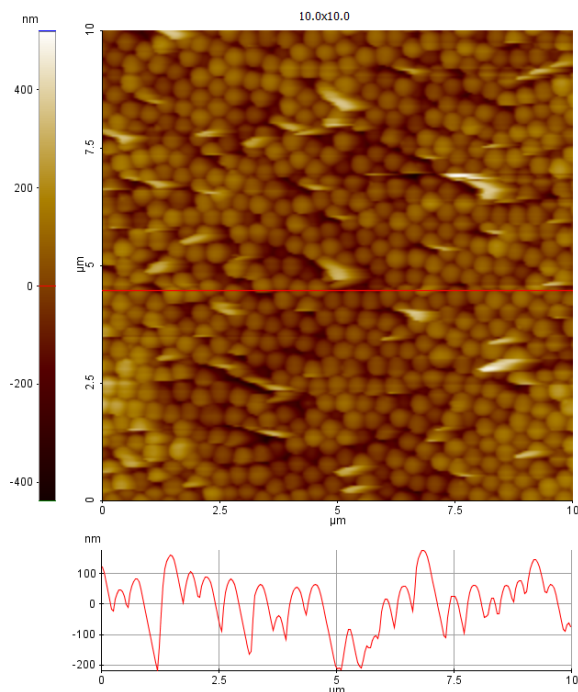


**Figure B.7:** AFM image over an area of  $10 \times 10 \mu\text{m}$  and similar to figure B.9. Here, the spheres seem to be arranged in a more disordered fashion. Over the whole area close packed spheres can be seen adsorbed to the surface. The profile of the horizontal red line is shown below the topography image.

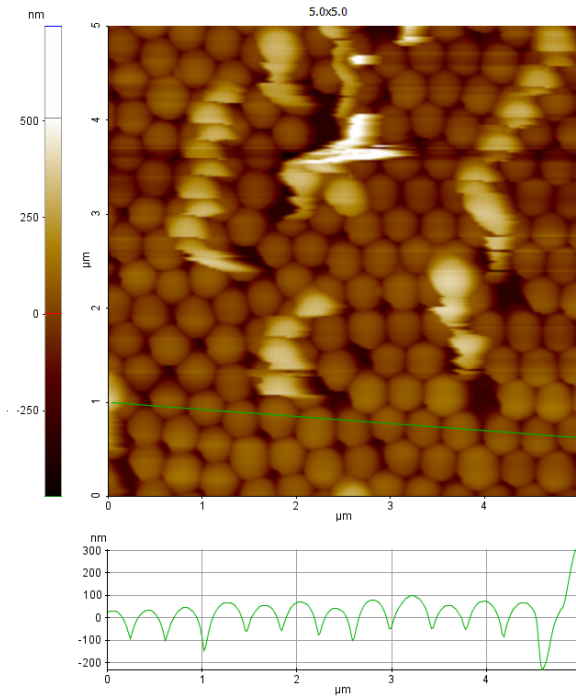


**Figure B.8:** AFM image over an area of  $5 \times 5 \mu\text{m}$ . This image shows a smaller surface area in which the local ordering of the silica spheres clearly can be seen. In addition, the close packing of the spheres is evident. The profile of the slanted green line is shown below the topography image.

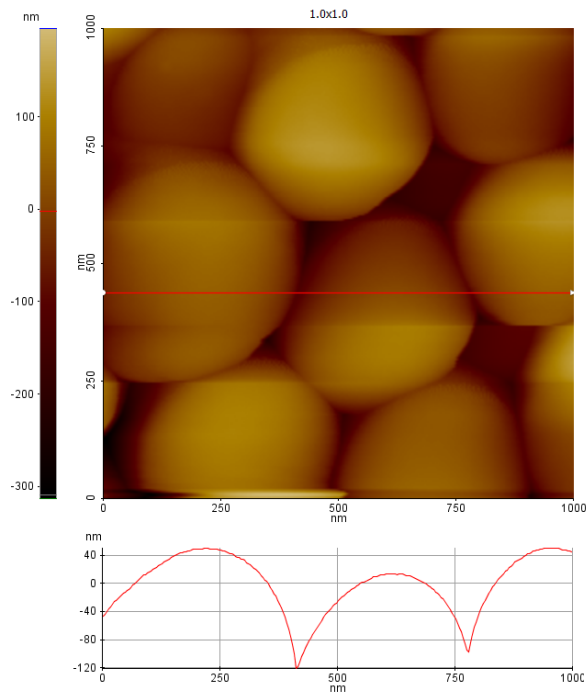


**Figure B.9:** AFM image over an area of  $1 \times 1 \mu\text{m}$ . By imaging an even smaller surface area, this image is obtained. Only a few spheres are visible and the profile of the horizontal red line (below) shows the number of spheres that are found along this line.



# Appendix C

---

## Quartz Crystal Microbalance with Dissipation Monitoring

---

### C.1 Technique

Quartz Crystal Microbalance (QCM) is an acoustic technique whereby an alternating current is applied to resonate coarse quartz crystals at multiples of their fundamental frequency. The resonance frequency changes as particles adsorb to the surface. From the Sauerbrey equation, the adsorbed mass can be deduced:

$$\Delta m = \left(\frac{C}{n}\right)\Delta f$$

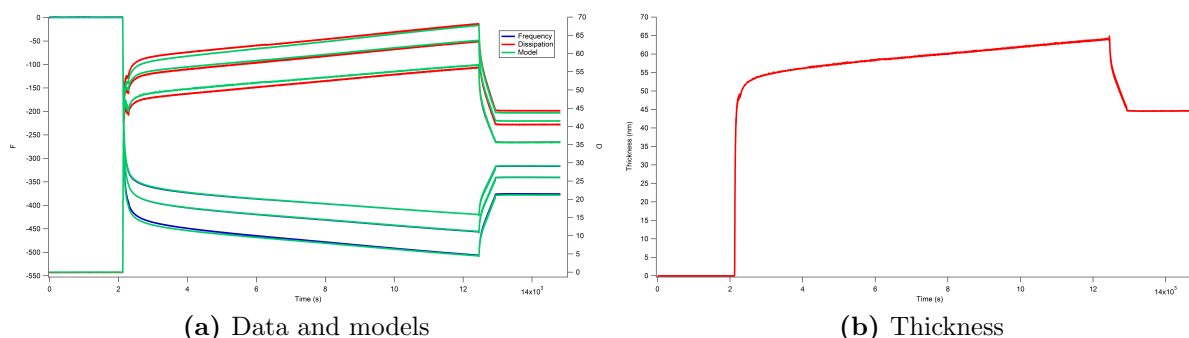
Here,  $C$  is the mass sensitivity constant and  $n$  is the overtone number. The Sauerbrey relation only holds for homogeneously distributed and rigid films. However, solvent molecules may couple to the adsorbed layer and hence increase the adsorbed amount. The wet mass of this viscoelastic film cannot be modelled with the simple Sauerbrey equation. When QCM is combined with measurements of the changes in energy dissipation (QCM-D), the frequency and dissipation changes can be modelled to yield the viscoelastic properties of the adsorbed layer [48], [49].

### C.2 Results

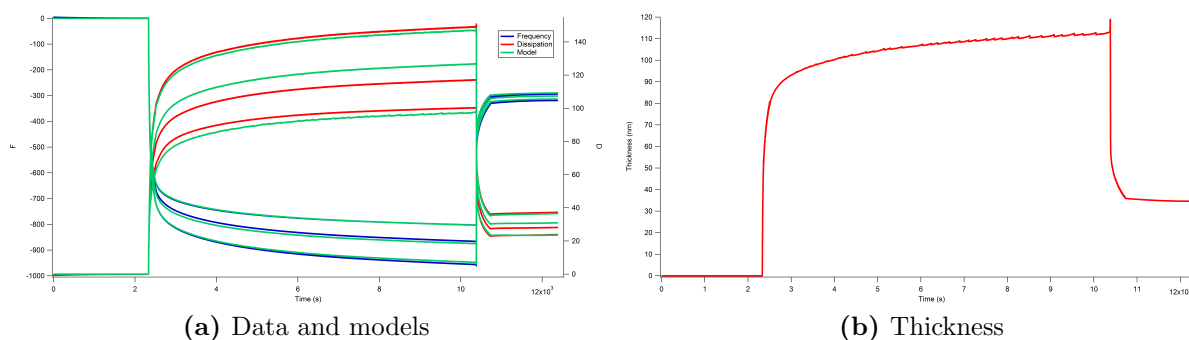
Several experiments were performed with QCM-D. The data were modelled to three overtone frequencies (usually 3, 5 and 7) using an extensive Voigt-based viscoelastic model. From the data the thickness and adsorbed amount were calculated. In figures C.1 to C.6 the raw data with the models and the resulting thickness is shown.

Figure C.1 shows that without depletion polymer, there is adsorption of silica spheres onto the quartz crystals. From figures C.1 and C.2 it can be deduced that the addition of polymer leads to an increase in the thickness of the adsorbed layer of silica spheres on the surface. Figures C.3 to C.5 show that a decrease in the PDMS concentration leads to a decrease in the thickness of the surface layer (however figure C.4 shows a thicker surface layer than figure C.3). When first the adsorption of PDMS is measured, followed by the

adsorption of the silica spheres (figure C.6), there is not a significant difference with the results from measurements of silica spheres only (figure C.1), indicating that PDMS does not adsorb to the surface.



**Figure C.1:** 0.58 V % SD1. (a) Raw data and models and (b) calculated thickness. Even without the addition of PDMS, silica spheres seem to adsorb to the silica surface.



**Figure C.2:** 0.58 V% SD1 and 20 mg/mL PDMS. (a) Raw data and models and (b) calculated thickness. Addition of PDMS leads to a thicker layer of silica on the surface.

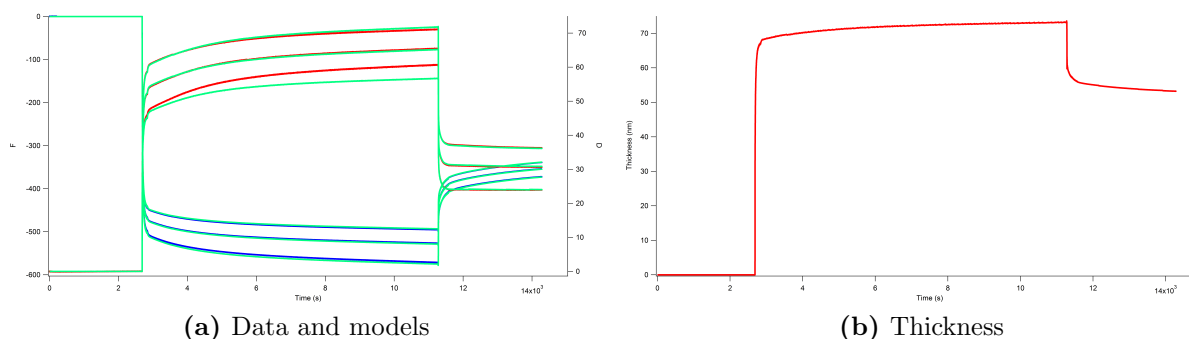


**Figure C.3:** 0.58 V% SD1 and 15 mg/mL PDMS. (a) Raw data and models and (b) calculated thickness. A decrease in the PDMS concentration results in a smaller thickness.

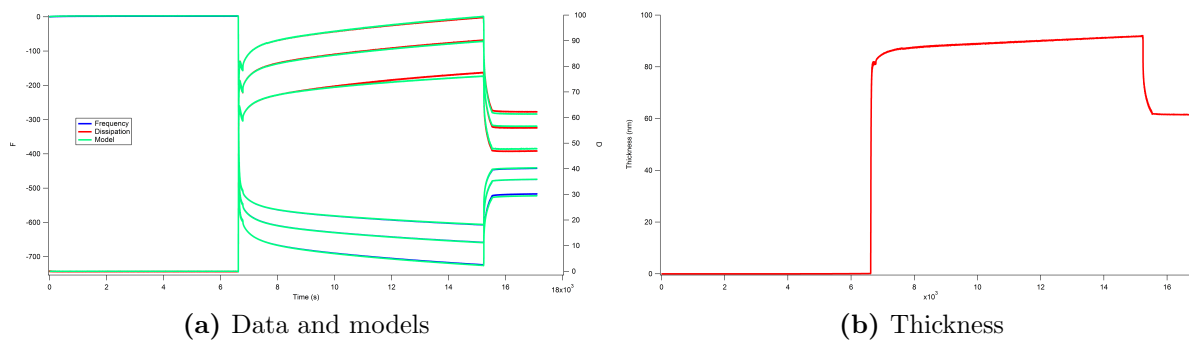


**Figure C.4:** 0.58 V% SD1 and 10 mg/mL PDMS. (a) Raw data and models and (b) calculated thickness. A decrease in the PDMS concentration results in a smaller thickness.

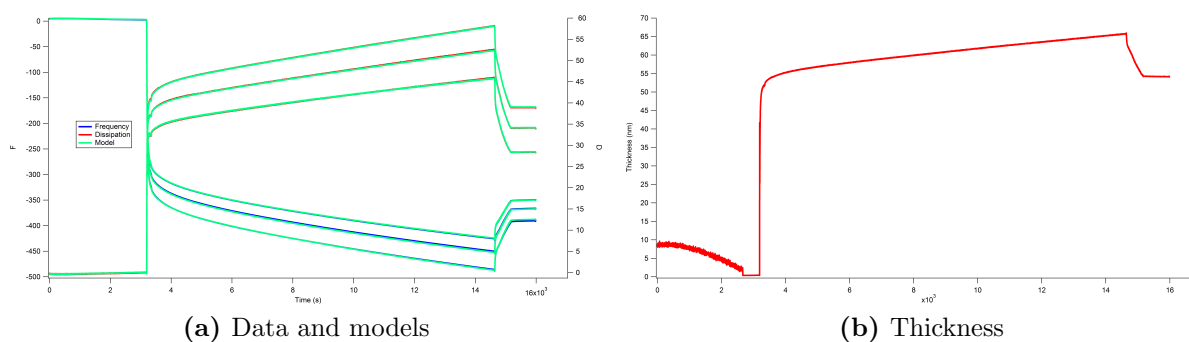


**Figure C.5:** 0.58 V% SD1 and 5 mg/mL PDMS. (a) Raw data and models and (b) calculated thickness. A decrease in the PDMS concentration results in a smaller thickness.

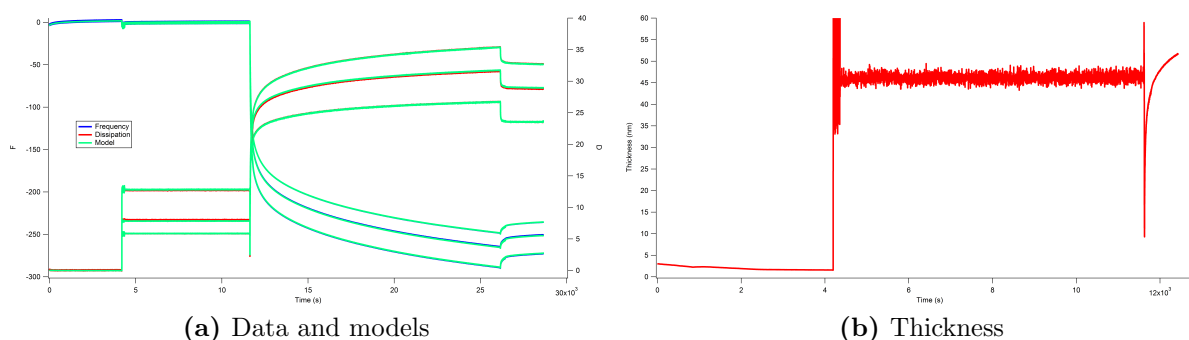


**Figure C.6:** First 20 mg/mL PDMS was flowed over the quartz crystal to measure the adsorption of the polymer followed by 0.58V% SD1. (a) Raw data and model and (b) calculated thickness. There is not a significant difference with the results from measurements of silica spheres only (figure C.1), indicating that the polymer does not adsorb to the crystal (as expected).

Injection of the sample occurs typically around 2000-4000 seconds (where a sharp transition can be seen) and rinsing typically start around 10000-15,000 seconds (where another sharp transition can be observed).

However, the QCM-D data could not be modelled in a satisfactory way. The modelling process yields models that do not overlap perfectly with the raw data, indicating that the model is not appropriate for these measurements. Another problem that was encountered, was the fact that the crystals were damaged after one experiment. Usually the crystals can be re-used at least ten times. It was found that the solvent, cyclohexane, damages the coarse crystals. For these two reasons, it was decided to abandon this technique.



# Appendix D

---

## Massive Adsorbed Amount

---

While performing ellipsometry experiments, it was found that the quality (that is the amount of hydrophobization) of the surfaces and the particles influence the adsorption process to a large extent.

### D.1 Incomplete Surface Hydrophobization

In figure D.1, the adsorbed amount and thickness per particle diameter, as measured by ellipsometry, can be found. The adsorption was measured from a 3V% silica particle dispersion in the absence of PDMS and onto a C<sub>18</sub>-TEP substrate. As can be seen here, the adsorbed amount is much larger than expected (and than usually measured; see chapter 4) and with values exceeding 150 mg/m<sup>2</sup>. In order to confirm these results, AFM was performed on the same substrate of which the images can be found in figure D.2.

As multiple experiments resulted in the same values, a surface was studied with AFM prior to an ellipsometry experiment (which eventually yielded similar thickness and adsorbed amount as in D.1). The AFM image of this surface can be found in figure D.3. The surface is covered with large aggregates of (most probably) stearyl alcohol, whereas other areas are completely bare. Due to incomplete hydrophobization of the surface, the substrate now consists of extremely hydrophobic parts on one side and hydrophilic parts on the other. If we now compare figure D.3 with D.2, it is motivating to state that the bare patches, i.e. where no particles adsorbed on the surface, in figure D.2, correspond to the patches with aggregates of hydrophobic material in figure D.2.

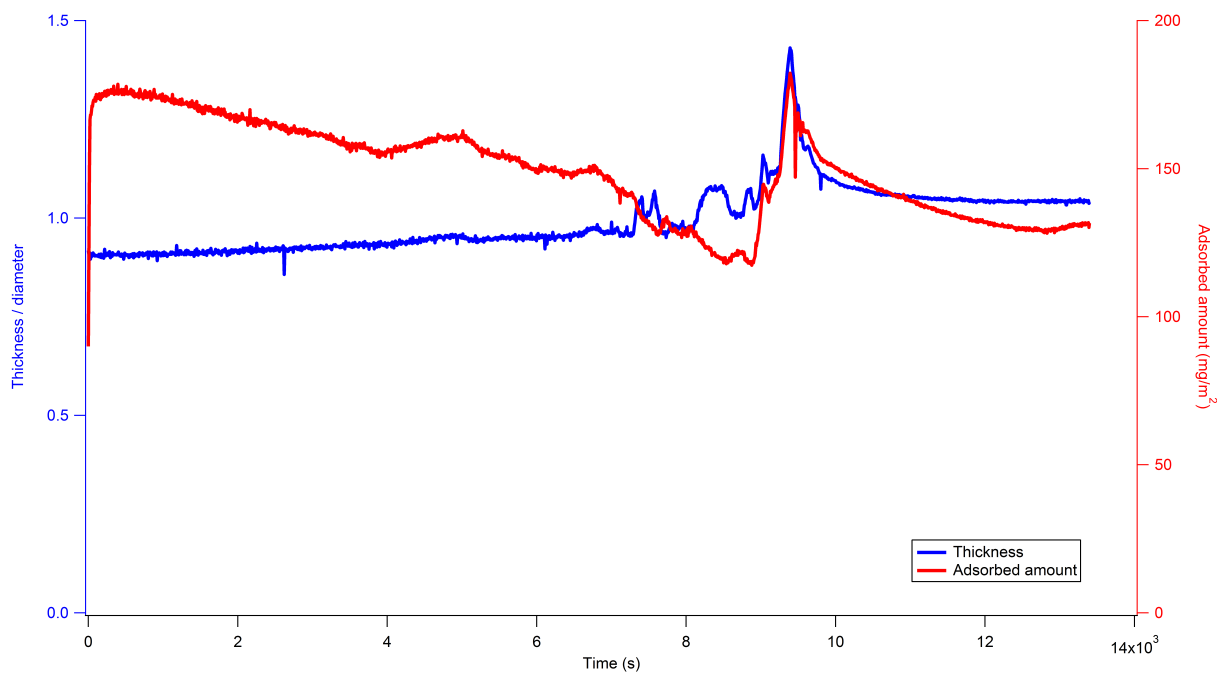


**Figure D.1:** Thickness per particle diameter and adsorbed amount versus time of adsorption from a 3V% silica particle dispersion on a  $C_{18}$ -TEP substrate.

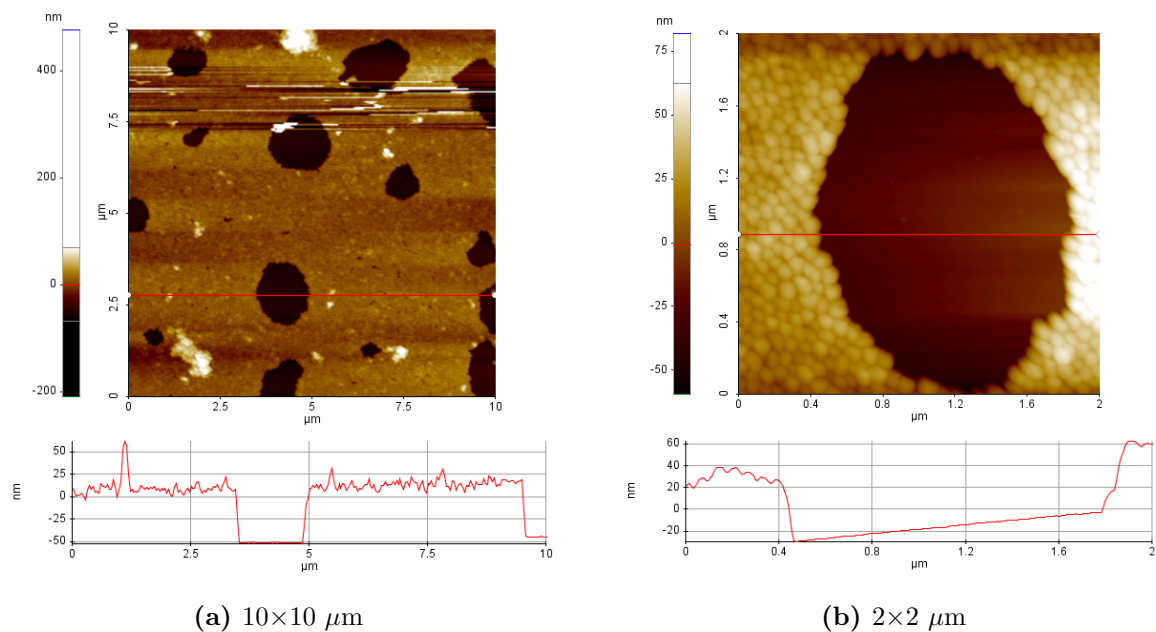


**Figure D.2:** AFM images of the substrate that showed a massive adsorbed amount with ellipsometry. (a) The surface is completely covered except for some bare patches that can be observed. (b) A zoom in of (a) shows that many particles are adsorbed on the surface and that there is a 'hole' where not even a single particle is adsorbed.

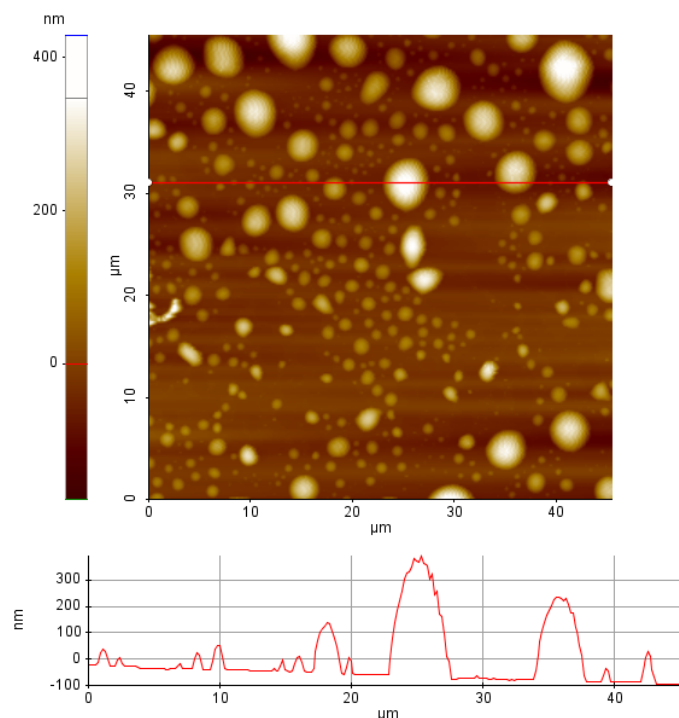


**Figure D.3:** AFM image,  $45.5 \times 45.5 \mu\text{m}$ , of bare  $\text{C}_{18}$ -TEP silica substrate prior to an ellipsometry experiment. The surface contains a number of large aggregates of (most probably) stearyl alcohol. Other parts of the surface are completely bare and are most likely still hydrophilic.

## D.2 Incomplete Particle Hydrophobization

Not only incomplete surface hydrophobization could lead to anomalous results, but so can incomplete particle hydrophobization. Three dispersions of hydrophobic silica spheres, that were all synthesized according to the protocol as described in Appendix A, but in different sizes and by different people, were used in additional adsorption experiments. The adsorption of 3V% silica particle dispersion was monitored by ellipsometry and the results are shown in figure D.4. Apart from the particle diameters, as indicated in the figure, the dispersions are supposed to be chemically equivalent. However, the measured adsorbed amount differs greatly from dispersion to dispersion. Therefore, it could be possible that the particle surface was incompletely hydrophobized; the less hydrophobic the particles, the more they tend to adsorb (similar as with incompletely hydrophobized surfaces). In order to quantify this, the zeta potential of the various dispersions was determined. These eventually yielded values of 0.548 mV for 74 nm,  $-0.841$  mV for 104 nm and  $-1.74$  mV for 86 nm spheres. Thus the zeta potential is indeed larger for the dispersion that shows the largest adsorbed amount. However, measuring the zeta potential in cyclohexane, an organic solvent, is extremely difficult and the results from various measurements vary enormously. The reliability of these values is thus questionable to say the least. Another method should be applied to quantify the amount of hydrophobization of the silica spheres (such as thermogravimetric analysis), but we do think that the differences that are observed are due to incomplete hydrophobization of the particle surface; the less hydrophobic the particles, the higher the adsorbed amount.

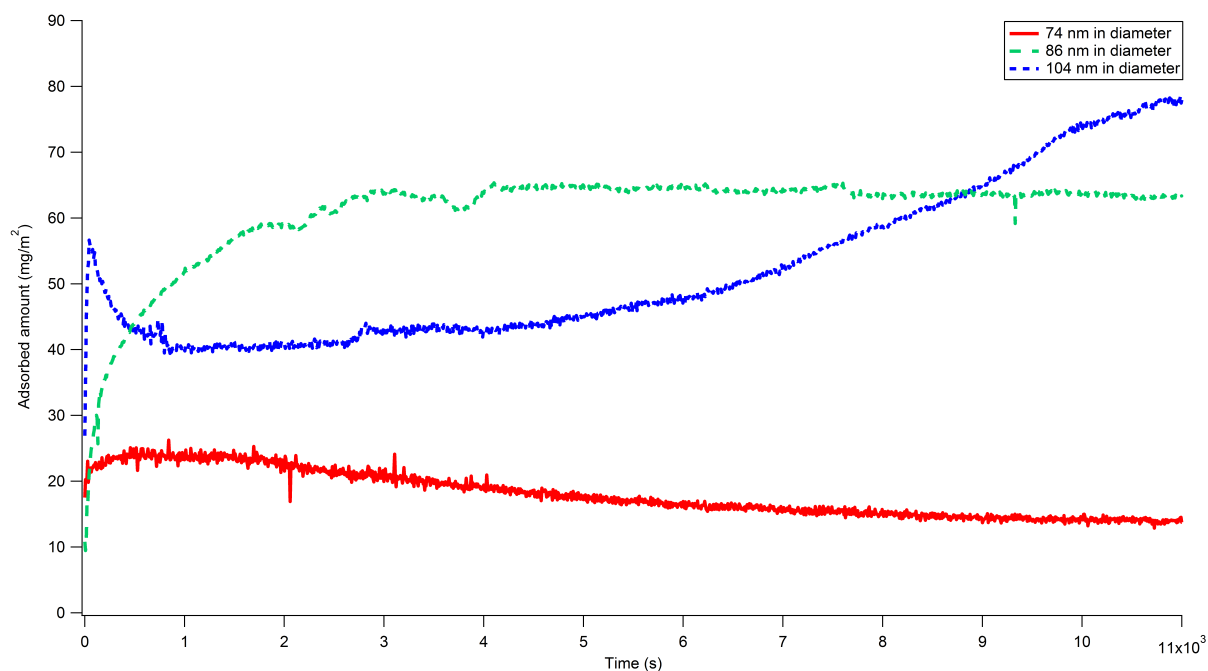


**Figure D.4:** Adsorbed amount versus time of adsorption from 3V% silica particle dispersion on C<sub>18</sub>-TEP surfaces of three different sizes: 74 nm, 86 nm and 104 nm in diameter. Even though the dispersions are supposed to be chemically equivalent apart from the size, the measured adsorbed amount differs greatly from dispersion to dispersion. No rinsing profile was measured.

In retrospect, we know that the the stability and reproducibility of C<sub>18</sub>-TEP surfaces has been questioned (see chapter 4). Nevertheless, the observed trends are believed to be valid, as not all the surfaces were of poor quality and usually a massive adsorbed amount ( $>150$  mg/m<sup>2</sup>) is obtained on insufficiently hydrophobized surfaces, which is not the case here. We thus hypothesize that in the limit of perfectly hydrophobic spheres and surfaces, the particles tend not to adsorb to the surface unless the interaction between them is increased.

# Appendix E

---

## Radius of Gyration of PDMS

---

The calculation of the radius of gyration of PDMS proceeded according to formulas derived by Vincent [50], [51].

The radius of gyration,  $R_g$ , of a depletion polymer is given by:

$$R_g = r_g^o r^{0.1} \quad (\text{E.0.1})$$

where  $r_g^o$  is the unperturbed value of the radius of gyration and  $r$  gives the number of effective segments per polymer chain.  $r$  is linked to the statistical segment length  $l$  through the extended polymer length  $L$ :

$$L = rl \quad (\text{E.0.2})$$

$r$  itself is defined by constants that are related to the nature of the polymer and is given by:

$$r = \left( \frac{0.408s}{AM_s} \right)^2 M_w \quad (\text{E.0.3})$$

Here,  $M_s$  is the real segment (repeat unit) molar mass,  $A$  is an empirical constant of the characteristic ratio for the polymer chains in a  $\theta$ -solvent,  $s$  is the length of each repeat unit and  $M_w$  is the molecular weight of the polymer. The unperturbed value of the radius of gyration,  $r_g^o$ , can then be calculated from equation (E.0.4):

$$r_g^o = \frac{A^2 M_s}{0.408s} \sqrt{r} \quad (\text{E.0.4})$$

The values of  $A$ ,  $M_s$  and  $s$  can be found in literature and have the following values for PDMS [50]:

$$\begin{aligned} A &= 0.027 \frac{nm\sqrt{mol}}{\sqrt{g}} \\ M_s &= 74 \frac{g}{mol} \\ s &= 0.25 \text{ nm} \end{aligned} \quad (\text{E.0.5})$$

PDMS that was used throughout this thesis had a molecular weight of 95000 g/mol. Filling these values out in equations (E.0.3) and (E.0.4) leads to:

$$\begin{aligned} r &= 248 \\ r_g^o &= 8.32 \text{ nm} \end{aligned} \quad (\text{E.0.6})$$

And finally a value for the radius of gyration of PDMS with a molecular weight of 95000 g/mol is obtained:

$$R_g = r_g^o r^{0.1} = 14.4 \text{ nm} \quad (\text{E.0.7})$$

## E.1 Relative Polydispersity

The PDMS that was used throughout this thesis has a  $M_w$  of 95000 g/mol, a radius of gyration of 14.4 nm (see above) and a polydispersity index of  $\frac{M_w}{M_n} = 1.9$ . In this section, the relative polydispersity in the radius of gyration is calculated from the polydispersity index by means of the moment expansion as described by A.P. Philipse in [52].

The  $n^{\text{th}}$  moment of a distribution of the number average over a total of  $N$  particles with radii  $a_i$ ,  $\langle a^n \rangle$ , is given by:

$$\langle a^n \rangle = \frac{1}{N} \sum_{i=1}^N a_i^n \quad (\text{E.1.1})$$

For  $n = 1$  we obtain the number averaged radius  $\langle a \rangle$  and  $n = 2$  defines the relative dispersity  $s_a$ :

$$s_a^2 = \frac{\langle a^2 \rangle - \langle a \rangle^2}{\langle a \rangle^2} = \frac{\sigma_a^2}{\langle a \rangle^2} \quad (\text{E.1.2})$$

where  $\sigma_a^2$  is the standard deviation. From (E.1.1) and (E.1.2) it follows that:

$$\frac{\langle a^n \rangle}{\langle a \rangle^n} = \left\langle \left( 1 + \frac{\sigma}{\langle a \rangle} \right)^n \right\rangle \quad (\text{E.1.3})$$

Equation (E.1.3) can be expanded by using the binominal theorem:

$$(1 + y)^n = \sum_{k=0}^n \frac{n!}{(n-k)!k!} y^k \quad (\text{E.1.4})$$

For distributions with  $\sigma_a^2 \ll 1$ , the expansion of (E.1.3) can be truncated at  $k = 2$  and yields:

$$\frac{\langle a^n \rangle}{\langle a \rangle^n} = 1 + \frac{n(n-1)}{2} s_a^2 \quad (\text{E.1.5})$$

The polydispersity index  $p$  of polymers is defined as the ratio between the weight-averaged molecular mass and the number-averaged molecular mass. For spheres with same mass density,  $p$  is given by:

$$p = \frac{\langle a^6 \rangle}{\langle a^3 \rangle^2} \quad (\text{E.1.6})$$

Substitution of (E.1.5) in (E.1.6) leads to:

$$p = 1 + 9s_a^2 \quad (\text{E.1.7})$$

PDMS that was used had a  $p$  of 1.9. This leads to a relative polydispersity,  $s_a$ , of:

$$s_a = \sqrt{\frac{0.9}{9}} * 100\% = 31.6\% \quad (\text{E.1.8})$$





# Appendix F

---

## Volume fractions

---

In literature, the amounts of colloids and polymer are usually given in terms of colloid volume fraction and relative polymer concentration. In this thesis, the colloid concentration is always given by volume percent (which is essentially  $100\times$  the volume fraction), but the amount of polymer is, for simplicity, given as an absolute polymer concentration. In order to be able to compare the results from this thesis with relevant literature, below the equation necessary to calculate the polymer volume fraction is given together with the formula that was used to determine the colloid volume percent.

### F.1 Colloid Volume Percent

Assuming that the volumes of solvent and colloids are additive, the colloid volume fraction ( $V_c\%$ ) can be calculated from:

$$V_c\% = \frac{\frac{w_c\%m_{dispersion}}{\rho_{colloid}}}{\frac{w_c\%m_{dispersion}}{\rho_{colloid}} + \frac{w_s\%m_{dispersion}}{\rho_{solvent}}} \quad (\text{F.1.1})$$

Where  $w_c\%$  and  $w_s\%$  are the weight percent of colloid and solvent respectively,  $\rho$  is the density of the colloids or solvents (as indicated) and  $m_{dispersion}$  is the mass of the dispersion. Equation (F.1.1) can be rewritten as:

$$V_c\% = \frac{\frac{w_c\%}{\rho_{colloid}}}{\frac{w_c\%}{\rho_{colloid}} + \frac{100\% - w_c\%}{\rho_{solvent}}} \quad (\text{F.1.2})$$

The density of cyclohexane that was used is 0.779 g/mL and for the silica dispersion SD1 a value of 1.70 g/mL was adhered.

### F.2 Relative Polymer Concentration

The following is largely based on a description of the relative polymer concentration as can be found in the book *Colloids and the Depletion-Interaction* by Lekkerkerker and Tuinier [14].

The relative polymer concentration is the polymer concentration normalized to the overlap concentration and is given by:

$$\phi_p = \frac{n_b}{n_b^*} = \frac{\varphi}{\varphi^*} \quad (\text{F.2.1})$$

Where  $n_b$  is the bulk number density of polymer molecules,  $n_b^*$  is the number density at the overlap concentration and  $\varphi$  corresponds with the volume fraction of polymer segments. At the overlap concentration the relative polymer concentration is equal to one. The overlap volume fraction where polymer segments start to overlap can be given by:

$$\varphi^* = \frac{Mv_s}{v_p} \quad (\text{F.2.2})$$

With  $M$  the number of monomers per chain,  $v_s$  the segment volume and  $v_p$  the coil volume. In terms of actual concentrations the overlap concentration,  $c^*$ , can be found from equation (F.2.3):

$$c^* = \frac{3M_p}{4\pi R_g^3 N_{AV}} \text{ in } g/L \quad (\text{F.2.3})$$

Where  $M_p$  is the molecular weight of the polymer,  $R_g$  is the radius of gyration of the polymer and  $N_{AV}$  is Avogadro's number.

In terms of concentrations the relative polymer concentration,  $\phi_p$ , is thus given by:

$$\phi_p = \frac{c}{c^*} = \frac{4\pi R_g^3 N_{AV} c}{3M_p} \quad (\text{F.2.4})$$

With the  $c$  the actual polymer concentration as used throughout this thesis.

# Appendix G

---

## Adsorbed Amount

---

Throughout this thesis values of the adsorbed amount in  $mg/m^2$  are given as results. To put things in perspective, we will calculate the adsorbed amount that corresponds with one full layer of close-packed spheres.

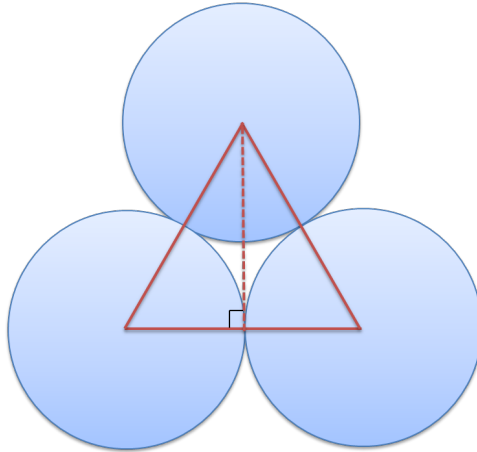


**Figure G.1:** Three close-packed spheres. An equilateral triangle is drawn onto the spheres of which the sides are equal to the diameter of the spheres. The three internal angles correspond to  $60^\circ$  each.

Figure G.1 shows three close-packed spheres. Within these spheres an equilateral triangle is drawn of which the sides are equal to the diameter of the sphere. Assuming a particle diameter of 74 nm (as is the case for dispersion SD1), the height of the triangle can be calculated using Pythagoras' theorem:

$$\text{Height} = \sqrt{74^2 - 37^2} = 64 \text{ nm}$$

The area of the triangle is then equal to:

$$\text{Area triangle} = \frac{74 \times 64 \text{ nm}}{2} = 2368 \text{ nm}^2$$

As each of the internal angles of an equilateral triangle corresponds to  $60^\circ$ ,  $\frac{1}{6}$  of each sphere is included in the triangle. Therefore, the area of the triangle consists of  $3 \times \frac{1}{6} = \frac{1}{2}$  sphere. The area of one sphere is thus equal to twice the area of the triangle and is equal to:

$$\text{Area per sphere} = \frac{74 \times 64 \text{ nm}}{2} \times 2 = 4736 \text{ nm}^2$$

The number of spheres on one  $m^2$  follows as:

$$\text{Number of spheres per } m^2 = \frac{1 \text{ m}^2}{4736 \cdot 10^{-18} \text{ m}^2} = 2.11 \cdot 10^{14}$$

The volume of one sphere corresponds to:

$$\text{Volume of a sphere} = \frac{4}{3}\pi R^3 = \frac{4}{3}\pi(37 \cdot 10^{-9} \text{ m})^3 = 2.12 \cdot 10^{-22} \text{ m}^3$$

The volume of all spheres amounts to:

$$\text{Total volume} = 2.11 \cdot 10^{14} \times 2.12 \cdot 10^{-22} \text{ m}^3 = 4.5 \cdot 10^{-8} \text{ m}^3 = 4.5 \cdot 10^{-2} \text{ mL}$$

Taking the density of SD1 as 1.70 g/mL, we find an adsorbed amount of:

$$\text{Adsorbed amount} = 1.70 \text{ g/mL} \times 4.5 \cdot 10^{-2} \text{ mL} = 7.599 \cdot 10^{-2} \text{ g/m}^2 = 76 \text{ mg/m}^2$$